



**Antibacterial Properties of Plasma Functionalized  
Surfaces Immobilization with Aggregation-Induced  
Emission Photosensitizers for Preventing Surgical  
Site Infection**

**by**

**Resmarani Sahu**

**Thesis submitted to Flinders University for**

**the degree of**

**Masters of Biotechnology**

College of Medicine and Public health

3<sup>rd</sup> of November 2023

Principle Supervisor: Prof. Youhong Tang

Co-Supervisors: Dr. Vi Khanh Truong

Prof. Krasimir Vasilev

Dr. Neethu Ninan

# Table of Contents

Abstract.....	5
Declaration.....	6
Acknowledgement.....	7
Figure List.....	8
Table List.....	10
LIST OF ABBREVIATIONS.....	11
CHAPTER 1: LITERATURE REVIEW.....	12
1.1. Introduction.....	12
1.2. Bacterial infections and surgical site infection.....	15
1.2.1. Cases worldwide and emergence of treatment.....	17
1.2.2. Current clinical treatments and biomedical application uses in prevention.....	<b>Error! Bookmark not defined.</b>
1.2.3. The causes affecting current treatment and roles of antibiotic resistance bacteria.....	21
1.3. Nanoparticles with anti-bacterial properties.....	21
1.3.1. Different research using different nanoparticle and their applications.....	22
1.3.2. Limitations of nanoparticle-based treatments.....	23
1.4. AIE- Aggregation induced emission.....	23
1.4.1. Properties of AIEgen.....	24
1.4.2. Research related to antibacterial AIEgens.....	24
1.5. Plasma polymerisation.....	26
1.5.1. Properties of plasma polymerisation.....	28
1.6. Hypothesis and aims.....	29
1.6.1. Hypothesis.....	29
1.6.2. Aims.....	29

CHAPTER 2: METHODOLOGY .....	31
2.1. Materials .....	31
2.2. Methods .....	31
2.2.1. Preparation of AIEgen immobilised plasma polymerised surfaces .....	31
2.3. Characterisation .....	33
2.3.1. Ellipsometer observation for stability of plasma polymerised surfaces .....	34
2.3.2. Immobilisation of the surfaces with AIEgen .....	35
2.3.3. Water contact angle .....	36
2.3.4. FTIR micro spectroscopy .....	37
2.3.5. UV-vis spectroscopy .....	38
2.3.6. Fluorescence microscopy .....	40
2.3.7. Live/dead staining .....	42
2.3.8. Colony formatting Unit .....	<b>Error! Bookmark not defined.</b>
2.3.9. ROS assay .....	<b>Error! Bookmark not defined.</b>
2.3.10. Membrane potential assay .....	45
2.3.11. Cell integrity .....	46
2.3.12. Scanning electron microscope .....	46
2.3.13. Zone Inhibition assay .....	48
2.3.14. Cyto-toxicity .....	48
CHAPTER 3: RESULTS AND DISCUSION .....	51
3.1. Results .....	51
3.1.1. Preparation of AIEgen-immobilised plasma polymerised surfaces and their characterisation	51
3.1.2. Antibacterial properties .....	57
3.1.3. Cell Viability/ Cyto-toxicity .....	64
3.2. Discussion .....	65
3.2.1. Characterisation of AIEgen-immobilised plasma polymerised surfaces .....	65

3.2.2. Performance of AIEgen-immobilised plasma polymerised surfaces with bacteria .....	67
3.2.3. Biocompatibility of the substrates .....	70
3.3. Conclusion and future research .....	70
Reference .....	73

## Abstract

Bacterial illnesses are major threats to human health because of the number of antibiotic-resistant bacteria causing significant mortality and morbidity in the general population. Surgical site infection (SSI) is one of the major bacterial infections that appears at the site of surgery with the entry of microorganisms. Aggregation-induced emission luminogens (AIEgens), with their distinct optical characteristics, biocompatibility, low toxicity, and target specificity, hold the potential for the treatment of SSIs as an antibacterial therapy with restricted reactive oxygen species (ROS) in their aggregation state. Herein, an AIEgen-immobilized plasma-polymerized substrate is reported to develop AIE active photosensitisers (PSs) with ROS generation ability for the successful prevention of drug-resistant bacteria at the surgical site. The plasma-polymerized surfaces are substrate-independent and it improves the binding of AIEgens to the substrate without changing the properties of either the substrate or AIEgens.

However, since the cyano group and cationic charge have such strong surface binding affinities, the cationic CN-TPAQ-PF6 exhibits outstanding photodynamic killing efficiency. It eradicates >90% of *S. aureus* and >99.99% of *P. aeruginosa* bacteria, respectively, at a very low concentration of 10 -14  $\mu\text{g/ml}$  under low-intensity light exposure ( $40 \text{ mW cm}^{-2}$ ) for 1 hour. Further, CN-TPAQ-PF6 have enhanced ROS generation capacity in compare to TPAQ-PF6 This CN-TPAQ-PF6 immobilised plasma coated surface showed a high cell viability rate towards HacaT cell in compared to the TPAQ-PF6 immobilised plasma coated surface. Furthermore, the cationic CN-TPAQ-PF6 is immobilized on a medical device suture for effective application in the biomedical field to prevent antibiotic-resistant bacterial infections. With more in-depth in-vivo research, our work illuminates potential future directions for innovative medicinal uses of AIEgens to combat antibiotic resistance.

## Declaration

I certify that this thesis:

1. does not incorporate without acknowledgement any material previously submitted for a degree or diploma in any university;
2. and the research within will not be submitted for any other future degree or diploma without the permission of Flinders University; and
3. to the best of my knowledge and belief, this work does not contain any material previously published or written by another person except where due reference is made in the text.

Signed..... *Resma* .....Resmarani Sahu

Date 3<sup>rd</sup> Nov 2023

## **Acknowledgement**

Firstly, I would like to thank all Prof. Youhong Tang, for his support and guidance throughout this research project. As a research student, it has been an enlightening journey for me to learn and grow because of his valuable advises and mentorship.

Also, I would like to express my deepest gratitude to Dr. Vi Khanh Truong, for his endless support and guidance. With all the experiments, his advises helped me to overcome difficult situations.

Further, I thank Professor Krasimir Vasilev and his wonderful research group at the Biomedical Nanoengineering Laboratory for their support in the lab and training with various apparatus and machines.

Furthermore, I thank Dr. Neethu Ninan, for her endless support in many experiments including training with plasma reactor, sample characterization and preparation following with great advises.

I want to thank Dr. Dennis Palms for the training and support in operating many equipment and machines such as ellipsometry, FTIR, UV Spectroscopy, and Fluorescence Spectroscopy.

I thank all my group members especially PhD student Ngoc Huu Nguyen for all the microbiology experiments, PhD student Manh Tuong Nguyen for the cytotoxicity experiment, PhD student Andrew Hayles, Associate Professor Jianzhong Wang for the help in every experiment, PhD student Markos Alemie, PhD student Borislav Stoilov and my colleagues, Mr Tien Thanh Nguyen, Ms Thi Giang Tuyet Pham, Mr Phuoc Ton and everyone for their support.

I want to thank Prof. Munish Puri, Dr. Liu-Fei Tan, Dr. Hanna Krysinska and Kushari Burn for all lab induction and biosafety sessions.

I would also like to thank my friends and family for their support and encouragement.

# Figure List

Figure 1 : (left) Surgical site infection .....	12
Figure 2 : Illustrate AIE materials are compared .....	14
Figure 3 : Illustration of an AIEgen-transduced .....	15
Figure 4 : Schematic presentation of different .....	16
Figure 5 : a) Examples showing aggregation-caused .....	25
Figure 6 : Schematic illustration of films .....	26
Figure 7 : Schematic illustration of surface coating .....	28
Figure 8 : The list of phases that needed to be obtained for the research objectives. ....	30
Figure 9 : The custom-built capacitively coupled bell .....	33
Figure 10 : Summary of the plasma polymerisation .....	34
Figure 11 : The properties of Ellipsometer (A) .....	35
Figure 12 : Illustrates the electrostatically binding of carboxylic.....	35
Figure 13 : illustration of water contact angle .....	37
Figure 14 : Schematic representation of .....	38
Figure 15 : Illustrates the steps for UV-Vis spectrometer function.....	39
Figure 16 : (A) Fluorescence Microscope, (B) excitation light .....	40
Figure 17 :(A) schematic illustration of bacterial staining .....	<b>Error! Bookmark not defined.</b>
Figure 18 : Use a serial dilution method for the colony forming ....	<b>Error! Bookmark not defined.</b>
Figure 19 : Suggested pathway via which DCFH- .....	45
Figure 20 : The main parts of an SEM machine .....	47
Figure 21 : Illustrates basic steps taken for the MTT assay. (1).....	49
Figure 22 : The intensity of AIEgen (AIE1 (TPAQ-PF6) .....	53
Figure 23 : The above graph represents that AIE2 is .....	54
Figure 24 : The absorbance pea for both .....	55

Figure 25 : Fourier transform infrared .....	56
Figure 26 : The figur represents the antibacterial assay .....	59
Figure 27 : The figur represents the antibacterial assay .....	57
Figure 28 : Colony forming unit count with 2 different concentrations. ....	60
Figure 29 : Samples for Zone of .....	61
Figure 30 : ROS staining images of .....	61
Figure 31 : The intensity of green, fluorescent.....	62
Figure 32 : Morphological changes in .....	63
Figure 33 : Cell integrity observation for <i>S. aureus</i> .....	64
Figure 34 : Chart illustrates the .....	65
Figure 35 : Illustration of cell membranes for both .....	68

## Table List

Table 1 : Important operative phases relates to the .....	18
Table 2 : Thickness measured for plasma deposited poly-oxazoline .....	51
Table 3 : Thickness measured for plasma deposited acrylic acid .....	51

# LIST OF ABBREVIATIONS

<b>Abbreviation</b>	<b>Full name</b>
ATR-FTIR	Attenuated total reflectance-Fourier transform infrared spectroscopy.
CFU	Colony forming unit.
CLSM	Confocal laser scanning microscopy.
DMEM	Dulbecco's modified eagle medium.
DMSO	Dimethyl sulfoxide.
FBS	Fetal bovine serum.
IF	Immunofluorescence.
MBC	Minimum bactericidal concentration.
MIC	Minimum inhibitory concentration.
MRSA	Methicillin resistant strains.
NADPH	Nicotinamide adenine dinucleotide phosphate.
NPs	Nanoparticles.
PBS	Phosphate buffered saline.
ROS	Reactive oxygen species.
SEM	Scanning electron microscopy.

# CHAPTER 1: LITERATURE REVIEW

## 1.1. Introduction

Bacterial illnesses are responsible for a great deal of major health problems in the general population. Some bacterial illnesses have significant mortality and morbidity rates and treating them can be costly (Taheri *et al.*, 2015). Numerous bacterial infections arise in a variety of fields, such as bacterial skin and soft tissue infections, blood stream infections, and infections of the urinary tract. The expense of hospital stays and treatments is rising, and surgical site infections (SSIs) are one of the most common bacterial infections to do so (Russo *et al.* 2019). SSI is one of the leading bacterial infections causing a higher economic burden with increasing costs for hospital stays including treatments (Russo *et al.* 2019). SSI develops after surgery around the body where the procedure was performed. Infections at the site of surgery can occasionally just affect the skin. Other, more serious SSIs might affect organs, tissues under the skin, or implanted material within 30 days of surgery. Purulent discharge from the wound or an isolated organism might cause the surgical site to become infected (Zabaglo & Sharman 2022). The occurrence of SSI varies based on the context, the accessibility of services, and a range of patient- and surgery-related variables, occurring in between 2% and 20% of patients globally after surgery (World Health Organization, 2018).

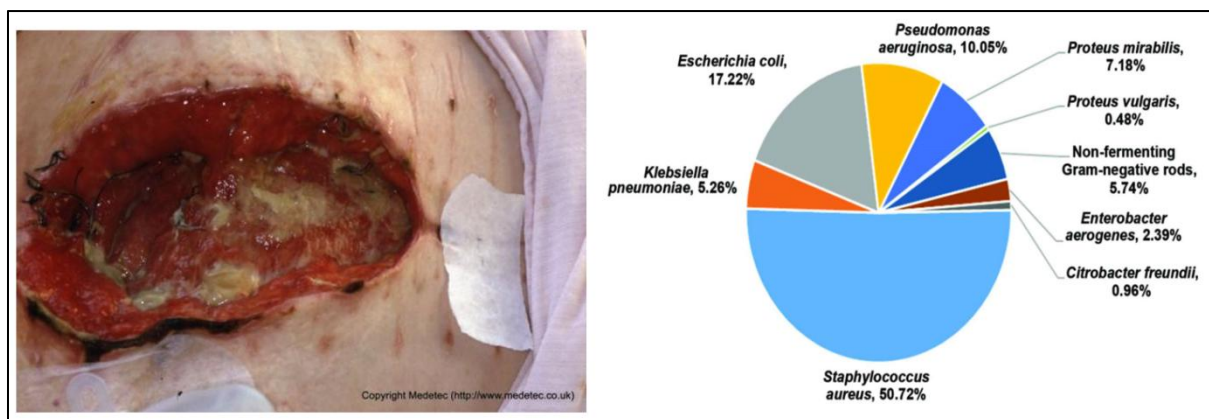


Figure 1: (left) Surgical site infection (Surgical Wound Dehiscence n.d.) and (right) different bacterial strain frequencies of causing the infection (Călina *et al.*, 2016).

Despite several preventive measures, surgical site or wound infection remains one of the most common and important healthcare-associated infections, which causes 17%–20% of all hospital-acquired infections (Lakoh *et al.* 2022). According to estimates by the World Health Organization (WHO) in 2011, the incidence of SSI in high-income countries (HICs) ranges from 1.2 to 5.2%, while that in low- and middle-income countries (LMICs) is 10.8% (Lakoh *et al.* 2022). SSI contributes up to \$3.4 billion in the US which includes extra stays at hospitals (Worth *et al.*, 2015). Even though numerous treatments, such as the "magic bullet" have already been found, the process has become frustrating due to some bacteria's antibiotic resistance traits (Liu *et al.*, 2023). For instance, the methicillin-resistant *S.aureus* and ceftriaxone-resistant *E. coli* bacteria are responsible for a variety of infectious illnesses (Wang *et al.*, 2022). Scientists have proposed several technologies in response to this serious predicament. Many studies have shown that nanoparticles related treatments are showing great antibacterial activity and wound infection applications, such as iron oxide, silver, curcumin, and wholly unrelated materials, are utilized to treat SSIs and antibacterial resistance (Juncker *et al.*, 2021). However, as different strains from the same species of bacteria have variable levels of antibiotic resistance, different antibacterial activities and different hazardous/ toxicity levels, a better solution for this aspect was needed (Duval *et al.*, 2019). These antibiotic-resistant bacteria can be eliminated by using near-infrared laser light and the photodynamic and photothermal properties of nanomaterials. Aggregation induced emission luminogens (AIEgens) with their distinct optical characteristics, biocompatibility, less toxicity, and target specificity have received a lot of attention recently in the field of antibacterial research. Aggregation-induced fluorescence enhancement is a property of AIEgens, which makes them excellent candidates for biosensing and imaging applications (Wu *et al.* 2022). Also, with the aid of surface engineering and a cutting-edge technique called plasma polymerisation, any type of material can have a nano-thin layer of polymer deposited on it, without altering the substrate or nanoparticle properties. This method's advantages include the ability to function without liquids, the need for the fewest precursors, and the extraction of less liquid organic waste (Ninan *et al.*, 2021). A detailed physico-chemical characterisation of these surfaces immobilised with AIE nanoparticles will be conducted, and their antibacterial properties will be investigated (Dabare *et al.*, 2021). There is various research that has already been conducted with AIE nanoparticles for antibacterial activities.

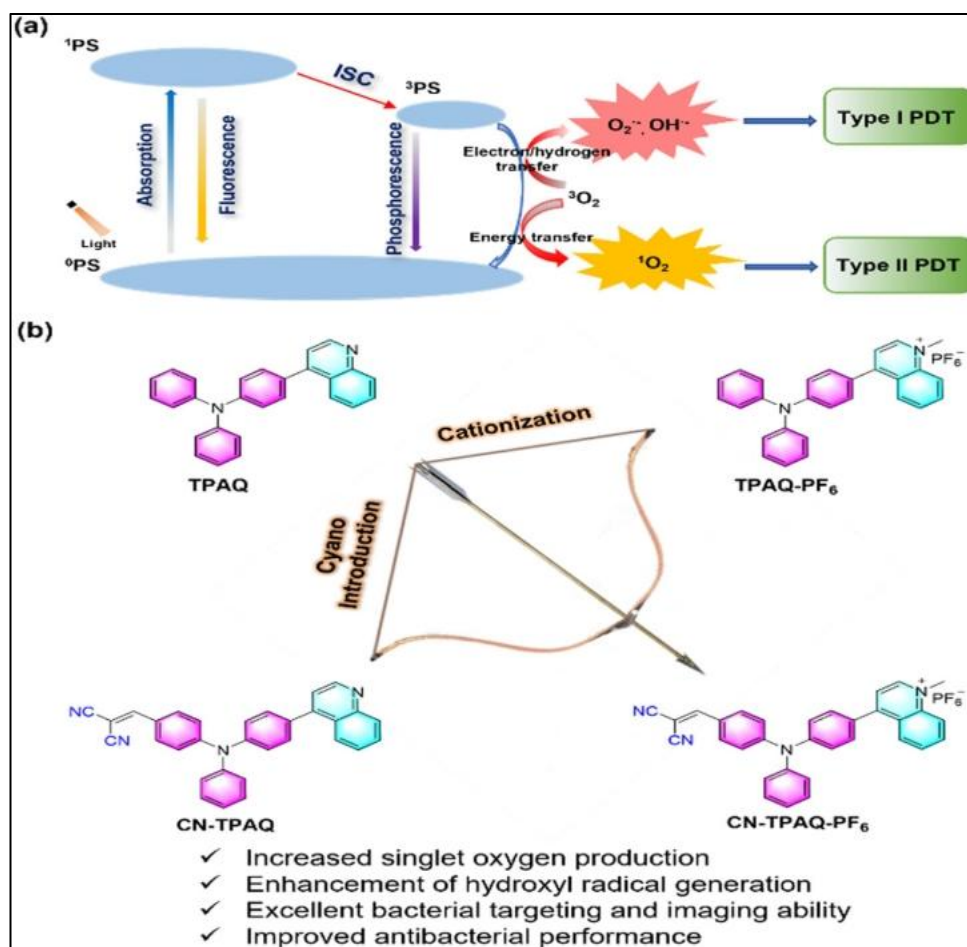


Figure 2: Comparison of AIE materials their cationic counterparts, TPAQ-PF<sub>6</sub> and CN-TPAQ-PF<sub>6</sub>, which demonstrates superior photodynamic killing of bacteria that are resistant to drugs. Here, (a) mechanism of ROS generation and (b) cyano introducing technique and molecular cationization to improve the production (Yu *et al.*, 2023).

Here, in this research project, using antibacterial plasma coating immobilised with AIEgens TPAQ-PF<sub>6</sub> (2,2,6,6-Tetramethylpiperidine-1-oxyl- hexafluorophosphate) and CN-TPAQ-PF<sub>6</sub> (cyano-2,2,6,6-Tetramethylpiperidine-1-oxyl- hexafluorophosphate), we expect to eradicate this bacterial biofilm. TPAQ is a neutral molecule which is converted to its cationic counterpart form. The plasma coating substrates can be applied on medical device to be used for SSI with a custom-built plasma reactor with selected monomers with further studies. In this research, the selected AIEgen will be immobilised on the top of the coated surface. Furthermore, the characterization of the AIEgen immobilised plasma functionalised surface will be done and advanced tools and data will be used to analyse with their respective

software (Dabare *et al.*, 2021). Also, the antibacterial activity will be determined with agar plate bacterial assay (Yu *et al.*, 2023) and the cytotoxicity will be determined using cell viability assay respectively (Ninan *et al.*, 2021).

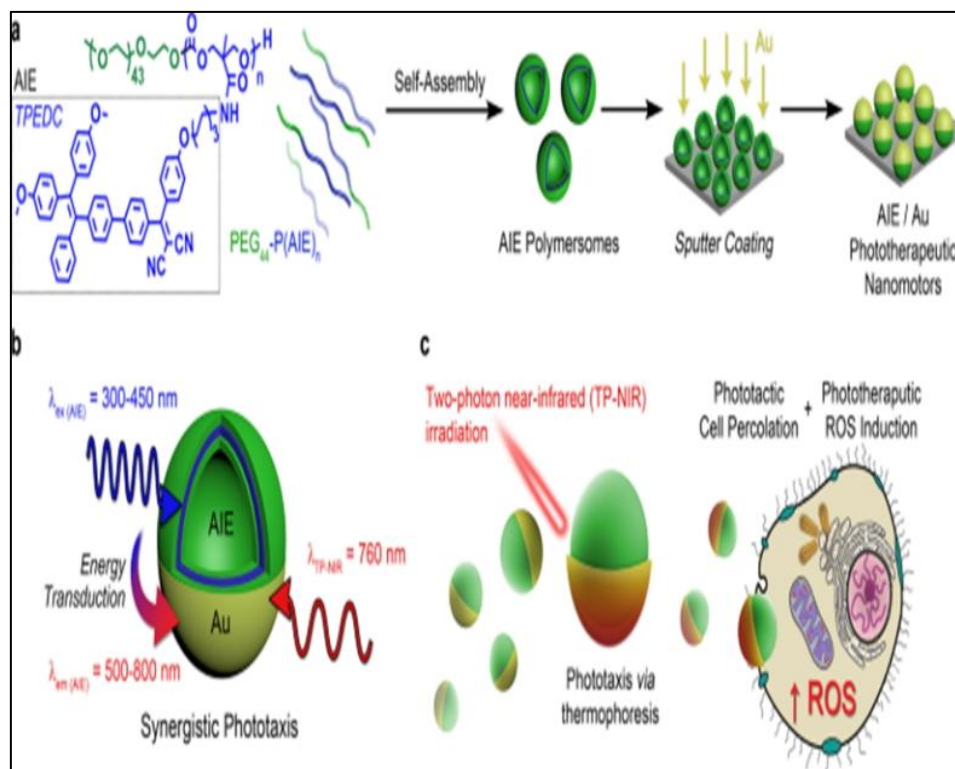


Figure 3: Illustration of an AIEgen-transduced hybrid that works in conjunction with Au phototherapeutic nanomotors. Here, (a) synthesis process of AIEgen-transduced hybrid with gold nanoparticle, (b) Characteristic of the new product, and (c) Mechanism of ROS production and bacterial infection resistance (Cao *et al.* 2021)

## 1.2. Bacterial infections and surgical site infection

A harmful microorganism develops at the locations of incisions, causing infection. Numerous locations, including the epidermis, deep skin layer, superficial subcutaneous fat, and occasionally organs and cavities, might experience it (Bagnall *et al.* 2009). An alarming rise in population mortality is a result of bacterial SSIs, a danger to the whole healthcare system. A prolonged hospital stay can be caused by several circumstances, including a patient's condition with other diseases, hygiene issues, contaminations, etc., all of which might increase the risk of infection. After an incision, this infection may spread to the tissues or

organs, posing a major risk. *S. aureus*, *P. aeruginosa*, *L. bacillus*, and other common bacteria are frequently identified to be the ones causing the infection site by establishing colonies. There are three different forms of SSI, depending on where the infection is located: superficial incisional infections, deep incisional infections, and organ infections (Cheadle 2006). The organism's exposure varies depending on the hygiene and wound site, which might lead to the infection spreading to nearby organs.

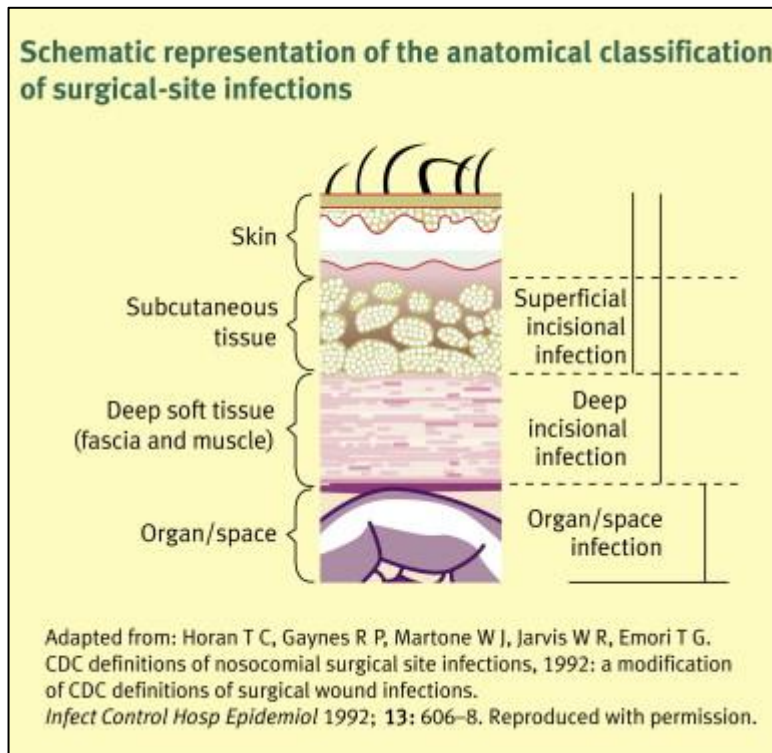


Figure 4: Schematic presentation of different types of surgical site infection (Bagnall *et al.* 2009)

Given that bacterial flora causes SSI, there may be clinical indications of the infection, such as fever, redness, swelling, etc. Severe instances of SSIs can pose a serious risk to life, such as bleeding from anastomotic dehiscence when an artificial vascular graft becomes infected (Bagnall *et al.* 2009). Many of these infections are resistant to several antibiotics, making it difficult to treat and maintain the wound site. As a result, it's critical to combat the infection more carefully so as not to harm the patient's organs.

### **1.2.1. Cases worldwide and the emergence of treatment**

Studies have shown that around 3% of surgical operations result in SSIs, which account for 20% of emergency cases (Barie & Eachempati 2005). Attributable to one-fourth of all aquatic infections, it is the most prevalent infection. An estimated 5% of individuals in the UK who had undergone surgery were found to have acquired an SSI, according to a prevalence survey conducted in 2006. About 14–16% of the 2 million nosocomial infections that hospitalised patients in the US are thought to be caused by SSIs. SSIs are linked to higher rates of morbidity, death, length of hospital stay, and treatment costs (Bagnall et al. 2009). Even with several preventative measures in place, surgical site or wound infections continue to rank among the most prevalent and significant healthcare-associated illnesses, accounting for 17% to 20% of all hospital-acquired infections. (Lakoh et al. 2022). In HICs (higher income countries), the incidence of SSI varies from 1.2 to 5.2%, but in LMICs (lower income countries), it is 10.8%, according to estimations made by the WHO in 2011. Infections from surgical sites can cost the US up to \$3.4 billion, including additional hospital stays (Worth et al., 2015).

Current clinical treatments and biomedical application uses in the prevention

One of the main causes of significant morbidity and death is SSI. It is crucial to clean and maintain incision sites to lower the incidence of SSI. Prior to surgery, it is important to focus on aspects like optimising the patient's condition by taking care of controllable variables like quitting smoking, increasing nutritional status, treating anaemia, and ensuring that diabetics have optimal glycaemic management. If prophylaxis is warranted, antibiotics ought to be given at the time of induction of anaesthesia. Microbes in the operating room air can be a significant source of pathogens that result in surgical site or wound infections. Therefore, it's imperative to have a less polluted operating room environment along with good hygiene with proper bathing with an antiseptic agent is also important. Patients with different diseases can be taken very ideal care which also includes their medication consumption at the right time. Also, infection would increase when hair gets into a surgical wound. Hence, hair removal from the area of surgery is also important. Different antibiotics can be used for some of the bacteria causing infection. However, not every bacterial strain can be treated with antibiotics (Alexander et al. 2011).

Table 1: Important operative phases relate to the prevention of surgical site infection (Bagnall *et al.* 2009)

<b>Pre-operative phase</b>	
Showering	All patients are to shower/bath with soap on the night prior to or on the day of the operation.
	Ensure assistance is provided if needed.
Hair removal	No need for routine hair removal. If indicated, use single-use electric clippers with a disposable head on the day of surgery. Do not use razors.
Theatre clothing	Appropriate clothing with easy access to the operative site, taking into account patient dignity.
	Staff are to wear appropriate clean non-sterile theatre wear in the operating department.
	Staff in non-sterile wear must minimize movement in and out of the theatre.
Nasal decontamination	Routine nasal MRSA decontamination is not indicated.
Mechanical bowel preparation	Mechanical bowel preparation is not routinely indicated.
Hand adornments	The operating team must remove all hand jewellery, nail polish and artificial nails.
Antibiotic prophylaxis	Give appropriate antibiotic prophylaxis only when indicated.
	Ensure local antibiotic formulary is utilized, and beware of adverse effects.
	Consider the timing of antibiotic prophylaxis (usually at induction, but an hour before operation if a tourniquet is to be used).
	Consider drug pharmacokinetics and the need for repeat

<b>Pre-operative phase</b>	
	dosing.
	Consider the need for further antibiotic treatment in addition to prophylaxis.
	Inform the patient of any antibiotic use as soon as is practicable.
<b>Intra-operative phase</b>	
Hand decontamination	Ensure meticulous hand hygiene in all members of the operating team.
	Use a disposable brush & nail-pick for the first procedure of the list.
Incise drapes	If an incise drape is required use an iodophor-impregnated drape, unless the patient has an iodine allergy. Do not use non-impregnated incise drapes routinely.
Sterile gowns and gloves	The operating team should wear sterile gowns and gloves in the operating theatre during the operation.
	Consider double-gloving if high risk of perforation and/or contamination.
Antiseptic skin preparation	Use povidone–iodine or chlorhexidine skin preparation immediately prior to incision.
	If diathermy is to be used, ensure that antiseptic skin preparations are dried by evaporation and that pooling of alcohol-based preparations is avoided.
Diathermy	Do not use diathermy for skin incision.
Maintaining patient homeostasis	Maintain patient temperature in line with ‘Inadvertent perioperative hypothermia’ (NICE clinical guideline 65).
	Maintain optimal oxygenation during surgery. In major

<b>Pre-operative phase</b>	
	surgery and recovery aim for >95% saturation. Maintain adequate perfusion during surgery.
	Do not give insulin routinely to patients who do not have diabetes to optimize blood glucose postoperatively as a means of reducing the risk of surgical-site infection.
Wound irrigation and intracavity lavage	Do not use wound irrigation or intracavity lavage to reduce the risk of surgical-site infection.
Antiseptic and antimicrobial agents before wound closure	Do not use intraoperative skin re-disinfection or topical cefotaxime in abdominal surgery to reduce the risk of surgical-site infection.
Wound dressings	Cover surgical incisions with an appropriate interactive dressing at the end of the operation.
<b>Postoperative phase</b>	
Changing dressings	Use an aseptic non-touch technique for changing or removing surgical wound dressings.
Post operative cleansing	Use sterile saline for wound cleansing up to 48 h after surgery.
	Advise patients that they may shower safely 48 h after surgery.
	Use tap water for wound cleansing after 48 h if the surgical wound has separated or has been surgically opened to drain pus.
Topical antimicrobial agents for wound healing by primary intention	Do not use topical antimicrobial agents for surgical wounds that are healing with the primary intention to reduce the risk of surgical-site infection.
Dressings for wound healing by secondary intention	Do not use Eusol and gauze, moist cotton gauze or mercuric antiseptic solutions to manage surgical wounds

<b>Pre-operative phase</b>	
	that are healing by secondary intention.
	Refer to a tissue viability nurse (or another healthcare professional with tissue viability expertise) for advice on appropriate dressings for the management of surgical wounds that are healing by secondary intention.
Antibiotic treatment of surgical-site infection and treatment failure (also see main text)	When surgical-site infection is suspected (i.e. cellulitis), either de novo or because of treatment failure, give the patient an antibiotic that covers the likely causative organisms. Consider local resistance patterns and the results of microbiological tests in choosing an antibiotic.
Debridement	Do not use Eusol and gauze, or dextranomer or enzymatic treatments for debridement in the management of surgical-site infection.

### **1.2.2. The causes affecting current treatment and roles of antibiotic resistance bacteria**

In addition to antibiotics, the use of other agents-namely, the readily available surface antibacterials-aimed at eliminating germs is growing. Still, this antibiotic-resistant bacterial cell affects the current system of treatment. As mentioned in the above table, numerous causes such as hygiene, different diseases, antibiotics, clean dressing, and regular baths with antiseptics are some of the important and common measures. Antibiotic resistance is mostly caused by the ability of resistance genes to proliferate to other bacteria via a variety of genetic routes. Antimicrobial therapy can lead to the selection of resistant forms, and antibiotic residues can linger in the environment for a considerable amount of time following treatment. Because of the emergency it holds, the production of antibiotics has expanded dramatically during the previous several years. However during the past few decades, the number of bacterial strains resistant to antibiotics has also been rising quickly (Levy 2002).

### **1.3. Nanoparticles with anti-bacterial properties**

One possible method for treating infections brought on by organisms resistant to several drugs is the use of nanoparticles (NPs). To evade the antibacterial activity of antimicrobial agents, NPs have antimicrobial activity that can overcome common resistance mechanisms, such as enzyme inactivation, decreased cell permeability, modification of target sites/enzymes, and increased efflux through overexpression of efflux pumps (Lee *et al.* 2019). A lot of scientific and technical attention is currently being paid to research pertaining to nanomaterials and nanoparticles, such as metal oxides, because of their special qualities that make them useful for a variety of applications across several industries. Their quantum size effects are the characteristics that make materials at the nanoscale promising for a range of technical and medicinal uses (Gupta *et al.* 2017). The study of nanomaterials has attracted a lot of attention recently due to the potential for direct solar energy utilisation, ecological harm, contamination of the environment, and scarcity of resources (Tang *et al.* 2019).

### **1.3.1. Different research using different nanoparticle and their applications**

A multitude of novel strategies are being employed by research to synthesise nanoparticles or nanomaterials for application in many biological domains. Several nanoparticles have been explored and are now being investigated further for potential applications in the biomedical sector. These include silver nanoparticles, zinc oxide nanoparticles, titanium oxide/gold nanoparticles, and others. Research has demonstrated the effectiveness of nanoparticles as a therapy for *S. aureus* infections both in vivo and in vitro, especially those containing an iron oxide component or an acidic capping agent. (Juncker *et al.* 2021). Numerous investigations showed the effective antibacterial qualities of synthesised silver nanoparticles against a range of drug-resistant bacteria that cause surgical site and wound infections (Kasithevar *et al.* 2017). Moreover, artificially produced clarithromycin nanoparticles have demonstrated strong antibacterial activity against *S. aureus* and have potential use as a drug delivery mechanism (Mohammadi *et al.* 2011). Furthermore, against *S. aureus*, ZnO-coated textiles with multipedal shapes have demonstrated outstanding antibacterial activity (Sricharussin *et al.* 2011). Zn<sup>2+</sup>-doped CdO nanostructures have also been shown in studies to have outstanding antibacterial activity against a variety of microorganisms (Gupta *et al.* 2017). Numerous investigations have also demonstrated the role of TiO<sub>2</sub>/Au nanoparticles in inhibiting *Escherichia coli* growth (*E. coli*) (Tang *et al.* 2019).

### 1.3.2. Limitations of nanoparticle-based treatments

After any surgical operation, the most frequent infection that develops is SSI. The incidence of SSI may result in worse life outcomes, longer hospital stays that are expensive, higher death rates, etc. Thus, one of the most crucial therapeutic objectives is to determine and put into practise evidence-based tactics intended to reduce SSI. Antibiotic selection, timing, and process optimisation have been the primary areas of previous studies (Anthony 2011). Preoperative and intraoperative measures should be done for the patient's health, as studies have demonstrated. It is also crucial to utilise wound barriers to prevent infection of the surgical wound during the surgery. Even though every safety precaution exists, not all of them have been extensively incorporated into clinical practise (Anthony 2011).

The bacteria that cause SSIs are known to have multiple strains within each species, and these strains vary in their characteristics. Many of the bacteria and their stains exhibit varying degrees of antibiotic resistance. Furthermore, evaluating a molecule's antibacterial properties cannot be done using a single, approved technique or media. In addition, certain research has found that treatments based on nanoparticles may be dangerous in both in vitro and in vivo settings (Duval *et al.*, 2019). Such as, silver nanoparticles are potentially toxic in large amounts, hence the use of a low concentration is preferred (Reithofer *et al.* 2014).

## 1.4. AIE- Aggregation induced emission

In this work, aggregation-induced emission luminogens (AIEgens) have been developed as a better technique to combat all the limitations and avoid SSI, which causes bacteria to thrive at the site of the incision. When BZ Tang and colleagues initially used the term "AIE" in 2001, it gained a lot of interest from several researchers throughout past years. According to research, when water is added to the AIEgen, which is a solution of 1-methyl-1,2,3,4,5-pentaphenylsilole in ethanol, it exhibits a substantial rise in fluorescence and precipitates, producing mostly amorphous organic nanoparticles that resemble inorganic semiconductor quantum dots. Conventional organic fluorescent compounds, such as uranine and perylene, exhibit emission self-quenching in the solid state or at high solution concentrations because of the conjugated groups'  $\pi$ - $\pi$  stacking, which is called aggregation-caused quenching (ACQ) phenomenon. On the other hand, luminous substances have AIE properties that overcome this ACQ phenomenon (Zuo *et al.* 2023). The stiffness of the chromophore in the aggregation

state prevented the otherwise rapid non-radiative decay of the photoexcited dyes in solution, which is important to understand the phenomenon. This was the reason behind the fluorescence enhancement, not the interaction between the dye molecules in the aggregation state (Würthner 2020).

#### **1.4.1. Properties of AIEgen**

When the fluorophore aggregation or binding to a biomacromolecule occurs, AIEgens often form a stiff structure with intermolecular interaction. Traditional organic dyes typically exhibit degraded emissions at high concentrations due to ACQ effects. Nevertheless, AIEgens overcome the quenching effect and emerge as a competitive contender for application in bacterial imaging due to its possible targeting and signalling features. Due to its exceptional photo-stability and biocompatibility, it is also utilised for bacterial staining and bacterial viability assays (Zhang et al. 2021). A thorough method for creating bioimaging materials now involves decorating AIE moieties onto polymer backbones.

Tetraphenylethene (TPE), neutral molecules TPAQ and CN-TPAQ, and their cationic equivalents TPAQ-PF<sub>6</sub> and CN-TPAQ-PF<sub>6</sub> are only a few of the AIEgens that researchers are working with in diverse fields. Each of the AIEgens listed above has a hydrophobic nature. Currently, AIE moieties are being converted onto polymer backbones to be delivered in several ways, conjugating with hydrophilic polymers, or encapsulating them with amphiphilic polymers to generate products that are both water-soluble and can target and circulate for an extended period. It is feasible to get improved hydrophilicity and externally triggered bioimaging by employing flexible polymers conjugated with AIEgens. The ability of cationic molecules to absorb negatively charged bacterial outer envelopes and then introduce hydrophobic moieties to rupture the membrane is one of their excellent antibacterial capabilities. Additionally, theranostic materials that serve both therapeutic and diagnostic objectives can be made from amine-containing AIEgens (Zhang et al. 2021).

#### **1.4.2. Research related to antibacterial AIEgens**

Many studies on AIEgens, conjugated AIEgens, and other materials have been conducted. The field of AIE macromolecular materials has gained attention recently due to its potential as an antibacterial solution. These materials present novel therapeutic approaches for treating

infections resistant to drugs, biofilms in bacterial infections, real-time monitoring, and targeted bacterial killing. The high brightness, stability, excellent bacterial targeting, tracking, distinguishing, wound-repairing, and biological safety of AIEgens have made them extremely useful in biological applications (Zuo *et al.* 2023). AIE-based nanostructures are gradually being employed in various research such as drug discovery, food industry, anti-bacterial drug production, wound treatment etc.

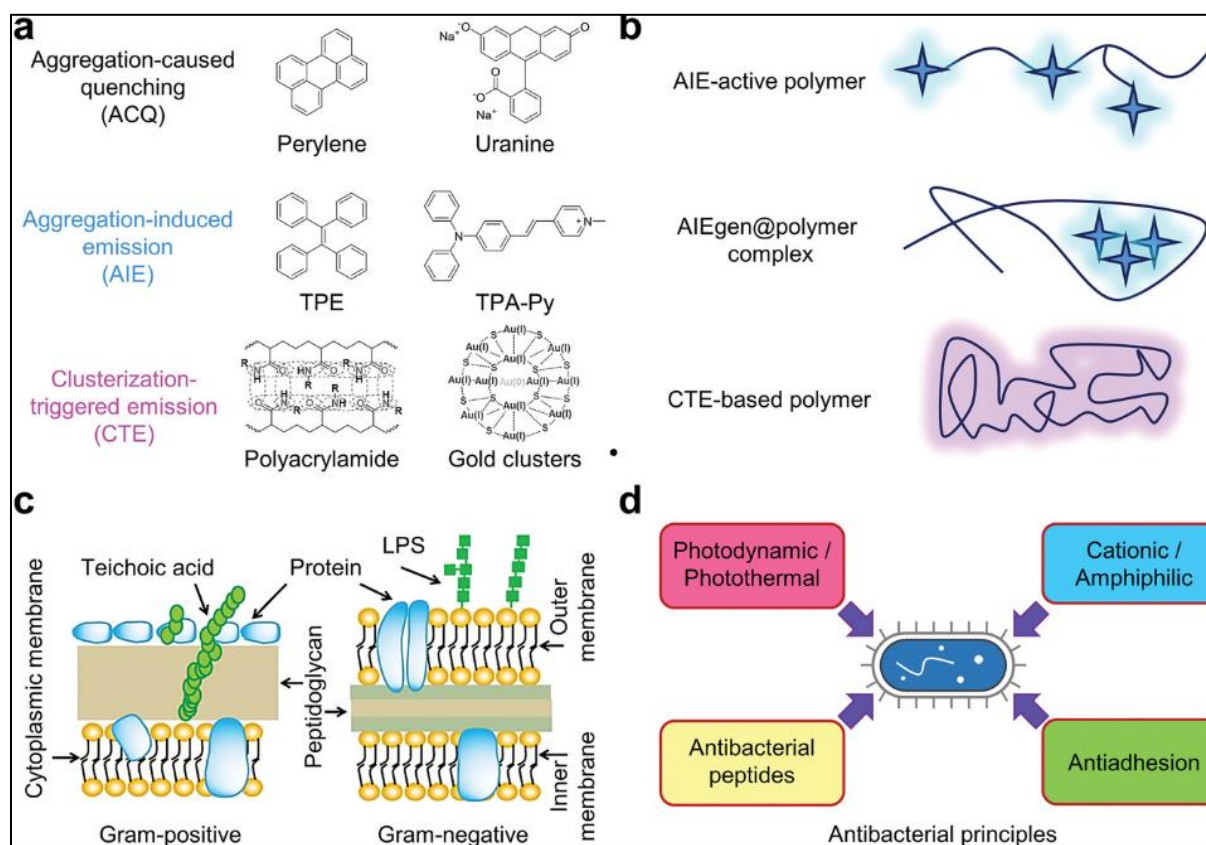


Figure 5: (a) Examples showing aggregation-caused quenching (ACQ), aggregation-induced emission (AIE), and clusterization-triggered emission (CTE). Reproduced with permission. (b) AIE macromolecular material classification for treatment against bacteria. (c) The schematic structure for the outer cell membrane of Gram-negative and Gram-positive. (d) Antibacterial principles of the AIE macromolecule (Zuo *et al.* 2023).

Various settings, including AIE-active polymers, AIEgen polymer complexes, and clusterisation-triggered emission (CTE), can make use of each AIEgen. By adding self-assembled berberine-cinnamic acid nanoparticles (BCNPs), which showed potent antibacterial activity against both *E. coli* and *S. aureus*, biodegradable and antibacterial

packaging films were successfully created for the food market by monitoring the ROS generation and fluorescence spectra of films under white light (Ma *et al.* 2022).

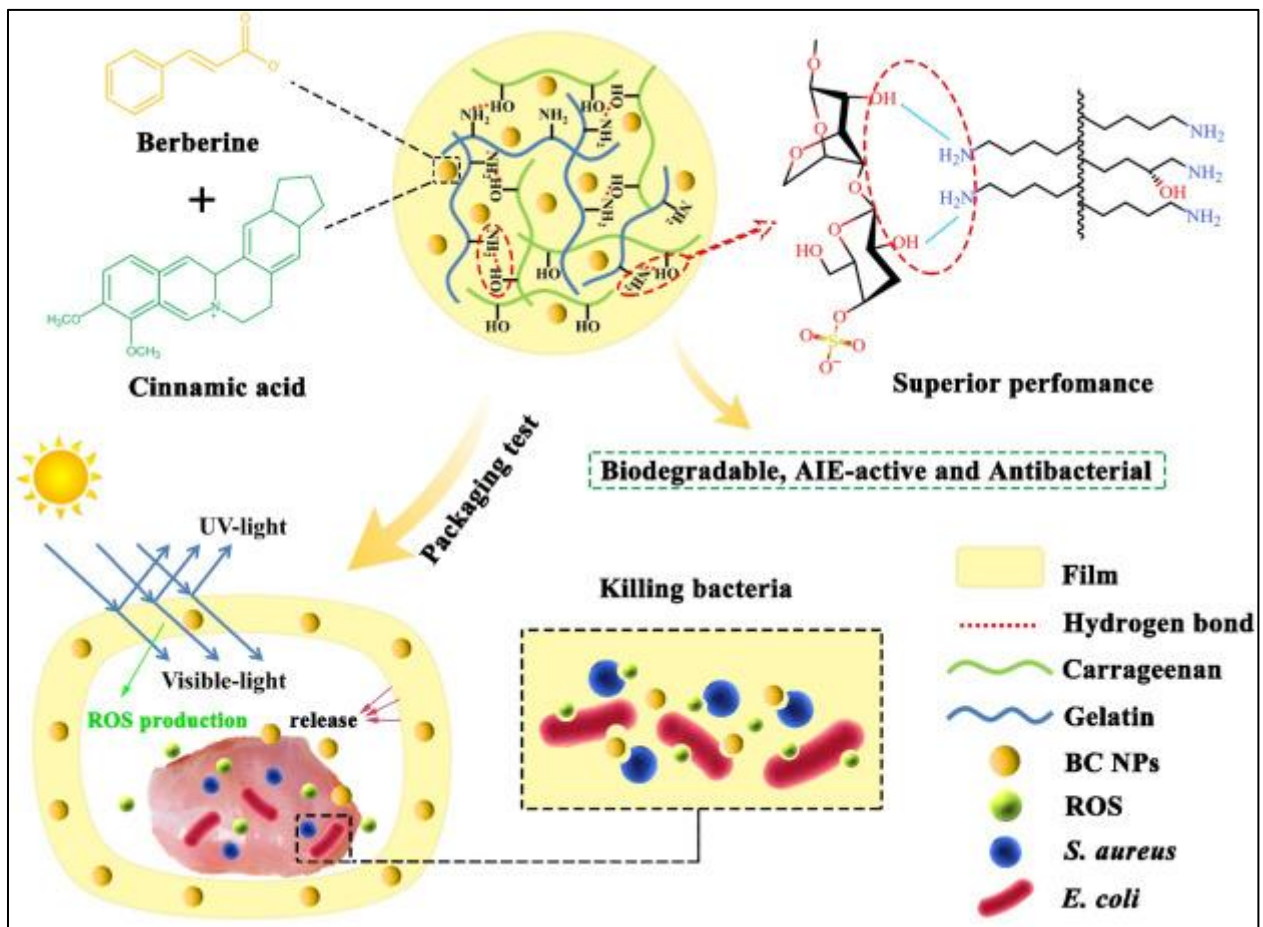


Figure 6: Schematic illustration of films containing AIE-active berberine-based nanoparticles with nanocomposite sustainable which shows anti-bacterial properties in food packaging (Ma *et al.* 2022).

Some studies have developed alternative methods to study the interactions between an AMP coated with AIEgen and bacterial membranes (Li *et al.* 2017). Also, AIEgen-based nanostructures can help with drug screening procedures, offer comprehensive recommendations for formulation optimisation, and support the investigation of pharmacological mechanisms as well as serve as well-known fluorescent agents for real-time and dynamic monitoring (Zhang *et al.* 2018).

## 1.5. Plasma polymerisation

The healthcare industry has seen a significant surge in the use of biomaterials due to their exceptional qualities and range of applications, which include prosthetics, diagnostics, imaging and sensing devices, and drug delivery systems. To enhance their inherent ability to regulate the reaction of foreign bodies and enhance the adhesion of various substances and molecules to the surface, much research has been conducted on the development of surface modifications for biomaterials (Dabare *et al.* 2022). Chemical grafting, self-assembled monolayers, or plasma polymerisation are simple methods for introducing diverse chemical functionalities that are physiologically plentiful and may be used to modify these biomaterial surfaces. These techniques can be used to maximise the adhesion or interaction of various molecules. The immunological response that follows cell attachment is triggered by surface chemistry, which also involves protein absorption. Based on the spectrum of surface charge and wettability states, four distinct surface chemical functions were created, i.e., oxazoline, amine, carboxylic, and methyl.

2-methyl-2-oxazoline (pOX) coatings deposited by plasma were selected due to their superior antibiofilm characteristics, elevated biocompatibility, and ability to mitigate inflammatory reactions. Moreover, the coating is appealing in a variety of biological applications because the oxazoline rings that are preserved at the surface enable the covalent attachment of molecules and nanoparticles with carboxylic acid functional groups. The use of plasma polymerised allylamine (AA) was made since these films are known to improve cellular adhesion and impart retention of amine functional groups. It is well known that coatings made of plasma polymers produced from acrylic acid (AC) promote cell migration and proliferation. To create hydrophobic coatings that add a second wetting state, 1,7-octadiene (OD) plasma polymerisation was employed. Flexibility and adaptability are provided by plasma polymerisation, which enables the single-step fabrication of pinhole-free nano-thin film coatings on any substrate material without the need for prior modification. Because this method of plasma polymerisation is substrate independent and act as an intermediate, it may be applied to a variety of biomaterial substances and enable the deposition of functional coatings for a range of biomedical purposes. These various surface chemical functions can be coated using plasma polymerisation under certain conditions using a plasma reactor and then placed on a substrate (Dabare *et al.* 2022).

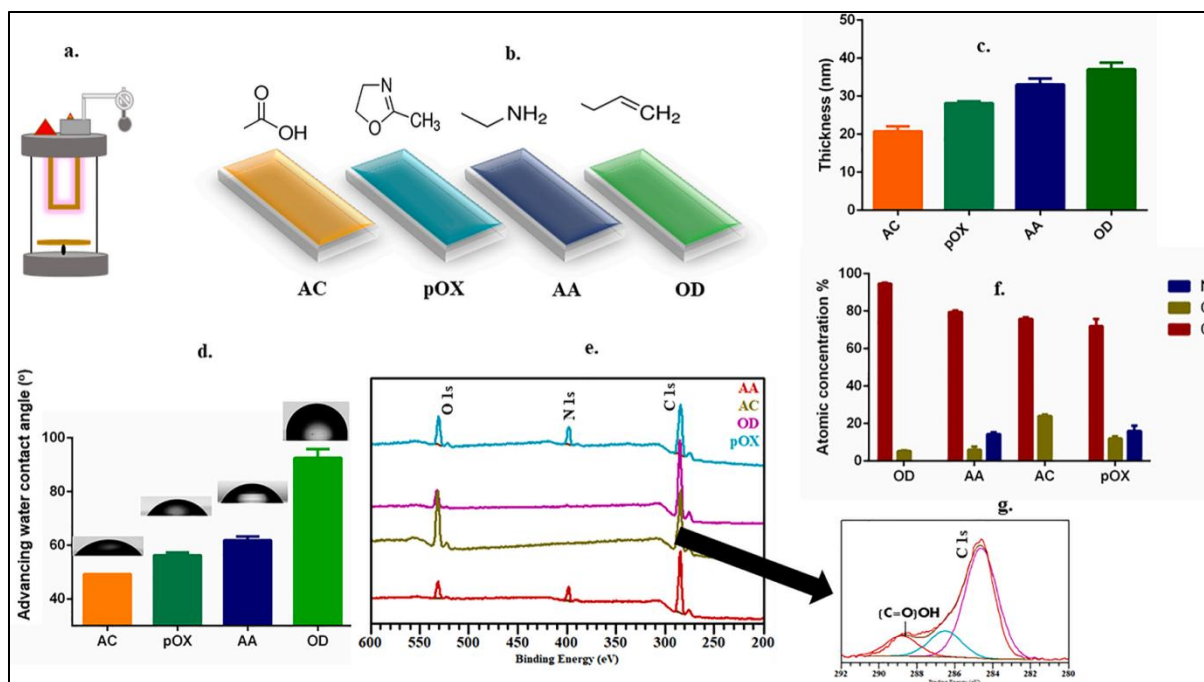


Figure 7: Schematic illustration of surface coating with plasma polymerisation technique and their characterization. (a) Plasma reactor used for surface modification, (b) molecular structure of chemical functionalities or monomer that have used for plasma deposition, (c) thickness comparison of all the precursors being used for plasma coating using spectroscopic ellipsometer, (d) comparison of water contact angle/wettability using ImageJ software, (e) XPS survey for functional group detection, (f) atomic concentration of an element on coated surfaces, and (g) high-resolution XPS for AC with retention of COOH group (Dabare *et al.* 2022).

### 1.5.1. Properties of plasma polymerisation

In essence, partly ionised gas influences the creation of a polymeric coating on surfaces during plasma polymerisation. Under various circumstances, the organic substance is deposited as a thin layer on the substrate due to the phenomenon known as electric discharge. The monomer's atoms seldom rearrange inside the molecule throughout the polymerisation process (Yasuda 2012). The introduction of organic vapour into an electric glow discharge of a gas, such as He, Ar, etc., causes the polymeric compounds to accumulate on top of the reactor's substrates (Yasuda & Gazicki 1982). Plasma-treated nano-thin substrates have superior biocompatibility as compared to traditional biomaterials. Furthermore, altering the

surface characteristics of a material without affecting its bulk qualities is made possible by thin coatings applied to substrates.

Numerous special benefits of the plasma polymerisation process include the ability to generate extremely thin films on a variety of substrates, strong attachment or binding to the substrate material, and the potential for long-lasting and chemically stable coatings (Yasuda & Gazicki 1982). Its applications span a wide range of fields, including biomedical, biomaterials research, textile manufacturing, antimicrobial research, etc. It is possible to coat any type of substrate with a thin coating of plasma monomer compounds by using electrical monomer discharges. The dry and environmentally friendly plasma-coated substrates may be utilised in the textile sector in place of wet chemical processes in a way that is more economical with the surface modification process (Hegemann 2006). Applications for the plasma polymerisation process include tissue engineering, cell-surface interactions, and anti-fouling (Bhatt *et al.* 2015).

## **1.6. Hypothesis and aims**

### **1.6.1. Hypothesis**

AIEgen immobilized plasma functionalized surfaces will generate ROS and eradicate pathogenic bacteria for promoting the healing of SSIs.

### **1.6.2. Aims**

Aim 1. Immobilize selected AIEgens on plasma polymerised surface.

Aim 2. Characterize plasma functionalized surface immobilized with AIEgen.

Aim 3. Determine antibacterial activities

Aim 4. Determine cytotoxicity and ROS generation abilities.

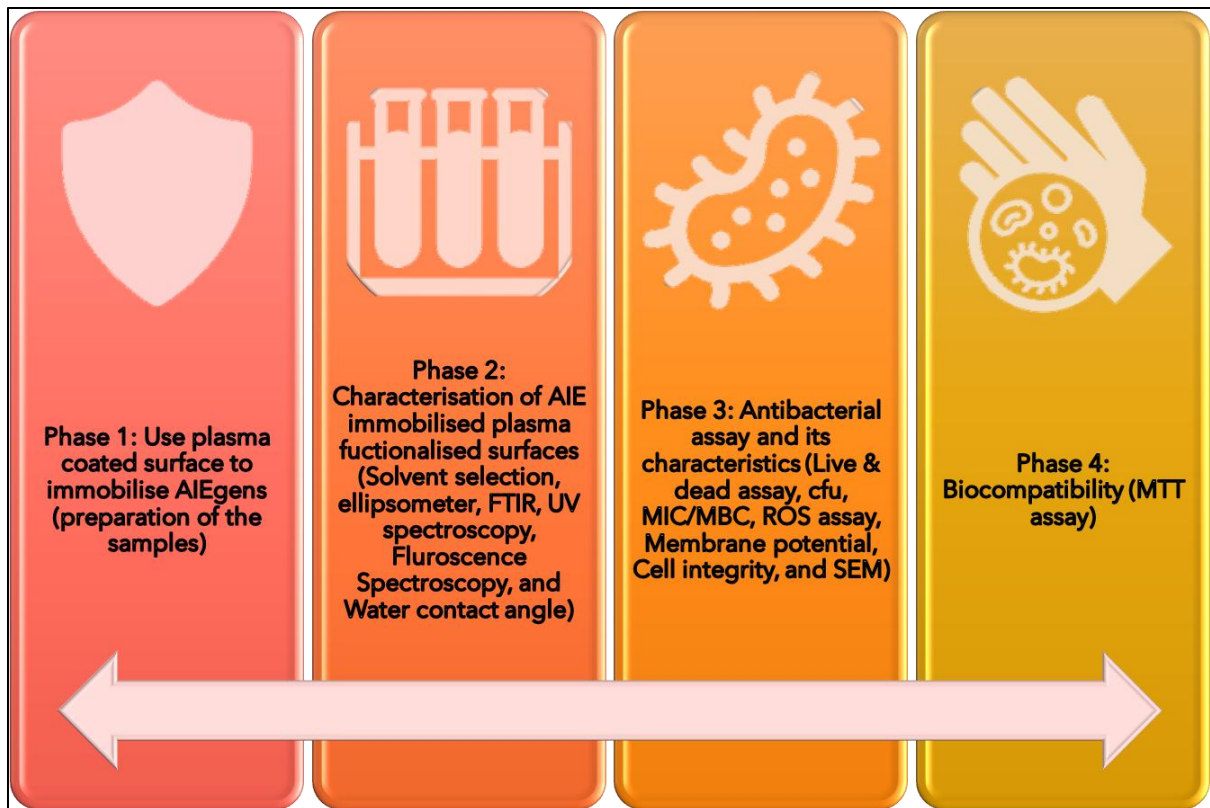


Figure 8: The list of phases that needed to be obtained for the research objectives.

# CHAPTER 2: METHODOLOGY

## 2.1. Materials

In regard to all experiments, we have used many facilities including custom-built bell-chamber plasma reactor, FEI Inspect F50 Field Emission SEM, USA; photography ellipsometer SENresearch, SENTECH, Germany; Digital Ultrasonic Cleaners Cleaning Equipment Bath Tank w/Timer Heated; BioTek Synergy HTX Multimode Reader; Fluorescence Microscope Olympus IX83, Light Microscopy; confocal laser scanning microscope (ZEISS LSM 880, Germany); Invitrogen™ Countess™ 3 Automated Cell Counter (USA).

The AIEgens used here were purchased from Aggregation Induced Emission Institute, South China University of Technology, China. Ultrahigh purity water was gained from a Milli Q system (Millipore Milli-Q Academic, USA), which was used to prepare the solution and washing steps. 2-methyl-2-oxazoline, silicon wafer (1 cm<sup>2</sup>), and some common organic solvents (ethanol, acetone, water, dimethyl sulfoxide (DMSO), and phosphate buffer saline (PBS) were purchased from Sigma-Aldrich, Australia and used without further purification. For the biological studies, (TSB) agar from Sigma-Aldrich Australia, common solvents from Sigma-Aldrich Australia, MTT solution from Sigma-Aldrich Australia along with different dyes for bacterial staining.

## 2.2. Methods

### 2.2.1. Preparation of AIEgen immobilised plasma polymerised surfaces

A cutting-edge method called plasma polymerisation makes it possible to apply a nanoscale coating to any kind of substrate material without first modifying its surface. Alternative processes, such as using silica for silanes or gold for thiols, require certain surface qualities to fabricate surface thin coatings (Vasilev *et al.* 2009). Because a wide range of monomers that are challenging to polymerise on a variety of substrates may be deposited, coatings made from plasma have the potential to have an extremely diverse range of physical and chemical characteristics. In low-pressure procedures, the introduction of all these monomers into the plasma chamber occurs either through the vacuum or, in atmospheric pressure discharges,

through the carrier gas in a volatile state. Additionally, by using the plasma polymerisation approach, the monomer deposition parameters, i.e., time, power, and pressure may be adjusted to regulate the characteristics of the plasma film (Vasilev 2013).

Two distinct types of monomers were used, depending on the charges on the AIEgens that were employed to immobilise the plasma coated surfaces. The precursor for 2-methyl-2-oxazoline (POx) and acrylic acid (AC) was plasma polymerised using a specially designed cylindrical reactor with an internal U-shaped top electrode and a circular bottom electrode. This process allowed the precursor to be deposited as a thin nanolayer on a variety of materials. When the substrates were positioned on top of the circular bottom electrode, a 13.56 MHz generator producing plasma was used, with settings for 10 and 20 watts of power and a monomer pressure of 0.2 Torr. It was discovered that the plasma-deposited POx and AC film preserved whole oxazoline rings and carboxyl (-COOH) groups on their surface, which go on to have several biological uses when they attach to proteins, antibodies, various antibacterial compounds, ligands, or particles (Vasilev *et al.* 2009).

### **2.2.2. Experimental Details**

The samples (1 cm<sup>2</sup> silicon wafer), which were thoroughly cleaned with acetone and ethanol and dried with nitrogen flow, are coated with a plasma polymerisation solution using a specially constructed connected bell chamber reactor. The precursor of 2-methyl-2-oxazoline/acrylic acid was added to the monomer flask using a needle valve when the operating plasma reactor achieved a base pressure of  $2.3 \times 10^{-2}$  mbar. By using the freeze-thaw process, the precursor flask was ignited and the pressure inside the chamber was allowed to stabilise. Utilising RF power, the plasma was ignited with 50 W and 100 W for POx and AC, respectively, for two minutes each, throughout the monomer deposition process, which included a working pressure of  $1.3 \times 10^{-1}$  mbar. The samples were vacuum sealed until further use.

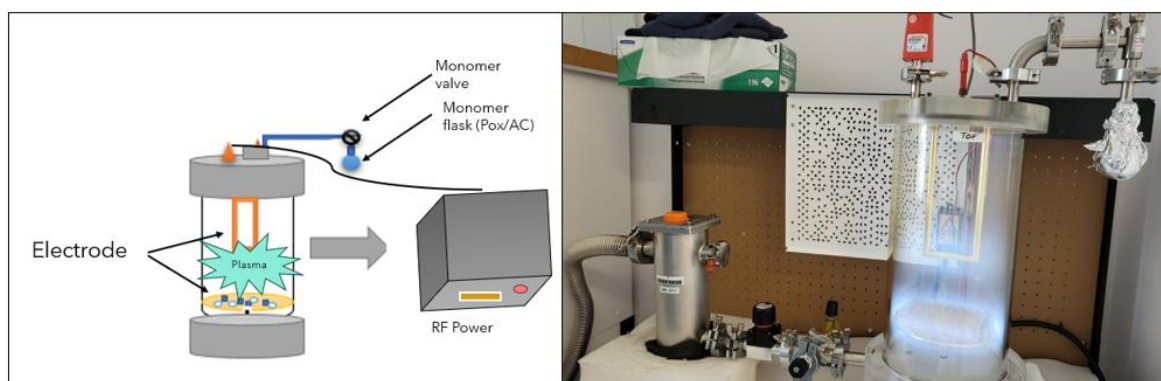


Figure 9: The custom-built capacitively coupled bell chamber with a top U-shaped electrode and a round bottom electrode to hold the samples. The pressure of the valve is maintained by RF power.

### 2.3. Characterisation

Numerous aspects related to the surface and the chemical structure employed in plasma deposition are included in the characterisation of plasma-coated surfaces. We selected two distinct precursors with negative surface charges for this investigation since the AIEgens we have chosen are positively charged. The procedure of plasma deposition makes it possible to preserve whole oxazoline rings on the coated surface, something that is often accomplished by traditional ring openings. Even in the absence of a catalyst, these rings react very quickly with carboxylic groups to create covalent bonds that bind biomolecules, ligands, and nanoparticles containing carboxyl acid groups that have a negative surface charge. These compounds have futuristic uses in a variety of fields. The ability of oxazoline-derived plasma polymer coatings to effectively modify immune responses was further established by the decrease of pro-inflammatory cytokine release, the modification of the protein corona that forms on the surface of biomaterials, and the suppression of biofilm formation (Vasilev 2019). Because the carboxyl acid functional groups are retained, plasma polymers based on acrylic acid (AC) have a negative surface charge throughout a broad pH range (Dabare *et al.* 2022). The acrylic acid-coated surfaces exhibit improved dirt resistance, wettability, dyeability, and reduced ageing when exposed to non-polymerized gases ( $O_2$ ,  $H_2O$ , Ar, and air). Furthermore, surfaces coated in acrylic acid are unable to improve cell adherence (Hegemann 2006).

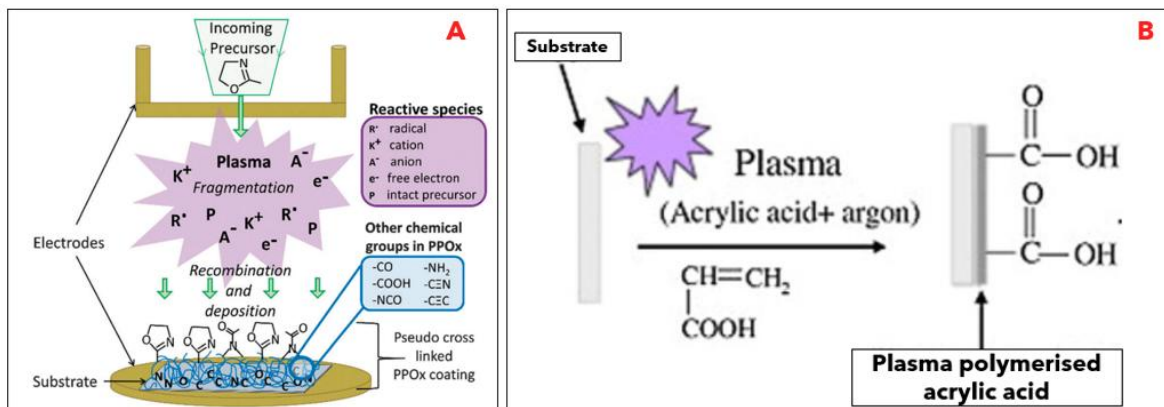


Figure 10: (A) Summary of the plasma polymerisation mechanism and chemistry of plasma deposited 2-methyl-2-oxazoline (MacGregor et al. 2015) and (B) acrylic acid coatings on substrates (Bitar *et al.* 2018).

### 2.3.1. Ellipsometer observation for stability of plasma polymerised surfaces

The most non-destructive optical reflectance measurement for thin film is ellipsometry. Ellipsometers are capable of providing information on the composition, thickness, and conductivity of the coated materials that are being observed, among other optical qualities. The amplitude ratio of two perpendicularly polarised beams, where the incidence angle may vary, is measured following the principle of change in the polarisation of light reflected off the sample surface. Given that it contains the two-measurement ratio of the perpendicular beam, the outcome is highly precise and devoid of variability. By fitting the measured data to a physical model of the layer, the thickness of the layers and the absorption coefficient were ascertained (Tilli *et al.* 2009).

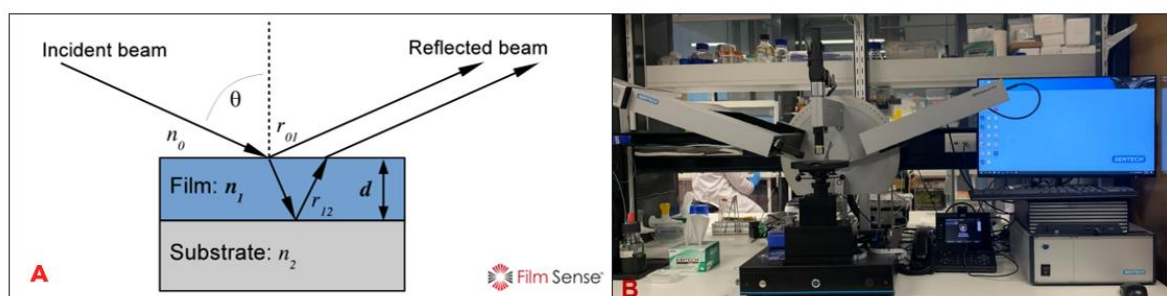


Figure 11: The properties of Ellipsometer (A) the surface of substrates when film strikes with incident beam and the reflected beam is observed (Ellipsometry Technology Information - Film Sense Ellipsometer 2023). (B) Ellipsometer system image.

The photographic ellipsometer from SENresearch, SENTECH, Germany was used to measure the thickness of the silicon wafer coated layer with plasma. The 2 nm SiO<sub>2</sub> layer on the silicon wafer substrate was removed, and SpectraRay/4 software was used to evaluate the layer's data. The substrates were positioned on the substrate platform, and the ellipsometer's operating settings were configured.

### 2.3.2. Immobilisation of the surfaces with AIEgen

In the traditional polymerisation process, the oxazoline ring opening is the most crucial step. The open oxazoline ring plays an important role in acting as a reactive agent to immobilise compounds and antibiotics for a variety of applications (MacGregor *et al.* 2015). The oxazoline ring reacts with carboxylic acid functionalities to generate a covalent amide-ester link (Macgregor-Ramiasa *et al.*, 2015). Two positively charged AIEgens (TPAQ-PF<sub>6</sub> (AIE1) and CN-TPAQ-PF<sub>6</sub> (AIE2)) are used in this work. and as they share a positively charged nitrogen group, the nucleophilic charge with higher density of electron from POx might create electrostatic binding. An additional nitrile group containing higher electron density might be drawn to the partial positive charge of carbon after the opening of oxazoline ring to form electrostatic bond.

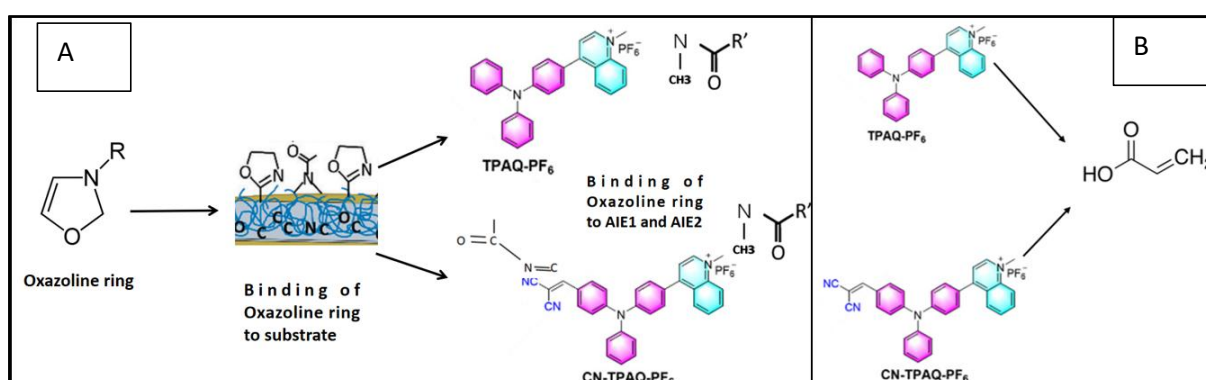


Figure 12: Illustration of (A) electrostatic binding of the nucleophilic site of the POx to the positively charged site of AIEgen (AIE1 and AIE2) where pOX surfaces containing intact

oxazoline ring and (B) negatively charged carboxylic group of acrylic acid (AC) to the AIEgen.

The AC (acrylic acid) also consists of carboxylic groups which can react to substrate even without any catalyst and forms covalent bond with biomolecules, ligands and nanoparticles containing carboxyl acid groups with a negative surface charge which further has many applications in various field. As the surface is negatively charged, a electrostatic force can be created between the surface and the positive site of the AIEgens (Ruvini L Dabare *et al.* 2022).

For each, distinct concentrations of AIEgen solutions (TPAQ-PF6 & CN-TPAQ-PF6) were created. Each AIE solution's initial concentration (A1b & A2b) contains 0.46 mg/mL of AIEgen in a 4:1 ratio dilution of ethanol and water, respectively. The AIEgen solutions' second concentrations (A1c & A2c) include 0.33 mg/mL of AIEgen in a 4:1 ethanol and water dilution ratio, respectively. These substrate coated with plasma polymerisation process immersed in the solution and left there for a full day of immobilisation. Following a 24-hour immobilisation period, the samples underwent a milli-Q water wash and a nitrogen gas flow drying process.

### 2.3.3. Water contact angle

The contact angle technique is a well-established approach to examine the surface characteristics of polymers. Surface wettability may be directly assessed using geometric measurements of the angle  $\theta$  that is created at the interface between the liquid, gas, and solid phases. This method is also useful for learning about the matrix's structure, particularly when working with substrates made of biopolymers. A mixed geometric/trigonometric technique was used to associate the contact angle (CA) analysis with image analysis (IA). The two main elements controlling the surface wetting process throughout the 60-second examination were spreading and absorption (Farris *et al.* 2011).

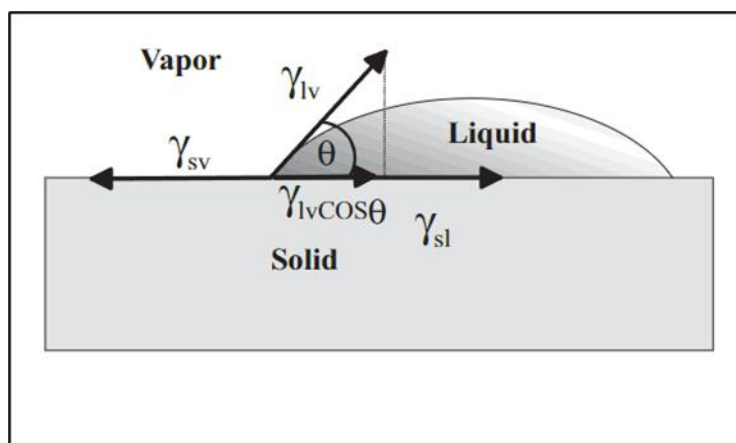


Figure 13: Illustration of water contact angle analysis around the water droplet on a solid (Rupp *et al.* 2002).

In this investigation, the AIEgen immobilised Pox coated substrates were employed as samples, and the light and camera attached to the designated stage were used. A water droplet of three to five microliters was deposited on top of the syringe held by the water contact angle instrument, and an image was taken with the camera and entered into the system. Additionally, the nature (hydrophobic/hydrophilic) of the functionalised surfaces was determined by measuring the contact angle using the drop snake analysis of ImageJ.

#### 2.3.4. FTIR micro spectroscopy

Fourier transform infrared (FTIR) spectroscopy is being used in many fields, including the examination of cells or tissues and tiny molecules or chemical complexes along with the functional groups. FTIR spectroscopy is also being used in biological protein studies. The molecular vibrations are investigated via infrared spectroscopy. The infrared absorption bands that are characteristic of functional groups can be linked to the basic vibrations of those groups. Depending on the kind of bonds and atoms involved, different areas will have different vibrational frequencies for a particular chemical group. The surroundings of the chemical groups inside these vibration areas affect their frequency (Berthomieu & Hienerwadel 2009).

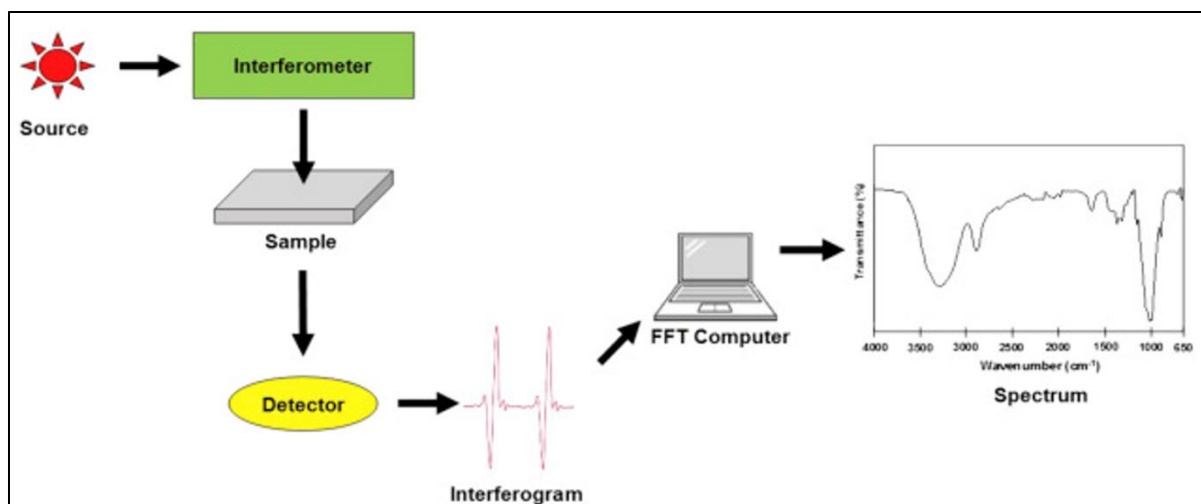


Figure 14: Schematic representation of the basic component of Fourier transform infrared (FTIR) spectroscopy, where the light beam passes through the sample and the emitted light is analysed to detect the vibration of the functional group from the infrared absorption band (Mohamed *et al.* 2017)

The blazing black-body source at the centre of the apparatus generates infrared light, which is then passed through an interferometer to encrypt the spectrum. Subsequently, the beam travels through the sample compartment, absorbing particular energy frequencies. The interferogram signals are then measured by the detector at all frequencies in terms of energy against time. The Fourier transform computer system may be used to extract the desired spectrum from the interferogram spectrum, which serves as the background reading for the instrument operation (Mohamed *et al.* 2017).

The AIEgen immobilised plasma polymerised surfaces/ potassium bromide surfaces were placed between two windows and arranged simultaneously were AIEgen-immobilised plasma polymerised substrates (transparent, i.e., coverslips) and potassium bromide disc. A Fourier transform computer system was used to evaluate the spectra of both AIEgen-immobilised and just plasma-treated samples.

### 2.3.5. UV-vis spectroscopy

As a spectrophotometric method for measuring light intensity in the UV (10–400 nm) and VIS (400–800 nm) areas as a function of wavelength, UV-VIS spectroscopy is regarded as

the oldest analytical technique. Based on the principle of light absorption, UV-VIS spectroscopy measures the amount of analyte present in a sample solution in direct proportion to the amount of light absorbed. The wavelength, expressed in nanometers (nm), of the radiation. After UV-VIS light is absorbed, a spectrum made up of organic, inorganic, biological, and medicinal components is created. This spectrum is produced from the interaction between the analyte and electromagnetic radiation (EMR) in the UV-VIS area. There are 3 types of energy levels present: electronic, vibrational, and rotational. In UV-VIS spectroscopy, radiation absorption takes place at the electronic energy levels (Akash & Rehman 2019).

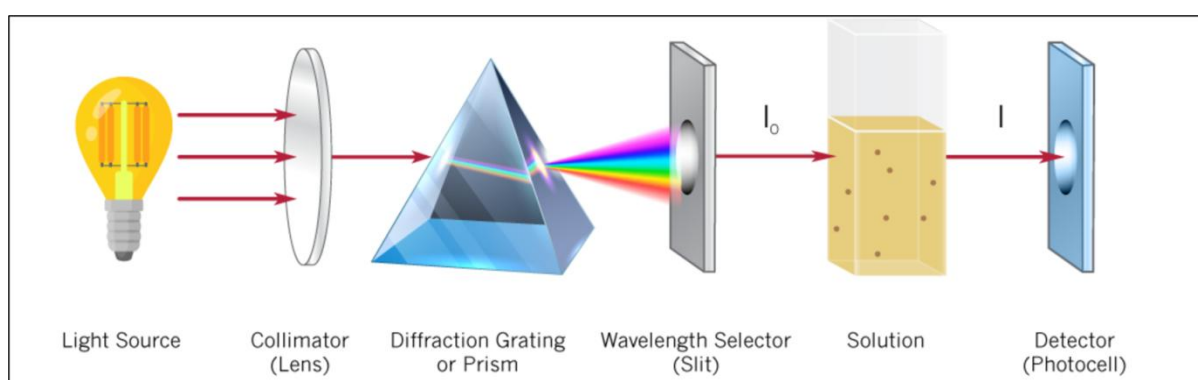


Figure 15: Illustrates the steps for the UV-Vis spectrometer function. The beam of light goes through the lens and prism which passes the solution. The beam that passes through the solution is then captured by the detector for further analysis (Implen, 2021)

Using the AIEgen-immobilised plasma coated substrate (with a transparent glass slide) the UV peak were observed to confirm the successful immobilisation of the AIE molecule. Further, shaking and sonicating were used to dissolve the plasma polymerised substrate that had been immobilised with AIEgen in acetonitrile. The immobilised AIEgen was diluted from the substrate and left for three distinct times-ten, twenty, and thirty minutes-in order to quantify the amount of AIEgen that bound to the surface of the plasma-coated surface. The findings were contrasted with concentration-known calibration standard curve data. Next, the cuvette containing the solution was put into the sample chamber. The adoption was assessed, and the data was examined in Microsoft Excel using UV-Vis spectroscopy scanning software.

### 2.3.6. Fluorescence microscopy

The technology known as fluorescence microscopy works by stimulating a fluorophore within a certain wavelength range (band) and then detecting the photons that are released using a camera system. The methods used for signal detection and specimen illumination vary. Photoluminescence is the name for the phenomenon where fluorescent molecules, also known as fluorophores or fluorochromes, can absorb and emit different parts of light, or photons (Dunst & Tomancak 2018). In addition to imaging molecular structure, sophisticated fluorescence microscopy may measure the physiological intactness of light-emitting molecules against a dark backdrop (Kubitscheck 2013).

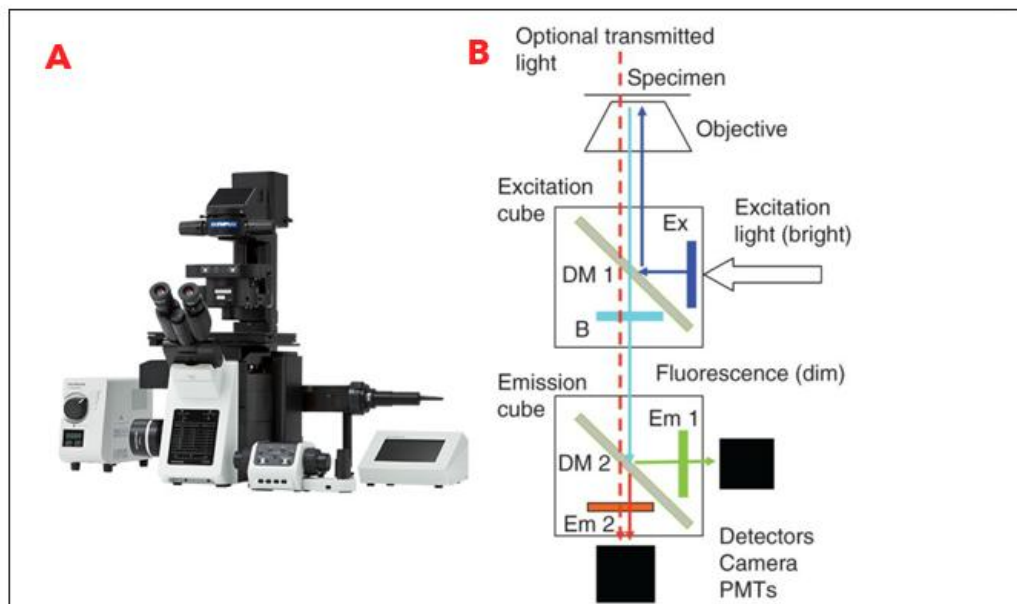


Figure 16: (A) Fluorescence Microscope, (B) excitation light is directed through substrate by dichroic mirror's light paths. The emission light gets separated by an emission cube. The emission of fluorescence splits into 2 beams through DM 2 and Em 1 and Em 2 are 2 designed emission filters that suppress light that is not needed. PMTs detect the fluorescence with long wavelength light used for a bright-field picture (Kubitscheck 2013).

The sample compartment was loaded with the AIEgen-immobilised plasma polymerised surface by modifying the suitable settings on the Olympus IX83 Inverted Fluorescence Microscope for Light Microscopy. The photographs were subsequently examined using

ImageJ to determine the binding intensity utilising pictures obtained from the cellSens Dimension programme in conjunction with a pE-800 LED light source that has eight independently controllable LEDs.

### 2.3.7. Live/dead staining

The live/dead staining method is a highly efficient approach for optical real-time measurement of the viability of bacteria. The fluorescence dye allows for the optical assessment of the bacterial membrane integrity, which is preserved in living bacteria and disrupted in dead ones. Green luminous fluorescent dye SYTO® 9 is often used to stain all live or destroyed bacteria, whereas harmless quantities of propidium iodide (PI) added to the culture medium are employed to stain dead bacteria. The excitation/emission maxima of STYO9 and PI were 480/500 and 490/635 nm. Fluorescence microscopy might be used to track this percentage of living and dead bacteria over time. In conclusion, the intensity diminishes when both fluorescence are combined for the staining assay. Green fluorescence indicates interacting living bacteria, whereas red fluorescence indicates destroyed bacteria (Vizcarra *et al.* 2013).

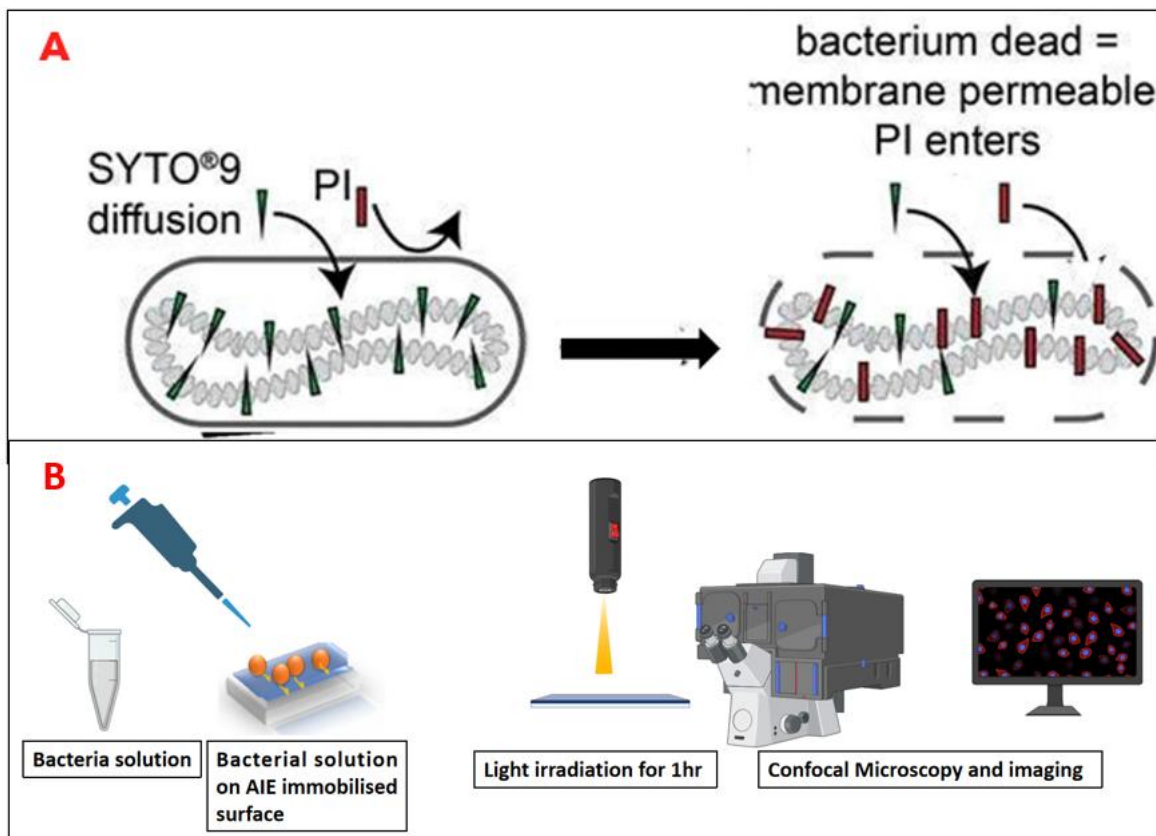


Figure 17:(A) Schematic illustration of bacterial staining for the cell viability assay where SYTO® 9 (green triangle) and propidium iodide (PI, red rectangle), Where SYTO® 9 stains the healthy bacterial DNA by diffusing into the bacterial cell with leaving green fluorescence to stains the healthy viable cell and PI stains the dead cell (Avalos Vizcarra *et al.* 2013). (B) Schematic illustration of the process of imaging the live/dead staining bacterial assay using a confocal microscope.

Here, *S. aureus* and *P. aeruginosa* were two of the strains of bacteria that were used. AIE1 (TPAQ-PF6) and AIE2 (CN-TPAQ-PF6) solutions immobilised on silicon wafers with POx coating were incubated with bacterial suspensions at different concentrations. In this experiment we prepared a set of bacterial strains which were exposed to light irradiation for one hour and 30 minutes ( $40 \text{ mW cm}^2$ ) without any disruption, while another set was exposed to light irradiation-free. Additionally, a confocal laser scanning microscope (ZEISS LSM 880, Germany) was used to image the samples stained using Syto9 and PI stains. Zen (Black Edition) was used to see and assess the pictures of the bacteria that were dyed red and green at their highest intensity. ImageJ software (NIH, USA) was then used to calculate the number of cells that were stained red and green by dividing the channel for green and red images.

### **2.3.8. Colony forming Unit**

The colony forming unit assay is carried out by serial dilution, incubation with an antibiotic substance, and counting the number of bacteria that survive after the mixture is plated on agar plates. The number of colony formations was then analysed to calculate the efficacy of the molecules against bacterial strains.(Putman *et al.* 2005).

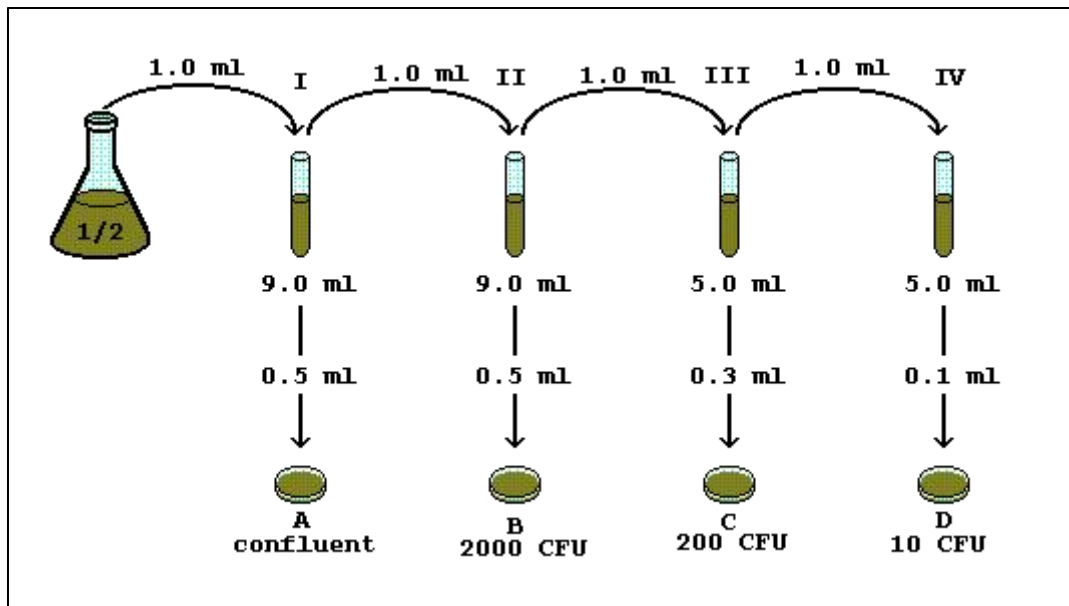


Figure 18: Use a serial dilution method for the colony-forming unit assay by dropping each fold of the dilution onto an agar plate to create bacterial colonies (Serial Dilution Problem Help n.d.)

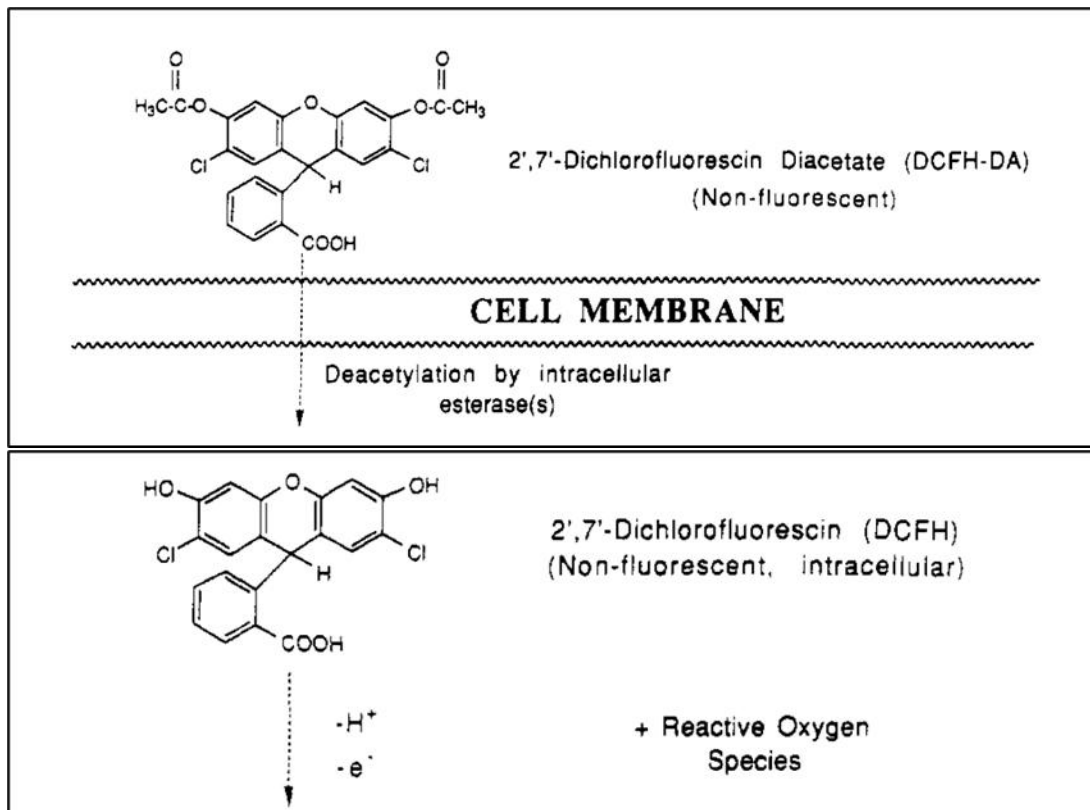
The TPAQ-PF6 and CN-TPAQ-PF6 immobilised plasma-coated samples were incubated with *S. aureus* and *P. aeruginosa* bacterial suspension ( $1 \times 10^8$  CFU mL<sup>-1</sup>, 10  $\mu$ l) for one hour at 37 °C. The samples were then treated in the dark or with white light irradiation (40 mW cm<sup>2</sup>, for one hour). After that, the suspension was shaken for five minutes and cleaned. The suspension was then serially diluted using the appropriate folds ( $10^4$ ,  $10^3$ ,  $10^2$ , and  $10^1$ ). Next, three parallel, independent plates from each group were incubated for 24 hours at 37 °C after 10  $\mu$ L of suspension was dropped onto an NB agar plate from each fold. Next, a count of the colony-forming units was made. The following formula is used to compute the number of surviving bacteria in suspension prior to dilution: C is equivalent to  $C_{\text{plate}} \times 10^A$ , where  $C_{\text{plate}}$  is the average number of colony-forming units on an agar plate, A is the diluted magnitude, and C is the actual CFU of the colony number prior to diluting.

$$\text{CFU/mL} = (\text{Number of colony formation} \times \text{Dilution factor}) / \text{Volume added (mL)}$$

### 2.3.9. ROS assay

Reactive oxygen species (ROS) are extremely reactive molecules and free radicals, which include both oxygen radicals (superoxide ( $\text{O}_2^{\cdot-}$ ), hydroxyl ( $\text{OH}^{\cdot}$ ), peroxy ( $\text{RO}_2^{\cdot}$ ), and hydroperoxyl ( $\text{HO}_2^{\cdot}$ ) radicals, as well as some nonradical oxidizing agents (hydrogen

peroxide ( $H_2O_2$ ), hypochlorous acid ( $HOCl$ ), and ozone ( $O_3$ )). ROS are also generated during regular metabolism and play a crucial role in gene expression, enzymatic processes, signal transduction, and mitochondrial electron transport (Bayr 2005). The ROS assay is a helpful approach for monitoring the quantity of ROS within cells to determine if bacterial mortality is due to oxidative stress. This investigation used the most widely used fluorescent probe, 2',7'-dichlorodihydrofluorescein (DCFH), which is readily incorporated into cells in its diacetate (DCFH-DA) form. Following its entry into the cell, DCFH-DA is deacetylated by cellular esterase to create a non-fluorescent chemical (DCFH). DCFH subsequently produces the fluorescent product 2',7'-dichlorofluorescein (DCF), which is detected by the detector in confocal laser scanning microscopy (LeBel et al. 1992).



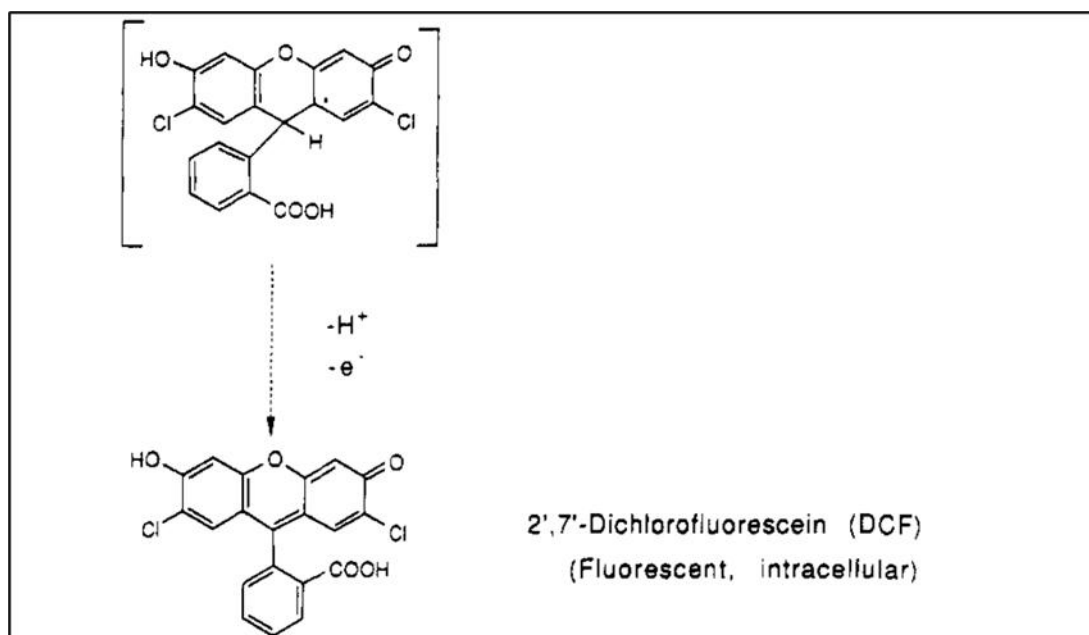


Figure 19: Suggested pathway through which DCFH-DA enters cells and over the membrane passage, DCFH-DA is de-esterified to DCFH, which generates ROS then oxidize to fluorescent DCF (LeBel *et al.* 1992)

To find intracellular ROS, the DCFDA / H<sub>2</sub>DCFDA - Cellular ROS Assay Kit (USA) was employed to evaluate oxidative stress-induced bacterial cell death. Using plain POx/uncoated silicon wafers as a negative control and bacteria grown on a silicon wafer as a positive control, the AIEgen solution (with minimum concentration i.e., c) immobilized on a silicon wafer with POx coating was soaked into the prepared bacterial solutions containing two strains, *S. aureus* and *P. aeruginosa*, with a one-hour light irradiation. Following a 45-minute staining period with 20 μM DCFDA, the samples were buffer-washed. Finally, using confocal laser microscopy (Zeiss LSM 880, Germany) with an excitation wavelength of 488 nm and an emission wavelength of 525 nm, the ROS level was examined. Software called ImageJ and Zen (Black Edition) were used to assess the photos for ROS intensity.

### 2.3.10. Membrane potential assay

The term "membrane potential" refers to the electric potential surrounding the cell membrane and provides the free energy necessary for the cell to perform all chemical and mechanical functions. A primary biological function of mitochondria is the generation of ATP, which is essential for the continuation of all productive cycles in the cell. It has an impact on bacterial

survival as well as metabolism, food absorption, and cell division. Antibiotics and other antibacterial chemicals can thus be used to target this location to destroy the bacterial cells (LeBel *et al.* 1992).

The AIEgen solution (with the minimum concentration) immobilised on silicon wafers polymerised with plasma was treated with *S. aureus* and *P. aeruginosa* using light irradiation for one hour. The uncoated samples containing bacterial strains and those lacking any strains were considered positive and negative controls. Following a PBS wash, the samples were stained for 10 minutes using the DiO/DPA membrane potential detection kit (Biotrum, USA). Green and red fluorescence was then measured using confocal laser microscopy (Zeiss LSM 880, Germany) at excitation/emission wavelengths of  $\lambda_{\text{abs}}/\lambda_{\text{em}} = 484/50$  nm for DiO and  $\lambda_{\text{abs}} = 406$  nm for DPA. Red and green fluorescence intensity was measured, and the ratio between them was computed, using Zen (Black Edition) and ImageJ software (NIH, USA) for image analysis.

### **2.3.11. Cell integrity**

The process of bacterial cell death involves several abrupt structural and morphological changes that compromise membrane integrity, harm cellular architecture, and release cellular contents into culture conditions. Consequently, the foundation of several cytotoxicity tests for determining cell membrane integrity is activity measurement in the extracellular environment (Cho *et al.* 2008).

Using two strains of *S. aureus* and *P. aeruginosa* and one hour of light irradiation, the AIEgen-(with minimum concentration) immobilised plasma polymerised silicon wafer was added to the bacterial solutions that had been prepared for the investigation. After that, they were exposed to the fluorescent dye Propidium Iodide (PI), and they were left for four hours to allow the dye to stain the bacterial strain and integrity of cell. In conclusion, the specimens were examined through confocal laser microscopy (Zeiss LSM 880, Germany) utilising an excitation wavelength of 488 nm and an emission wavelength of 525 nm.

### **2.3.12. Scanning electron microscope**

Powerful tools like scanning electron microscopy are utilised to identify different surface characteristics in materials. The sample, which is concentrated in a tiny area, is bombarded

by an electron beam from an electron gun in a scanning electron microscope, which causes the sample to travel randomly across each point of the object. The electron current exiting the item is gathered and examined in an electron detector to ascertain the material's composition and shape (Smith & Oatley, 1955). It is considered a useful technique for analysing both organic and inorganic materials at the nanoscale to microscale ( $\mu\text{m}$ ) scale, with high magnification ranging from 5x to 300,000 x (Mohammed, A., & Abdullah, A., 2018). Magnetic field lenses and metal slits within a vacuumed column concentrate and restrict the electrons that are released from the SEM to a monochromatic beam with a diameter of 100 nm or less (Akhtar *et al.*, 2018). The generated signals provide information on morphology, composition, topography, grain orientation, and crystallographic structure, among other aspects of the material. Topography refers to surface characteristics like texture, smoothness, or roughness, whereas morphology deals with the sample's size and form (Akhtar *et al.*, 2018).

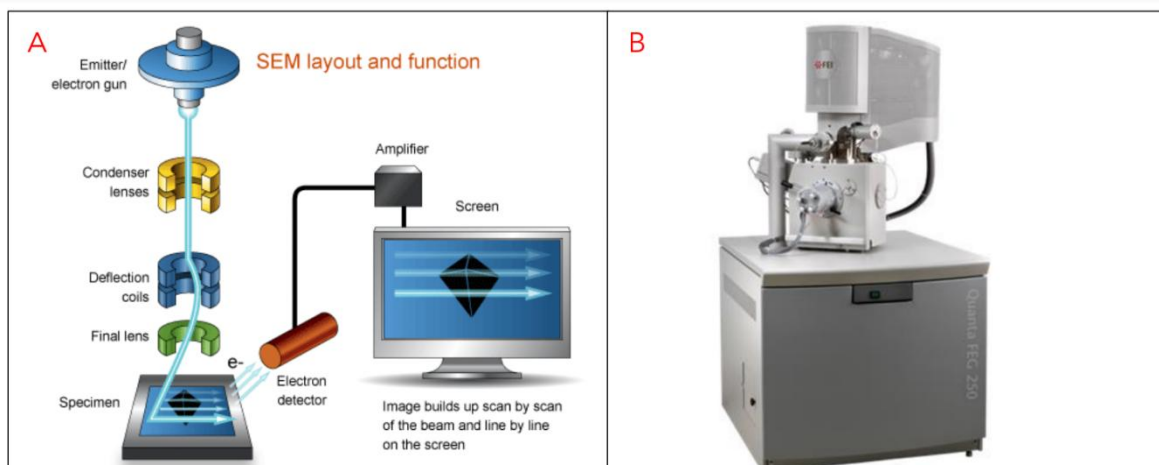


Figure 20: The main parts of an SEM machine (A) include the detectors, imaging system, column, specimen chamber, vacuum system, electron gun, and water chilling system (Myscope, 2012a). (B) A SEM and EDS system (FEI Inspect F50 Field Emission SEM, USA) at Flinders University.

*P. aeruginosa* and *S. aureus* ( $\text{OD} \approx 0.1-0.03$ ), two bacterial strains, were deposited on AIEgen immobilised plasma coated surfaces and subjected to one hour of light irradiation to investigate the morphology of the bacteria after being exposed to a coated surface. The samples were then cleaned with PBS, fixed with glutaraldehyde in 0.1 M sodium cacodylate

buffer pH 7.4, 4% (ProSciTech, Australia) for 45 minutes, and then cleaned and resuspended. Gradient dehydration was carried out under room temperature using ethanol aqueous solutions (20, 40, 60, 70, 80, 90, 95, 99, and 100%) in succession, with each incubation period lasting 10 minutes. Ultimately, the specimens underwent air drying and were thereafter coated with a thin layer of platinum using an Ion Sputter Coater (TB-SPUTTER, Quorum Technologies, UK) before SEM imaging.

### **2.3.13. Zone Inhibition assay**

The antibacterial activity of the AIEgen immobilised Pox coated surface was investigated using the zone inhibition test. Within the biosafety cabinet, 10 µl of the bacterial stock solution ( $1 \times 10^9$  CFU mL<sup>-1</sup>) was applied to the agar plates and evenly distributed using a sterile inoculating spreader. The bacterial stock solution was generated using overnight cultured broth solution. The samples were further prepared by adding 5 µl of sterilised Milli-Q water to AIEgen-immobilised Pox coated samples. Pox coated samples were used as a positive control, while uncoated samples were used as a negative control. The samples were then activated with light irradiation for one hour. The agar plate was incubated with bacteria for 24 hours at 37 °C held these samples. Each solution's generated inhibitory zone's diameter was measured.

### **2.3.14. Cytotoxicity**

It is vital to investigate whether the antibacterial activity of the AIEgen-immobilised Pox coated surfaces causes cellular toxicity upon contact since this will aid with the final product's use in various biomedical applications. The MTT test, a popular colourimetric cell viability assay, counts the number of viable cells using a few simple procedures. This method involves the cellular oxidoreductase enzymes of nicotinamide adenine dinucleotide phosphate (NADPH)-dependent tetrazolium dye MTT solution reducing to its insoluble formazan state, which leaves the mitochondria of live cells stained purple.

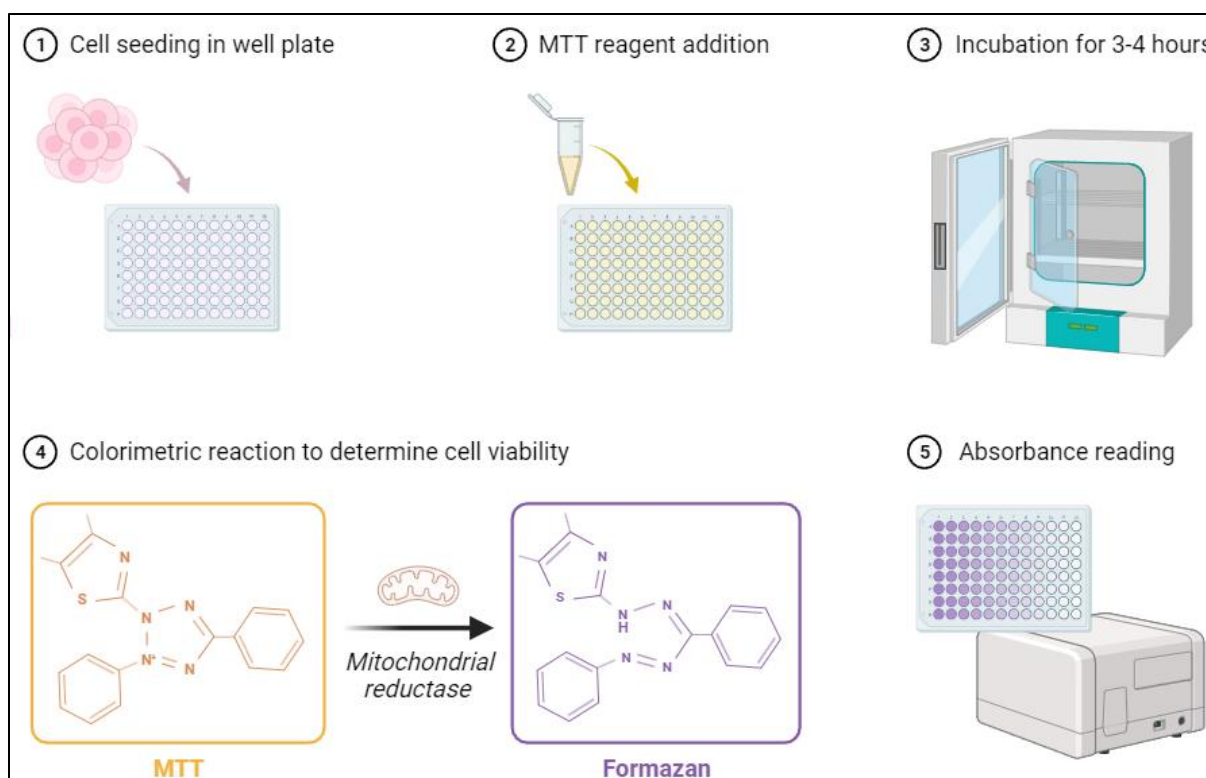


Figure 21: Illustration of basic steps used in the MTT assay. (1) Cells were added to the sample-based well plate and kept for incubation, (2 & 3) The reagents for MTT assay were added and kept for incubation for reaction, and (4 & 5) Plate reading after the reaction was completed.

To immobilise the molecule for a whole day in the presence of previously produced Pox coated and uncoated wells (controls) with triplicates of each sample, half-masked Pox coated 96-well plates were made and -AIEgen-solutions (with both concentrations i.e., b and c) were added. To monitor epidermal homeostasis, human keratinocytes (HaCaT cells) were used for our investigation. Each marked well of coated 96-well plates held about  $1 \times 10^5$  HaCaT cells, which were then grown in Dulbecco's modified Eagle's medium (DMEM). To achieve a final concentration of 50-100 I.U./mL of penicillin and 50-100 ( $\mu\text{g}/\text{mL}$ ) of streptomycin, penicillin-streptomycin solution was added to the cell culture medium. The plates were then incubated for around 24 hours at  $37^\circ\text{C}$  with 5%  $\text{CO}_2$ . The media was taken out of each well after incubation, and a fresh medium was added. To get a final concentration of 0.2 - 0.5 mg/ml, MTT (sigma-Aldrich, AU) solution was applied to each well. The plates were then placed in a humidified environment and incubated for 4 hours. The solution from each well was removed, and then the DMSO solubilization solution was added. The mixture was then incubated for an additional 30 minutes in the incubator. Next, we use the plate reader at 570

nm absorbance of the 96-well plate. GraphPad Prism 9 was used to record and process the data. The absorbance values were determined by calculating the cell viability % using the equation below.

$$\text{Cell viability (\%)} = \frac{\text{Mean absorbance of the sample}}{\text{Mean absorbance of the control}} \times 100$$

# CHAPTER 3: RESULTS AND DISCUSSION

## 3.1. Results

### 3.1.1. Preparation of AIEgen-immobilised plasma polymerised surfaces and their characterisation

Correct selection and cautious step optimisation are necessary for the plasma reactor's parameters to prepare stable plasma deposition on the substrates. Here, 50W of power, two minutes, and a base pressure of  $1.3 \times 10^{-1}$  mbar are the conditions used for plasma deposition in the reactor. The thickness of POx was measured using an ellipsometer, yielding a result of  $23.648 \pm 1.5$  nm.

Table 2: Thickness measured for plasma deposited poly-oxazoline

Sample number	1	2	3	4	5	Mean	Standard deviation
The thickness of POx in nm	21.55	23.71	25.12	25.05	22.81	23.648	1.519875

Table 3: Thickness measured for plasma deposited acrylic acid

Sample number	1	2	3	4	5	Mean	Standard deviation
Thickness of AC in nm	11.53	11.19	10.52	11.11	11.47	11.164	0.401846

POx and AC coated silicon wafers were submerged in 300  $\mu$ l of AIE1 (TPAQ-PF6) and AIE2 (CN-TPAQ-PF6) solutions for two distinct times, i.e., four hours and twenty-four hours, after which three Milli-Q water washes were performed. The AIEgen concentration in the solutions was 0.66 mg/ml (4:1 ratio of ethanol to water). The samples were examined using an Olympus IX83 inverted fluorescent microscope to evaluate the strength of AIEgen binding to the plasma-deposited surface since AIEgens are also extremely fluorescent when they are

aggregates. It was shown that as the immobilisation time rises, so does the AIE PSs binding to the plasma-deposited surfaces.

Additionally, there were differences in binding intensity and plasma polymer for each AIEgen, specifically AIE1 (A1) and AIE2 (A2). In this instance, the Pox coated surface exhibited a greater binding intensity compared to the Ac coated surfaces. This observation was verified using fluorescence microscopy analysis of the AIEgen-immobilised surfaces. Similar to this, the 24-hour immobilised samples had a greater binding density than the 4-hour immobilised samples. After a 24-hour immobilisation period, the investigation revealed that the AIEgen had a strong binding affinity for the plasma-coated substrate. Additionally, the Pox coated substrates exhibited greater binding intensities compared to AC because the nucleophilic sites in both AIE with increased electron density functions creates the repulsive force to the negatively charged surface forming less binding with the nitrogen-containing functional group with covalently binding to the carboxylic group in the molecule. On the other hand, POX has intact oxazoline functions that enable them to bind with the nucleophilic sites and nitrogen-containing functional group of both AIE through the electrostatic attraction (Ruvini L Dabare *et al.* 2022) For our additional research, we thus employed Pox coated substrates.

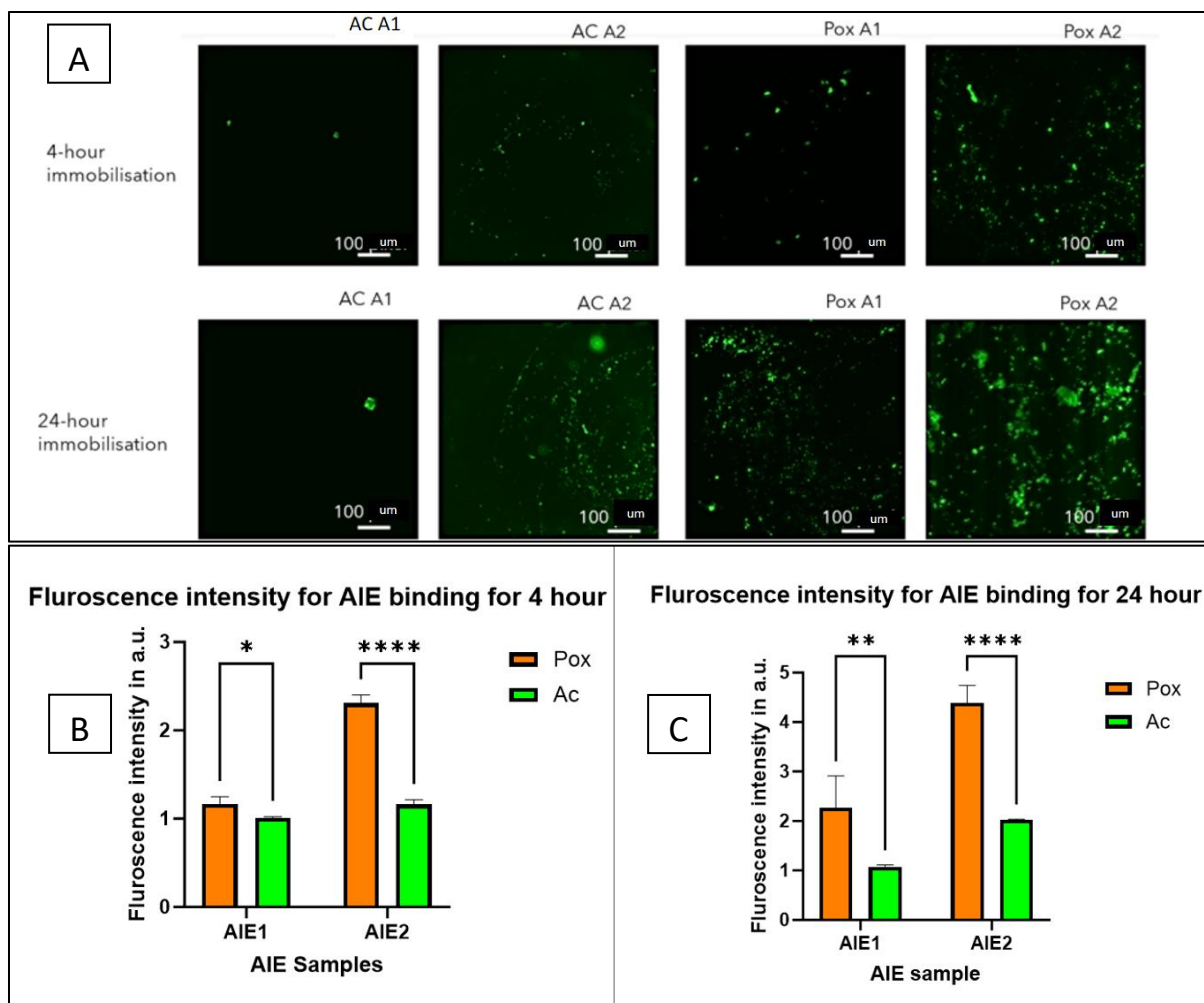


Figure 22: The intensity of AIEgen (AIE1 (TPAQ-PF6) and AIE2 (CN-TPAQ-PF6)) to Pox and AC deposited surfaces were analysed and quantified. (A) Images taken from cellSens Dimension software by using fluorescence spectroscopy for 4- and 24-hour immobilisation. (B and C) The intensity of AIE binding was determined in image J software and Graphpad prism was used for graphical analysis to conclude the higher binding intensity of AIE2. Here, mean  $\pm$  SD, n = 3. \*  $p < 0.05$ , \*\*\* $p < 0.001$ , \*\*\*\*  $p < 0.0001$ .

Next, the water contact angle for the surface characteristics pertaining to the sample surface's wettability (hydrophobicity/hydrophilicity) was calculated. The wettability of substrates was observed using the water contact angle machine on top of AIEgen-immobilised plasma polymerised samples. Here we observed, AIE1 (TPAQ-PF6) was shown to be more hydrophilic, whereas AIE2 (CN-TPAQ-PF6) had a larger value of contact angle, making it hydrophobic.

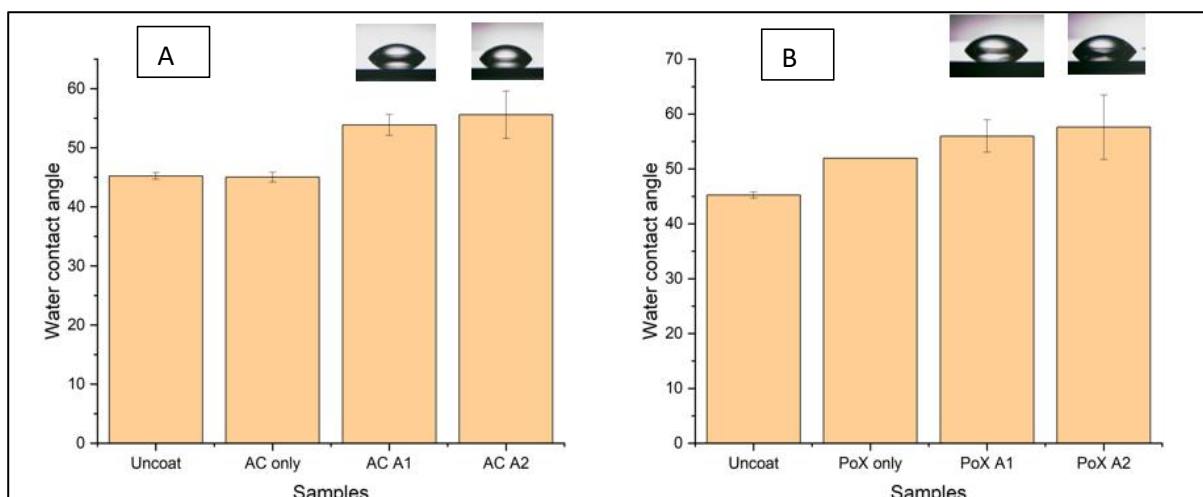


Figure 23: The above graph represents the water contact angle analysis for (A) AIE PSs immobilised AC coated surfaces and (B) AIE PSs immobilised POx coated surfaces. It was observed, AIE2 is more hydrophobic than AIE1 along with control samples (uncoated). Further, in comparison to the AC coated plasma polymerised substrate the Pox coated surfaces were more hydrophobic.

From the above characterisation technique, we observed the binding of AIE PSs to the POx coated surfaces were higher incompare to the AC coated surfaces and from here the optimised surfaces for further investigation were choosed, which are; POX A1 and POX A2.

With UV spectroscopy, the binding of the AIE PSs after immobilization can be observed with the presence of absorbance peak of both AIE PSs. However, the binding is unstable because of plasma coated substrate. We performed a Fourier transform infrared (FTIR) spectroscopy investigation to gain a deeper understanding of the chemical functions of both AIEgen-immobilised plasma-coated substrates. Potassium bromide, or KBr, whose chemical makeup is known, is utilised in this work as the substrate to read the solid-state chemical functions of the AIEgen sample.

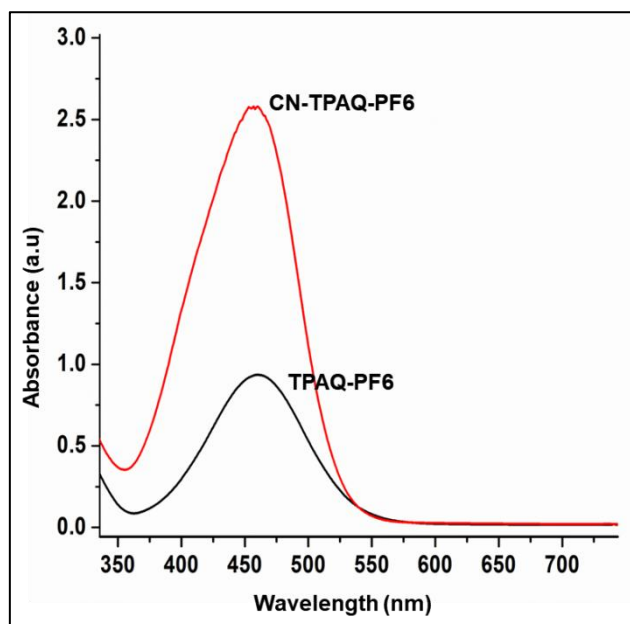


Figure 24: The absorbance pea for both AIEgens (TPAQ-PF6 and CN-TPAQ-PF6) immobilized on a plasma polymerized surface.

The distinctive functional groups of AIE1 and AIE2 consist of hydroxyl groups (O-H) located at 3775 and 3780  $\text{cm}^{-1}$ , aromatic CHx extending between 3000 and 3100  $\text{cm}^{-1}$ , and alosematic CHx extending between 2800 and 3000  $\text{cm}^{-1}$ . PF6 groups credit the peak in the fingerprint area, which is between 700 and 800  $\text{cm}^{-1}$  (Chen *et al.* 2012).

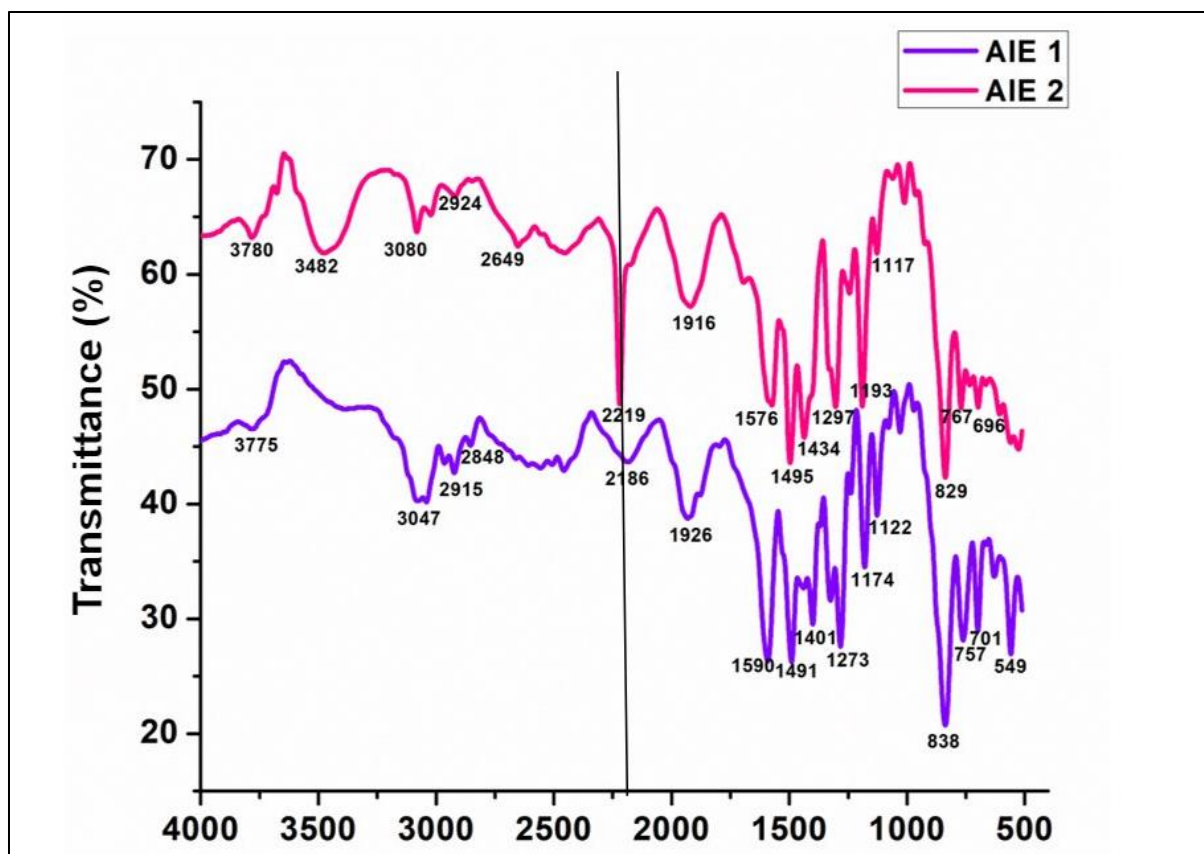


Figure 25: Fourier transform infrared spectroscopy was used to detect the chemical functionalities present in AIE1 (TPAQ-PF6) and AIE2 (CN-TPAQ-PF6) where the difference of functional groups was determined.

As for AIE1, it holds C=C/C=C at  $1926\text{ cm}^{-1}$ , and AIE2 holds the same group at  $2219\text{ cm}^{-1}$  are among its typical functional groups. Further, the differentiation of these 2 AIEgen can be observed at AIE2  $3482\text{ cm}^{-1}$  represents the extra nitrile group in it. N-H bending occurs at  $1576\text{ cm}^{-1}$  for AIE2 and  $1590\text{ cm}^{-1}$  for AIE1, with the aromatic rings falling between  $1400$  and  $1450\text{ cm}^{-1}$ . Macgregor-Ramiasa *et al.* (2015) revealed that the C-N amide triple band, C-O-C polysaccharide, and carbohydrate (C-O) exist within the range of  $1300\text{-}1000\text{ cm}^{-1}$  for both AIE1 and AIE2.

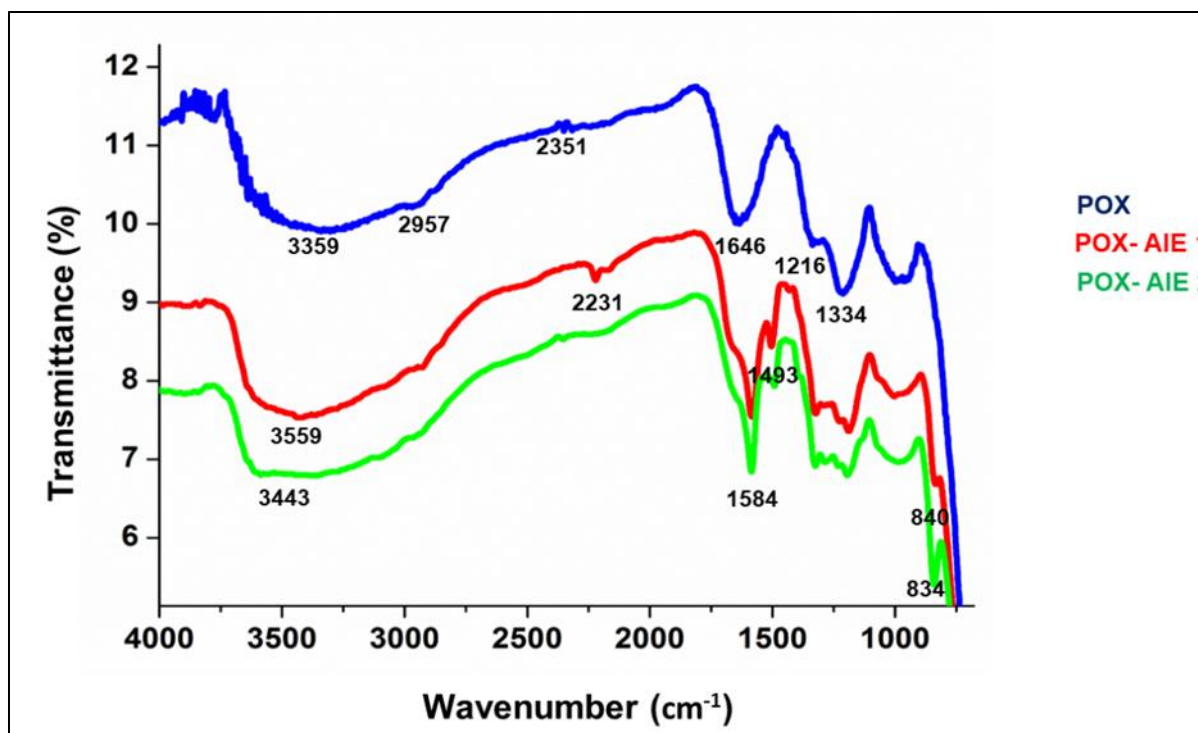


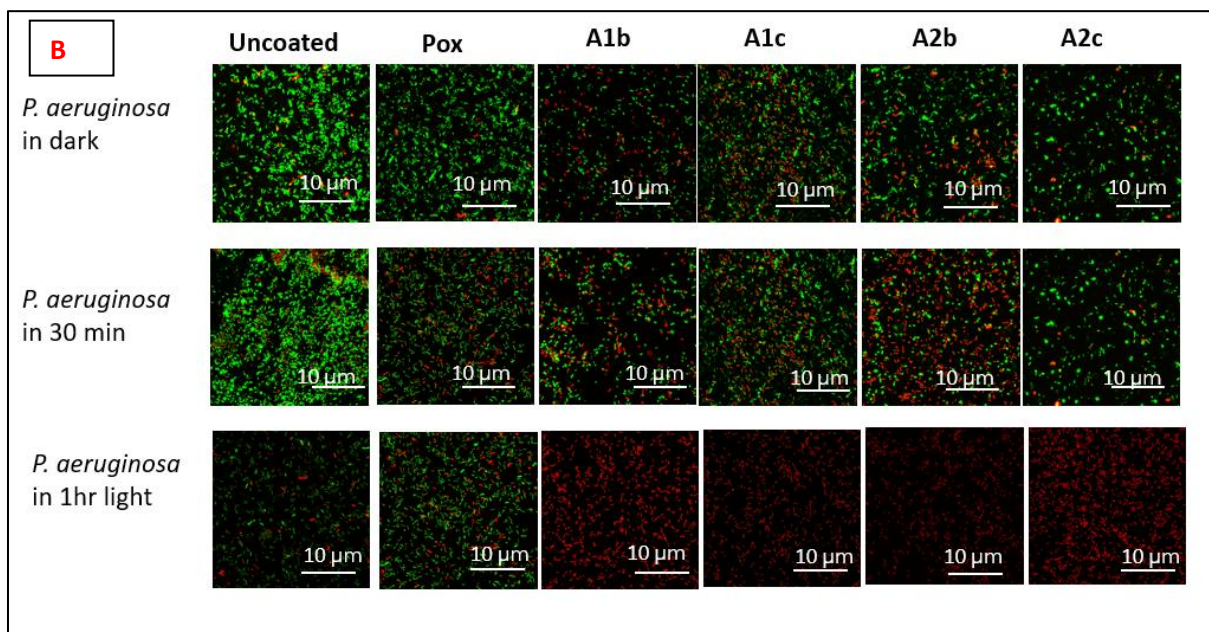
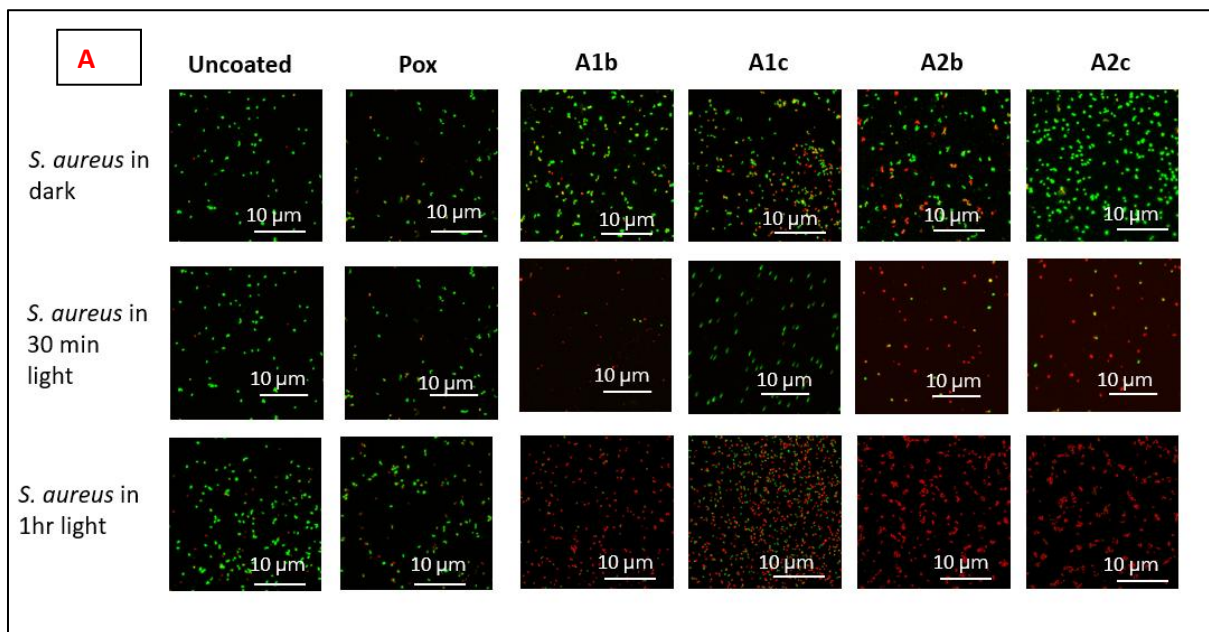
Figure 26: Fourier transform infrared spectroscopy was used to detect the chemical functionalities present in POx-AIE1 (TPAQ-PF6) and POx-AIE2 (CN-TPAQ-PF6) where the difference of functional groups was determined.

The spectra of POX-AIE1 and POX-AIE2 show the presence of all significant vibrational characteristics linked to AIEgen, indicating the immobilisation of AIEgen on plasma-coated surfaces was effective. However, the nitrile group was not visible on POx- AIE2 coated surfaces.

### 3.1.2. Antibacterial properties

Numerous antibacterial studies were conducted to investigate the facts related to bacteria, among which the antimicrobial test using Live/Dead staining was one of the significant findings. It is made up of two dyes with distinct properties, propidium iodide (PI) and SYTO9. SYTO9 dye is replaced with PI dye due to the latter's greater binding affinity to nucleic acid and red fluorescence in unhealthy cells were observed. This results in the bacterium culture's viable cells being the only ones that are stained green and the non-viable cells being red. For each stain, we had samples with AIE1 and AIE2 immobilised plasma coated substrate and negative control (Pox and uncoated samples). In this work, we employed two distinct bacterial cell cultures, namely *S. aureus* and *P. aeruginosa*.

The proportion of killed bacterial cells following light irradiation is greater than under dark conditions, according to image analysis results obtained using ImageJ software. Less dead bacteria were seen in the dark conditions of the AIEgens (AIE1 and AIE2) immobilised plasma coated samples containing *S. aureus* and *P. aeruginosa*, demonstrating their antibacterial activity with <50% and <40% efficiency, respectively. However after one hour of light irradiation, the surfaces showed a discernible rise in dead cells, as shown by the improved antibacterial qualities with > 95% for *P. aeruginosa* bacterial strains and > 90% for *S. aureus* bacterial strains.



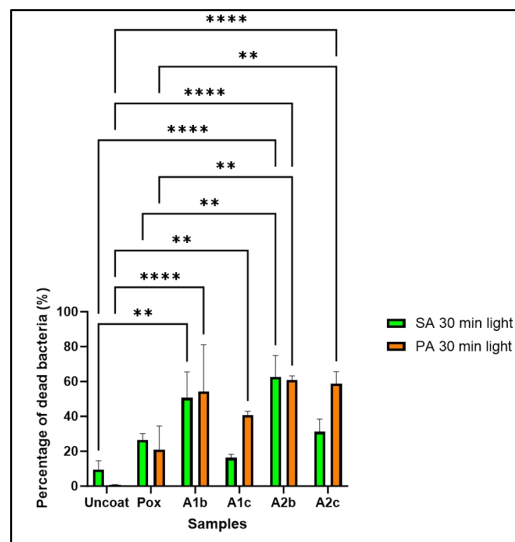
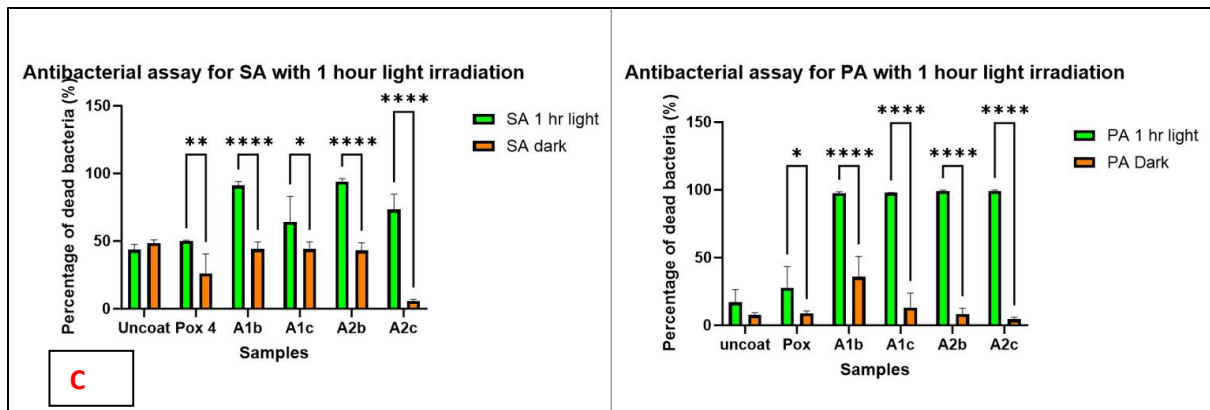


Figure 27: The figure represents the antibacterial assay for dead/live bacterial staining with (Fig. A and B) *S. aureus* and *P.aeruginosa* for uncoated, pox coated and 2 different concentrations of both AIE1 and AIE2 i. e., b=0.46 mg and c=0.33 mg respectively under 30 min, 1 hr light irradiation and dark condition (c). The percentage of dead bacteria was calculated and represented in the graph where *P.aeruginosa* has >99% dead bacterial cells. Here, mean  $\pm$  SD, n = 3. \* p<0.05, \*\* p<0.01p, \*\*\*p<0.001, \*\*\*\*p<0.0001.

When the combination is plated on agar plates from each fold of dilution, the colony-forming unit is an additional antibacterial test to count the surviving bacterial colony. The AIEgen-immobilised sample is to observe the capacity for individual cell growth and differentiation.

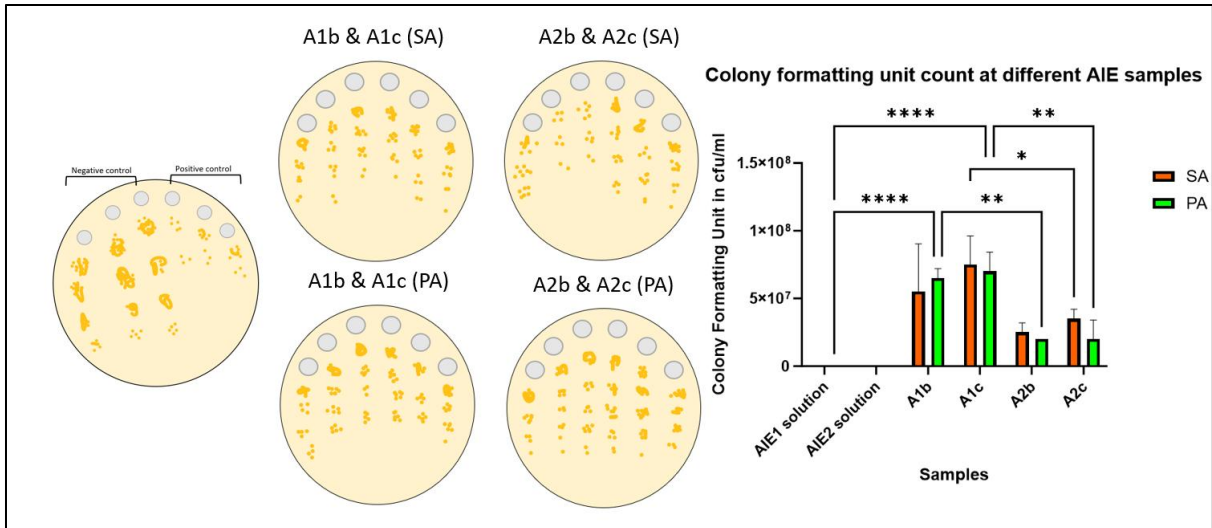


Figure 28: Colony forming unit count with 2 different concentrations of both AIE1 and AIE2 i. e., b=0.46 mg and c=0.33 mg and a chart illustrating the CFU count where *P.aeruginosa* showed less colony formation than *S. aureus*. Data illustrates mean  $\pm$  SD, n = 3. \* p<0.05, \*\* p<0.01p, \*\*\* p<0.001, \*\*\*\* p<0.0001.

AIEgen-immobilised plasma coated surfaces are tested for their antibacterial efficacy against harmful bacterial strains of Gram-positive *S. aureus* and Gram-negative *P. aeruginosa* using the straightforward and universal Zone Inhibition Assay. After a 24-hour incubation period, the base of the positive control, which has avancomycin (10  $\mu$ l) on top of the substrate, remained transparent due to its solution state. The AIE molecules were immobilised to the surface and the stability of the binding was strong, so the AIE samples did not exhibit any zones of inhibition.

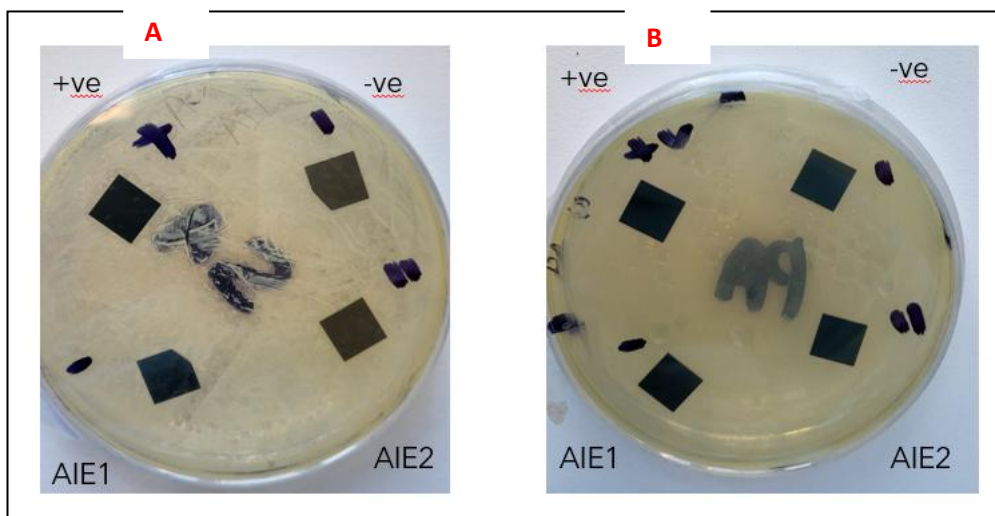


Figure 29: Samples for Zone of inhibition assay, where A1=AIE1 (TPAQ-PF6) and A2=AIE2 (CN-TPAQ-PF6) along with Vancomycin as positive and uncoated substrate as negative control where image (A) for *S. aureus* and (B) *P. aeruginosa* cultured plate.

One of the key drivers of antibacterial activity is the production of ROS, which supports one of our theories about the activity's ability to combat Gram-positive *S. aureus* and Gram-negative *P. aeruginosa*. Oxidative stress in bacterial cells was identified and quantified using a fluorescent dye (DCFDA / H2DCFDA - Cellular ROS Assay Kit). Greater amounts of intracellular ROS are indicated by green fluorescence signalling intensity. In this investigation, microorganisms from AIE2 immobilised samples showed higher levels of green fluorescence than strains from AIE1 immobilised samples or the control sample. *P. aeruginosa* has a higher fluorescent signal intensity than *S. aureus*, according to the findings.

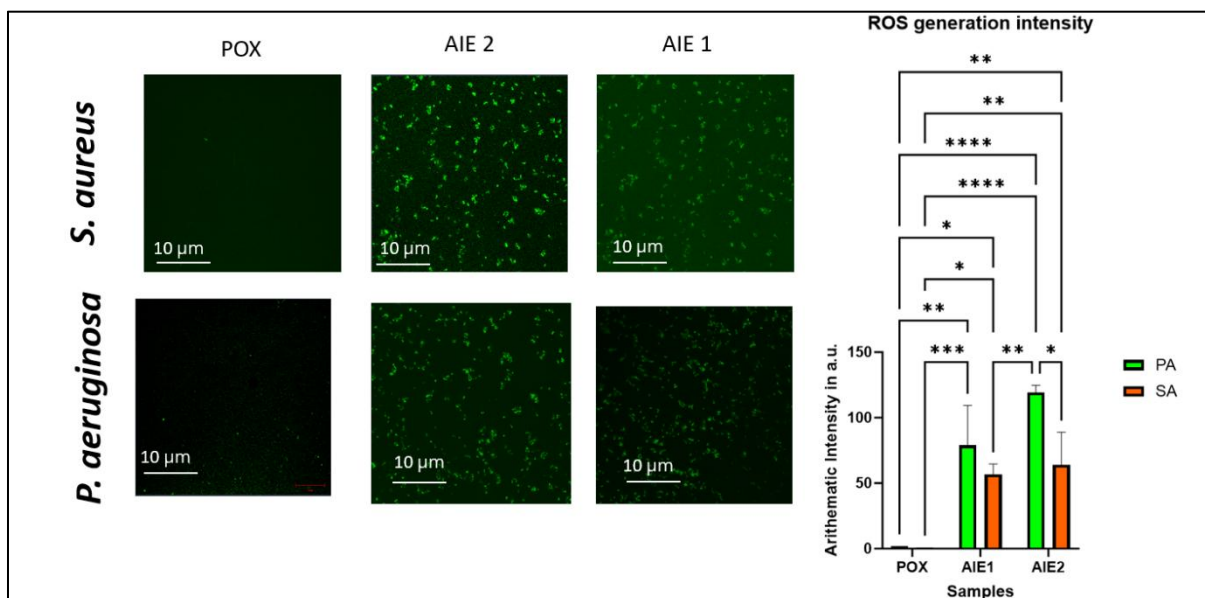


Figure 30: ROS staining images of *P. aeruginosa* and *S. aureus* from AIE1 and AIE2 immobilised samples along with ROS fluorescence intensity chart where AIE2 generates more ROS than AIE1. Data illustrates mean  $\pm$  SD, n = 3. \* p < 0.05.

The membrane potential test was used to determine whether the bacterial membrane had changed following exposure in order to further investigate the antibacterial qualities of the AIEgen-immobilised sample. DiO/DPA Membrane Potential was utilised for this test, which offers DPA, premixed buffer, and the fluorescent membrane potential indicator dye DiOC16. All bacterial cells are penetrated by DiOC16, a substance that displays green fluorescence, sometimes referred to as stationary fluorescence resonance energy transfer, or FRET. When

DPA anion reducing agent that functions as a mobile fluorescence resonance energy transfer (FRET) acceptor is introduced to this dye, it changes to red fluorescence. When healthy bacterial cells are exposed to this DPA dye, they undergo red fluorescence, the intensity of which varies according to the degree of bacterial membrane alterations. The population of green and red luminous bacteria was examined using a confocal laser scanning microscope. Analyses of the pictures obtained from the programme were conducted using Image J to determine the intensity of the red fluorescence.

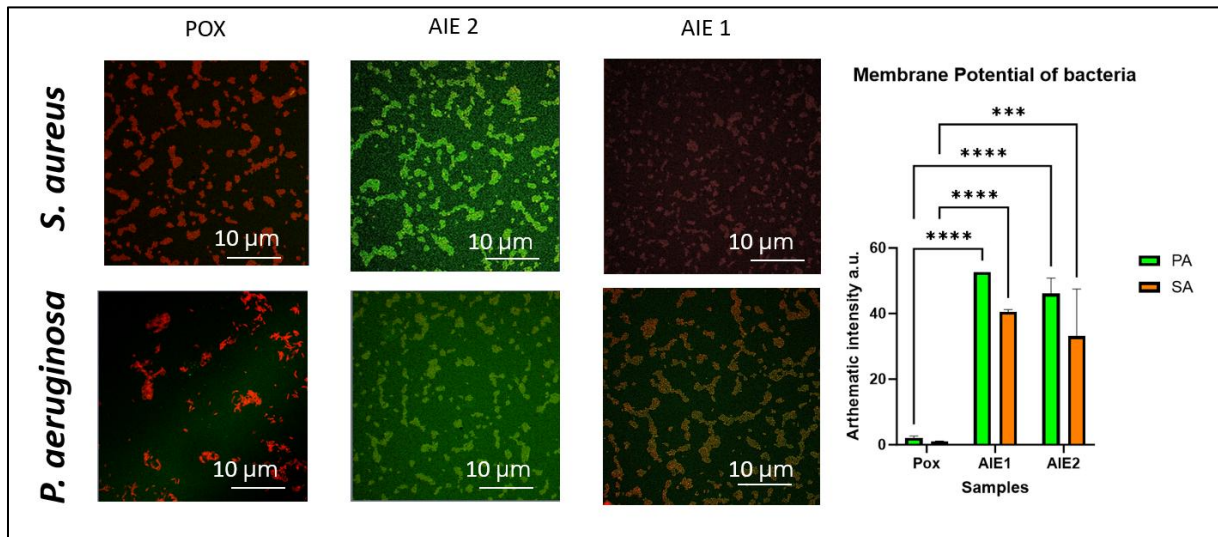


Figure 31: The intensity of green, fluorescent bacteria for both *P. aeruginosa* and *S. aureus* on AIE (AIE1 and AIE2) immobilised samples where the intensity of disrupted bacterial cells was measured. Here, *S. aureus* showed higher membrane potential with low intensity of damaged or disrupted membrane. Data illustrates mean  $\pm$  SD, n = 3, \* p<0.05, \*\* p<0.01p, \*\*\* p<0.001, \*\*\*\* p<0.0001.

Scanning electron microscopy (SEM) was utilised to see how the AIEgen-immobilised plasma coated surfaces affected the morphological alterations of the *S. aureus* and *P. aeruginosa* bacteria. Under a microscope, the bacteria had their normal, healthy cell morphologies- rod-shaped for *P. aeruginosa* and spherical for *S. aureus* when the AIEgen were absent from the substrates (control group). The bacterial cells, however, were distorted and wrinkled by the AIEgen-immobilised plasma-covered substrates. The integrity of the cell was compromised by damage to the cell membrane from the membrane side. AIE2 and AIE1 had extremely strong antibacterial effects on both Gram-positive and Gram-negative bacteria with ruptured and swollen cell membranes, according to a SEM picture. Furthermore, *P. aeruginosa* bacterial cells are more disrupted than *S. aureus*.

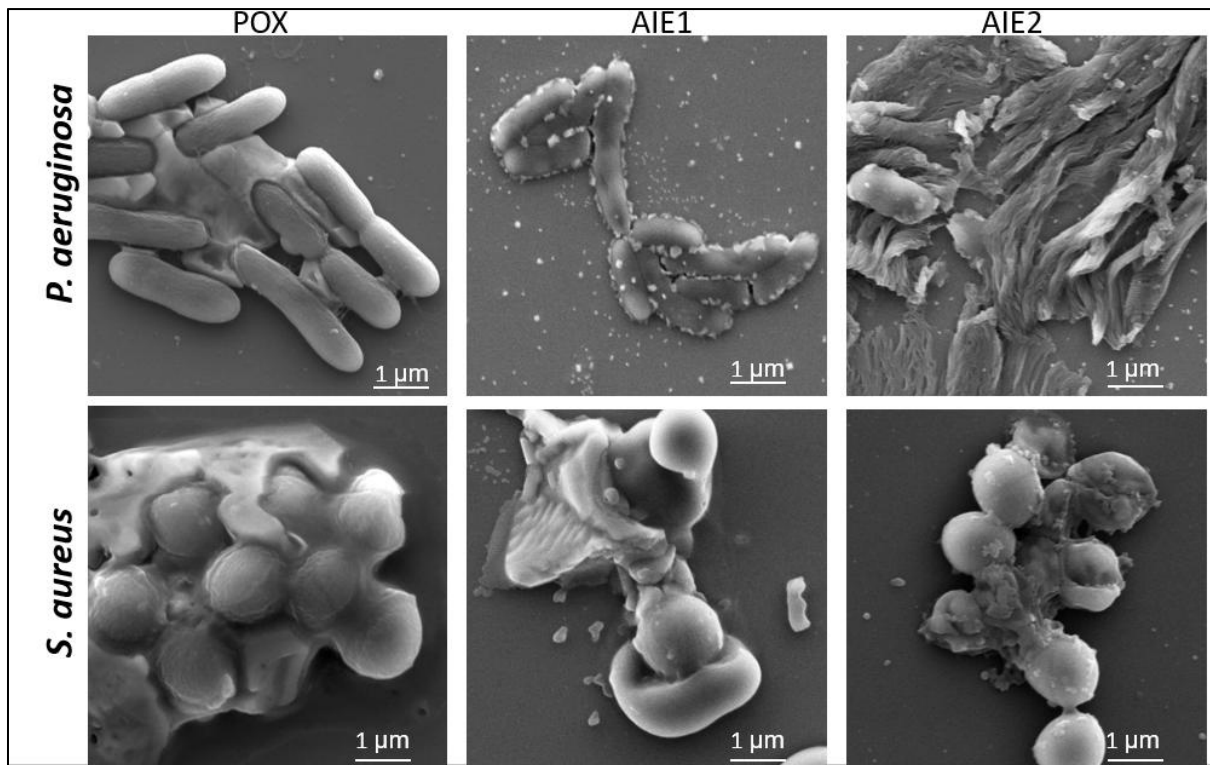


Figure 32: Morphological changes in bacterial cells after exposure to AIEgen-(AIE1 and AIE2) immobilised plasma coated substrates using SEM.

The cell permeability experiment was performed to demonstrate cell death and not only structural damage or morphological alterations to make more in-depth observations regarding how antibacterial activity relates to cell death. In addition to causing morphological damage to the bacteria, exposure to AIEgen-immobilised samples also caused cellular architecture destruction and the extrusion of all intramolecular components into the culture fluid. It stains the cell with (PI) fluorescence dye. Next, photos were captured for confocal laser scanning microscope examination. It was noted that the killing percentage rate of AIE2 was higher than that of AIE1.

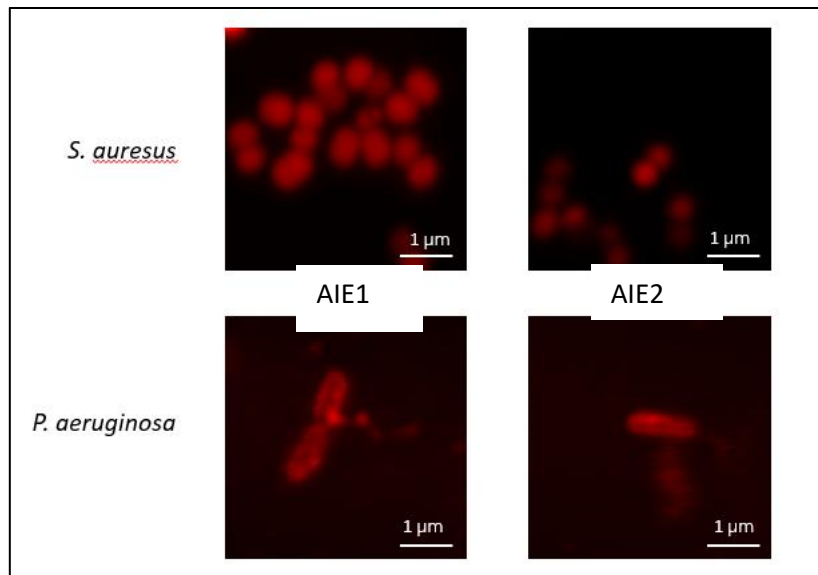


Figure 33: Cell integrity observation for *S. aureus* and *P. aeruginosa* on AIE1 and AIE2 immobilised surface.

### 3.1.3. Cell Viability/ Cytotoxicity

To determine the viable cell count in the current AIEgen-immobilised surface, the biological biocompatibility assay is crucial. The HaCat cell was used for this investigation's to analyse the cell viability and multiplication rate on the AIE PSs-immobilised substrate. The reading was obtained using a plate reader following the addition of MTT solution and seeding. It was noted that, in contrast to AIE1, AIE2 had good cell viability. In contrast to AIE2, which demonstrated about 100% vitality even after one hour of light irradiation, AIE1 only demonstrated around 50% viability.

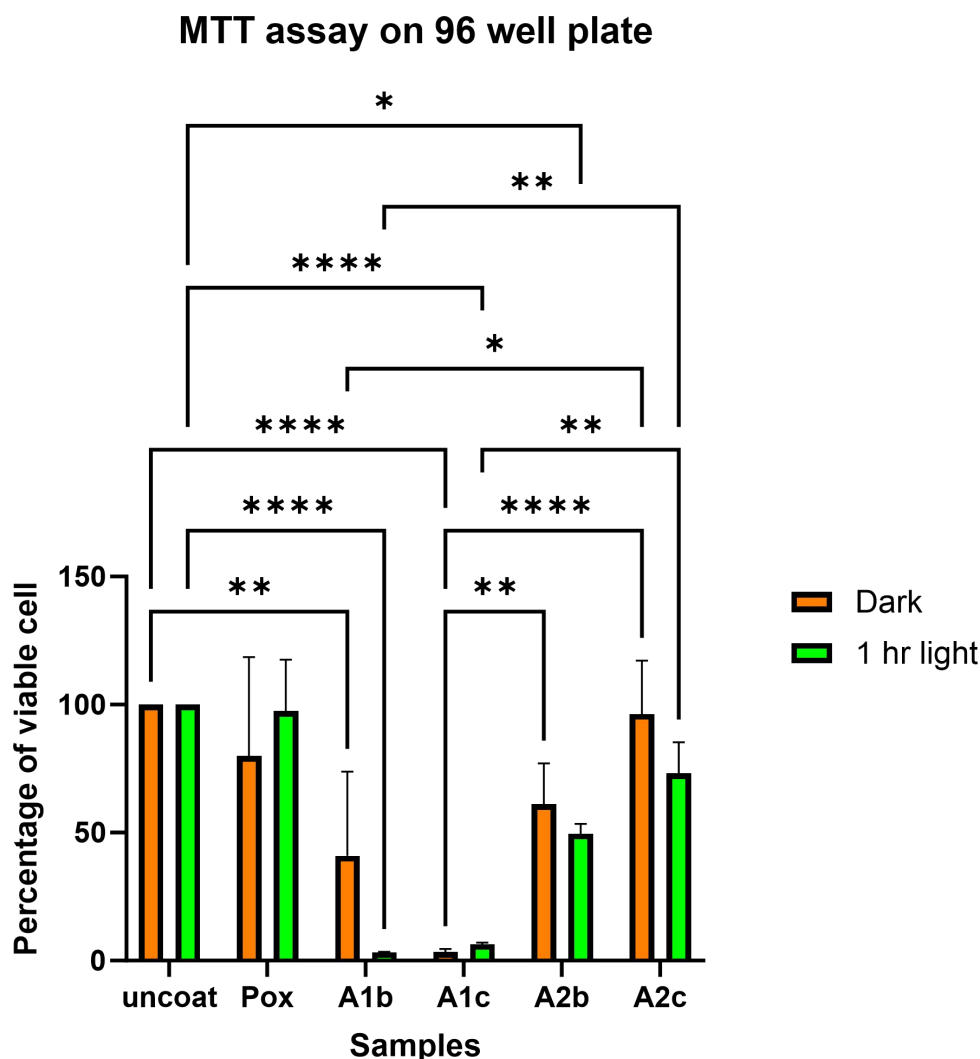


Figure 34: The chart illustrates the percentage of viability measured for each AIE1 and AIE2 with different concentrations i. e., b=0.46 mg and c=0.33 mg which demonstrates that AIE1 is highly toxic even in dark conditions. Data illustrates mean  $\pm$  SD, n = 3. \* p<0.05, \*\* p<0.01p, \*\*\* p<0.001, \*\*\*\* p<0.0001.

## 3.2. Discussion

### 3.2.1. Characterisation of AIEgen-immobilised plasma polymerised surfaces

The majority of photodynamic treatment uses photosensitisers, which excite a material to a singlet excited state before intercrossing to a triplet state. Upon reacting to the current substrate through an electron transfer mechanism and an energy exchange process, they may create type I ROS with oxygen radicals ( $O_2^-$ , HO-, and  $H_2O_2$ ) as well as type I ROS with

singlet oxygen ( $^1\text{O}_2$ ). These planar-structured photosensitisers, however, have a quenching effect related to stacking that results in significant fluorescence quenching and minimal ROS production when they are in their aggregation state. AIEgen is a mixture of photosensitisers and organic fluorophores that, when aggregates, exhibit strong fluorescence emission without exhibiting any quenching effect brought on by aggregation. Because of intramolecular mobility, they exhibit opposing properties while in their aggregation state and exhibit almost little fluorescence when in the molecular state. Its property makes it a suitable photosensitiser for bacteria that are image-guided and photodynamically inactivated (Yu *et al.* 2023).

During the investigation, two distinct molecular AIEgens were chosen for economic cationization and cyano introduction. These molecules can generate high levels of ROS of both type II and type I, as well as improve the bacterium's binding affinity for very effective photodynamic treatment of drug-resistant bacteria. Propeller-configured triphenylamine (TPA) is used as the electron donor because of its twisted geometry, which also lessens the aggregate's tight  $\pi$ - $\pi$  stacking and radiates the quenching effect. To create the asymmetric acceptor-donor-acceptor (A-D-A') subtype AIEgen CN-TPAQ-PF<sub>6</sub>, which also enhances light harvesting and ROS production, the quinolinium hexafluorophosphate (PF<sub>6</sub>) group and cyano group with a strong electron-withdrawing capacity were conjugated with TPA. Thus, because of its nonplanar structure and potent electron-donating capability, TPA is used as an AIE active electron donor (D) group. In addition, we selected TPA, i.e., the quinoline fragment and AIE1, i.e., TPAQ-PF<sub>6</sub>, which has a single electron acceptor group, to form a donor-acceptor (D-A) type. (Yu *et al.* 2023). Since AIEgen is hydrophobic, this pair of AIEgen was utilised to make a solution first using ethanol and then water (both mixed). For the solution's molecule to attach to the substrate surface, it was submerged in it.

Using a plasma polymerisation process, we prepared the substrate for coating with AC (acrylic acid) and Pox (poly-oxazoline). Ellipsometer measurements of the substrate thickness following the plasma polymerisation process were used to verify the coating of plasma polymer on surfaces. Following AIEgen-immobilisation on the plasma-coated surface, we employed fluorescence microscopy to measure the degree to which each AIEgen bound to the Pox and AC-coated substrates. We discovered that, due to the availability of their binding sites, AIE2's binding intensity is significantly higher than AIE1's. Furthermore, compared to negatively charged surfaces with carboxylic acid groups, the binding of AIEgen to POx coated substrates was significantly greater than that of AC coated substrates. This could be

the result of the opening of the oxazoline ring in both AIEgens responds to the positively charged nitrogen/nitrile group more efficiently to the higher electron density site of POx. The binding intensity to the surface of acrylic acid is substantially lower than that of Pox-coated substrates because there was less electrostatic interaction between the nitrile group and the hydroxylic group. Therefore, we continue our additional tests using just substrates coated with Pox.

By using water contact angle observation to examine the surface's wettability, the binding stability of the AIEgen was achieved. In comparison to all other samples and controls, the results verified that the surface of AIE2 immobilised plasma coated is more hydrophobic. The absorbance peak in UV spectroscopy on POX coated glass slide immobilised with AIEgens also showed the peak at 448 nm and 472 nm for CN-TPAQ-PF6 and TPAQ-PF6 respectively confirming their presence. However, using the calibration standard curve the values that were obtained showed different concentrations as the binding affinity of AIE1 is less. Except for the additional nitrile group that is present in the range of 2300 and 2100  $\text{cm}^{-1}$ , both AIE1 and AIE2 had similar related peaks in an FTIR spectroscopy research that was carried out to provide a more thorough analysis of the chemical functions present in each of the AIEgen. Heat activation and AIE characteristics are combined in a way that makes AIEgens particularly desirable in many biological applications. Because of their excellent photobleaching resistance, little toxicity, and effective emission, AIE materials are predicted to replace inorganic quantum dots in the areas of biological tests and bio-imaging. (Zhao & Sun 2016).

### **3.2.2. Performance of AIEgen-immobilised plasma polymerised surfaces with bacteria**

AIE1 (TPAQ-PF6) and AIE2 (CN-TPAQ-PF6) both demonstrated considerable mortality of *S. aureus* and MRSA after 30 minutes of light irradiation, according to a prior comparison research (Yu *et al.* 2023). For the antibacterial test in this investigation, gram-negative *P. aeruginosa* and gram-positive *S. aureus* were employed. The gram-negative bacteria have a thin peptidoglycan cell wall which was surrounded by a lipopolysaccharide membrane. Whereas gram-positive bacteria only have thick layers of peptidoglycan (Silhavy *et al.* 2010).

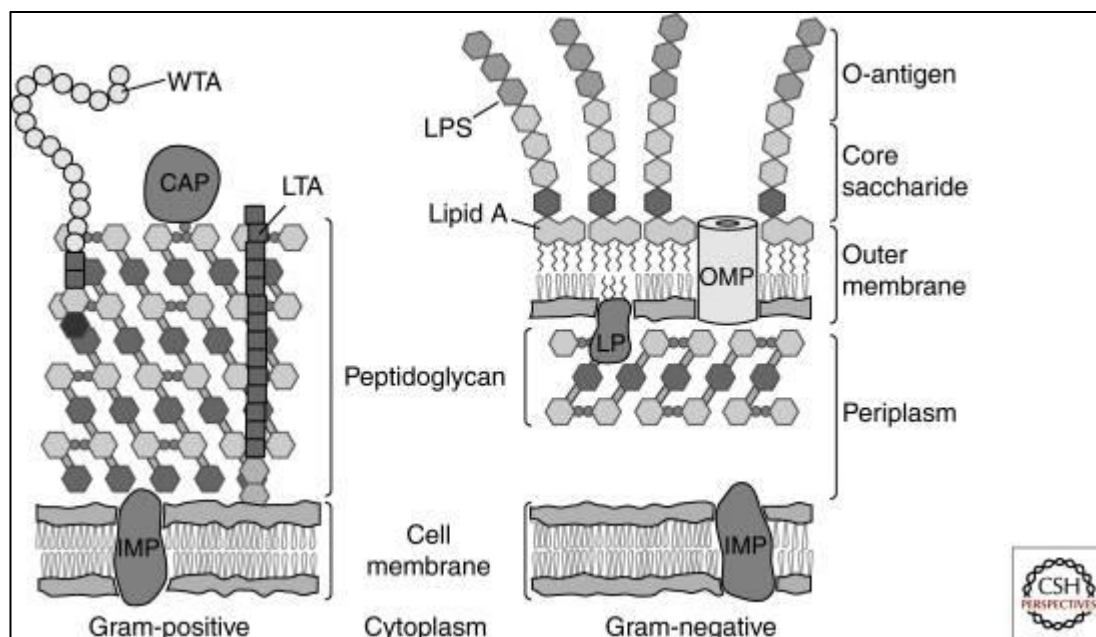


Figure 35: Illustration of cell membranes for both gram-positive and gram-negative bacteria where CAP = covalently attached protein; IMP, integral membrane protein; LP, lipoprotein; LPS, lipopolysaccharide; LTA, lipoteichoic acid (Silhavy *et al.* 2010).

The cationic AIEgen have a good binding affinity towards gram-negative bacteria. However, nitrile-containing molecules in the AIE NPs showed high binding affinity to the phospholipid membrane of the bacterial cell wall by hydrogen bonding interaction (Yu *et al.* 2023). Experiments using live and dead bacteria staining, well diffusion, and colony forming unit were used to assess the antibacterial activity of immobilised AIEgen to plasma treated substrate. The zone inhibition experiment demonstrated that the immobilised plasma polymerised surface of AIEgen was unable to produce inhibition zones because the immobilised AIEgen which is hydrophobic did not release into the surrounding environment leaving the surface of the substrate clear.

To evaluate the antibacterial effectiveness of AIEgen-immobilised plasma coated substrate, a live/dead bacterial cell staining study was performed. AIEgen immobilised on the surface demonstrated strong inhibition against both *P. aeruginosa* and *S. aureus*, according to the results from confocal laser scanning microscope images. It was shown that *P. aeruginosa* has a higher proportion of dead bacteria ( $\geq 95\%$ ) than *S. aureus* ( $\geq 90\%$ ) in 1 hour light irradiation for AIE2 immobilised plasma surfaces. While in dark conditions, AIE2 immobilised surface

showed less than 10% of inhibition against both *P. aeruginosa* and *S. aureus*. Identical samples were observed under 30 min light irradiation as well, which showed below <55% of bacterial inhibition for both bacterial strains on AIE1 immobilized samples and <65% for AIE2 immobilized samples. Additionally, the capacity of bacterial cells inside an AIE sample to proliferate and differentiate was measured using the colony forming unit (CFU) test. Colony formation was shown to be impacted by changes in sample concentration and bacterial solution dilution. In this investigation, it was shown that for both bacterial strains, the AIE1 sample formed more colonies than the AIE2 sample. Furthermore, compared to *S. aureus*, the positive control with AIEgen demonstrated significant suppression of colony development. Negative control, on the other hand, revealed both bacterial strains growing out of control.

The antibacterial mechanism of these two metal particles was investigated by the use of membrane potential tests and reactive oxygen species (ROS). Alpha-oxygen ( $\alpha\text{-O}$ ), singlet oxygen ( $^1\text{O}_2$ ), hydroxyl radicals ( $\cdot\text{OH}$ ), superoxide anions ( $\text{O}_2^-$ ), hydrogen peroxide ( $\text{H}_2\text{O}_2$ ), and other highly reactive molecules and free radicals produced from molecular oxygen are together referred to as reactive oxygen species (ROS). Numerous physiological and pathological disorders can arise from these ROS-induced damages to cellular structures and processes (Pizzino *et al.*, 2017). According to the results of the previous paper, TPAQ-PF6 and CN-TPAQ-PF6 were able to generate more ROS than their neutral counterparts in a short period ( $20 \text{ mW cm}^{-2}$ ), as demonstrated by the DCFH fluorescence enhancement factors. These results are approximately 15.0- and 2.5-fold higher than those of TPAQ and CN-TPAQ, respectively. This suggests that cationization is a progressive strategy to increase the efficiency of ROS generation. The ROS generation of CN-TPAQ-PF6 was likewise superior to that of TPAQ-PF6, indicating that the insertion of the cyano group to enable this kind of A-D-A structure is also advantageous for enhancing ROS production (Yu *et al.* 2023). DCFH dye solution's fluorescence intensity was measured between 500 nm and 550 nm at a wavelength of 488 nm for excitation. This work shows that after one hour of light irradiation ( $40 \text{ mW cm}^{-12}$ ), AIE2 (CN-TPAQ-PF6) creates more ROS than AIE1 (TPAQ-PF6) even with a small concentration of AIEgen solution ( $10 \mu\text{g/ml}$ ).

Additionally, after exposing bacteria to AIEgen-immobilized materials, we observed changes in their membrane potential using probe DiOC16(3). Cell membrane potential, or the electric potential surrounding the cell membrane, is what gives the cell its free energy to perform all chemical and mechanical functions. It influences the ability of bacteria to divide, as well as

their metabolism, intake of nutrients, and survival. Therefore, by using antibiotics and other antibacterial treatments to target this location, the bacterial cell can be destroyed (LeBel *et al.* 1992). Our research revealed that AIE2 had a significant impact on the membrane potential of *S. aureus* and *P. aeruginosa* bacterial cells with a smaller concentration (10 µg/ml). Moreover, *S. aureus* have a greater degree of membrane alteration in both AIEgens following exposure to an immobilised plasma polymerised sample.

Furthermore, after coming into direct contact with a chemical that has antibacterial action, the bacterial cell membrane causes modifications to the membrane's integrity, including wrinkling, cracking, and the creation of holes. These actions cause bacterial cells to become inactivated by drastically changing their shape. The process of bacterial cell death results in cellular content leakage into the culture medium and damage to cellular architecture (Cho *et al.* 2008). In this study, we observed the death efficacy related to bacterial cell integrity was determined using propidium iodide (PI) dye on AIE2 immobilised (10 µg/ml) on plasma-coated surface and confocal laser scanning microscope.

### **3.2.3. Biocompatibility of the substrates**

An essential preliminary experiment for the biomedical field's use of AIEgen-immobilized samples is the *in-vitro* cytotoxicity observation. HaCaT cells with an immobilised plasma surface from AIEgen were employed in this investigation for the biocompatibility analysis. After the cells were seeded and allowed to grow in the sample wells of the 96-well plate, Tetrazolium dye MTT solution was applied. Nicotinamide adenine dinucleotide phosphate (NADPH)-dependent cellular oxidoreductase enzymes converted it to its insoluble formazan state, giving live cells' mitochondria a purple staining hue. AIE1 demonstrated a very low percentage of viable cells-less than 15%-both in the presence and absence of light, according to the measured observations. On the other hand, AIE2 demonstrated noticeably high vitality at low concentrations (10 µg) of AIEgen, under 1 hour of light irradiation (>70%), and in complete darkness (100%). However, after one hour of light irradiation, >60% of the concentration of b (14 µg/ml) demonstrated less viability than the concentration "c."

## **3.3. Conclusion and future research**

One of the biggest issues facing healthcare, as well as the general public is bacterial infections. Numerous fields, including the bloodstream, skin, tissue, and SSIs, are susceptible

to these illnesses. Depending on how bad the infection is, the expense of treatment may increase and need further hospital stays. For various bacterial strains, there are several antibiotics available. All the present treatment features, however, are seriously threatened by antibiotic-resistant microorganisms. Among the frequent microorganisms that cause these infections are the methicillin-resistant *S. aureus* and *P. aeruginosa*. To stop microorganisms from entering the site of surgical site infection (SSI), we prepared, a surface covered with antibacterial agents. With the use of the plasma polymerisation approach, we were able to create a surface that included the specific molecules, which will show antibacterial activities against the infection-causing bacteria. We next examined its biocompatibility, antibacterial qualities, and potential uses by introducing it into different substrates. The selected AIE molecules (AIE1=TPAQ-PF6 and AIE2=CN-TPAQ-PF6), were immobilised on the surface covered with plasma. The nitrogen groups in both AIE molecules, which have greater electron density as nucleophilic charge, bind to the surface. AIE2 (CN-TPAQ-PF6) has an additional nitrile group that is present due to nucleophilic interactions. This group is drawn to the electrophilic charges of the oxazoline ring by nucleophilic-electrophilic contact. When compared to substrates coated with Pox, the binding intensity to the surface of acrylic acid is noticeably lower because there was less nucleophilic interaction between the hydroxylic and nitrile groups. Therefore, we solely use Pox coated substrates in all other research.

It has been shown that AIEgen-immobilised plasma coated substrates are highly effective at inhibiting the growth of two common pathogenic gram-positive and gram-negative bacteria, *Staphylococcus aureus* and *Pseudomonas aeruginosa* when exposed to a 40mW cm<sup>-2</sup> light source for one hour (>90% and >95%). AIE2 did, however, outperform AIE1 in every antibacterial assay and showed high biocompatibility. There are a few tests that may be used to acquire the dead bacterial cell mechanism, including the production of ROS, disruption of membrane potential, and destroyed cell integrity. It is possible to conclude from all of the results that AIE2 has significantly greater antibacterial activity than AIE1. AIE2 has also shown outstanding biocompatibility in the cytotoxicity testing in both light and dark conditions (>70% & 100%). Conversely, in both light and dark conditions, AIE1 displayed relatively few viable cells (<15% & <40%). Applications in biomedicine, such as sutures, can take advantage of the AIEgen-immobilised plasma coated substrate. This device can be used to prevent germs from entering the surgical site.

Despite the progress made in this study, several important research questions have emerged that warrant further investigation. For instance, it remains unclear how much AIE ions are

released under different pH conditions, and what the size and surface charge of the particles is. Also, will it get dissolved in the blood stream causing any threats after applying at the surgical site? Further, some of the other antibacterial mechanisms are still unclear such as bacterial membrane penetration and genetic material destruction for better understanding. Moreover, some more study needs to be done to get to know about the prior action of these AIEgen-immobilised plasma coated substrates for their characteristics for cell viability. In-vivo studies can clarify the chemistry of different cytotoxic levels of these 2 AIEgens (TPAQ-PF6 and CN-TPAQ-PF6). In order to clarify all these questions, more in-vivo analysis for the mechanism part needs to be done as per the future perspective.

# References

- Ahmed, S. 2021. Welcome to molecular medicine communications! *Molecular Medicine Communications* 1(1), 01.
- Akash, M.S.H., Rehman, K. 2019. Ultraviolet-Visible (UV-VIS) Spectroscopy. *Essentials of Pharmaceutical Analysis* , 29–56.
- Alexander, J.W., Solomkin, J. S., Edwards, M. J. 2011. Updated recommendations for control of surgical site infections. *Annals of Surgery* 253(6), 1082–1093.
- Anthony, T. 2011. Evaluating an evidence-based bundle for preventing surgical site infection. *Archives of Surgery* 146(3), 263.
- Argemi, X., Martin V., Loux, V., Dahyot, S., Lebeurre, J., Guffroy, A., Martin, M., Valay, A., Keller, D., Riegel, P., Hansmann, Y., Paul, N., Prevost, G. 2017. Whole genome sequencing of 7 strains of *Staphylococcus lugdunensis* allows identification of mobile genetic elements. *Genome Biology and Evolution*. 9(5),
- Bagnall, N. M., Vig, S., Trivedi, P. 2009. Surgical-site infection. *Infection*, 27(10), 426.
- Balavandy, S.K., Shameli, K. and Abidin, Z.Z., 2015. Rapid and green synthesis of silver nanoparticles via sodium alginate media. *International Journal of Electrochemical Science*, 10(1), 486-497.
- Barie, P. S., Eachempati, S. R. 2005. Surgical site infections. *Surgical Clinics of North America* 85(6), 1115.
- Bayr, H. 2005. Reactive oxygen species. *Critical Care Medicine* 33(Suppl), S498.
- Beckmann, J. S., Lew, D. 2016. Reconciling evidence-based medicine and precision medicine in the era of big data: challenges and opportunities. *Genome Medicine* 8(1).
- Benarroch, J. M., Asally, M. 2020. The microbiologist's guide to membrane potential dynamics. *Trends in Microbiology* 28(4), 304.

- Berthomieu, C., Hienerwadel, R. 2009. Fourier transform infrared (FTIR) spectroscopy. *Photosynthesis Research* 101(2–3), 157.
- Bhatt, S., Pulpytel, J., Arefi-Khonsari, F. 2015. Low and atmospheric plasma polymerisation of nanocoatings for bio-applications. *Surface Innovations*, 3(2), 63.
- Bitar, R., Cools, P., De Geyter, N., Morent, R. 2018. Acrylic acid plasma polymerization for biomedical use. *Applied Surface Science* 448, 168.
- Burr, T. 2010. Phylogenetic trees in bioinformatics. *Current Bioinformatics* 5(1), 52.
- Călina, D., Docea, A. O., Rosu, L., Zlatian, O., Rosu, A. F., Anghelina, F., Rpgpveanu, P., Arsene, A. L., Nicolae, A. C., Dragoi, C. M., Rsiaoussis, J., Tsatsakis, A. M., Spandidos, D. A., Drakoulis, N., Gofita, E. 2016. Antimicrobial resistance development following surgical site infections. *Molecular Medicine Reports* 15(2), 681.
- Cao, S., Shao, J., W, H., Song, S., De Martino, M. T., Pijers, I. A. B., Friedrich, H., Abdelmohsen, L. K. E. A., Williams, D. S., van Hest, J. C. M. 2021. Photoactivated nanomotors via aggregation induced emission for enhanced phototherapy. *Nature Communications*, 12, 2077.
- CHANG, B., GUO, J., LIU, C., QIAN, J. & YANG, W. 2010. Surface functionalization of magnetic mesoporous silica nanoparticles for controlled drug release. *Journal of Materials Chemistry*, 20, 9941-9947.
- CHEADLE, W. G. 2006. Risk Factors for Surgical Site Infection. *Surgical Infections*, 7, s7-s11.
- Chen, Y., Mastalerz, M. & Schimmelmann, A. 2012. Characterization of chemical functional groups in macerals across different coal ranks via micro-FTIR spectroscopy. *International Journal of Coal Geology*, 104, 22-33.
- Chen, Y.-J., Chang, W.-A., Wu, L.-Y., Hsu, Y.-L., Chen, C.-H. & Kuo, P.-L. 2018. Systematic Analysis of Transcriptomic Profile of Chondrocytes in Osteoarthritic Knee Using Next-Generation Sequencing and Bioinformatics. *Journal of Clinical Medicine*, 7, 535.

Dabare, P.R.L., Bachhuka, A., Palms, D., Parkinson-Lawrence, E., Hayball, J.D., Mierczynska, A. and Vasilev, K., 2022. Surface chemistry mediated albumin adsorption, conformational changes and influence on innate immune responses. *Applied Surface Science*, 596, p.153518.

Dabare, P.R.L., Bachhuka, A., Parkinson-Lawrence, E. and Vasilev, K., 2021. Surface nanotopography mediated albumin adsorption, unfolding and modulation of early innate immune responses. *Materials Today Advances*, 12, p.100187.

Diniz, F. R., Maia, R., Rannier, L., Andrade, L. N., M, V. C., Da Silva, C. F., Corrêa, C. B., De Albuquerque Junior, R. L. C., L, P. D. C., Shin, S. R., Hassan, S., Sanchez-Lopez, E., Souto, E. B. & Severino, P. 2020. Silver nanoparticles-composing alginate/gelatine hydrogel improves wound healing in vivo. *Nanomaterials (Basel)*, 10.

Dunst, S. & Tomancak, P. 2019. Imaging Flies By Fluorescence Microscopy: principles, technologies, and applications. *Genetics*, 211, 15-34.

Duval, R. E., Gouyau, J. & Lamouroux, E. 2019. Limitations of Recent Studies Dealing with the Antibacterial Properties of Silver Nanoparticles: Fact and Opinion. *Nanomaterials (Basel)*, 9.

Ellipsometry Technology Information - Film Sense Ellipsometer. 2023.

Emidio Capriotti 1, N. L. N., Maricel G Kann, Yana Bromberg 2012. Bioinformatics for personal genome interpretation. *Briefings in Bioinformatics*, 13(4).

Farris, S., Introzzi, L., Biagioni, P., Holz, T., Schiraldi, A. & Piergiovanni, L. 2011. Wetting of Biopolymer Coatings: Contact Angle Kinetics and Image Analysis Investigation. *Langmuir*, 27, 7563-7574.

Feoktistova, M., Geserick, P. & Leverkus, M. 2016. Crystal Violet Assay for Determining Viability of Cultured Cells. *Cold Spring Harb Protoc*, 2016, pdb.prot087379.

Gudimalla, A., Jose, J., Rajendran, J. V., Gurram, G. & Thomas, S. 2022. Synthesis of silver nanoparticles by plant extract, incorporated into alginate films and their characterizations. *Chemical Papers*, 76, 1031-1043.

Gunasekaran, T., Nigusse, T. & Dhanaraju, Magharla D. 2011. Silver Nanoparticles as Real Topical Bullets for Wound Healing. *Journal of the American College of Clinical Wound Specialists*, 3, 82-96.

Gupta, A., Briffa, S. M., Swingler, S., Gibson, H., Kannappan, V., Adamus, G., Kowalczyk, M., Martin, C. & Radecka, I. 2020. Synthesis of Silver Nanoparticles Using Curcumin-Cyclodextrins Loaded into Bacterial Cellulose-Based Hydrogels for Wound Dressing Applications. *Biomacromolecules*, 21, 1802-1811.

Gupta, A., Briffa, S.M., Swingler, S., Gibson, H., Kannappan, V., Adamus, G., Kowalczyk, M., Martin, C. and Radecka, I., 2020. Synthesis of silver nanoparticles using curcumin-cyclodextrins loaded into bacterial cellulose-based hydrogels for wound dressing applications. *Biomacromolecules*, 21(5), pp.1802-1811.

Gupta, V. K., Fakhri, A., Tahami, S. & Agarwal, S. 2017. Zn doped CdO nanoparticles: Structural, morphological, optical, photocatalytic and anti-bacterial properties. *Journal of Colloid and Interface Science*, 504, 164-170.

Hankinson, S. E. & Eliassen, A. H. 2010. Circulating sex steroids and breast cancer risk in premenopausal women. *Horm Cancer*, 1, 2-10.

Harro, J. M., Peters, B. M., O'May, G. A., Archer, N., Kerns, P., Prabhakara, R. & Shirtliff, M. E. 2010. Vaccine development in *Staphylococcus aureus*: taking the biofilm phenotype into consideration. *FEMS Immunol Med Microbiol*, 59, 306-23.

Hegemann, D. 2006. Plasma polymerization and its applications in textiles.

Hu, Q., Nie, Y., Xiang, J., Xie, J., Si, H., Li, D., Zhang, S., Li, M. & Huang, S. 2023. Injectable sodium alginate hydrogel loaded with plant polyphenol-functionalized silver nanoparticles for bacteria-infected wound healing. *International Journal of Biological Macromolecules*, 234, 123691.

Humphreys, H. 2009. Preventing surgical site infection. Where now? *J Hosp Infect*, 73, 316-22.

IX83 | Fully-Motorized and Automated Inverted Microscope | Olympus LS.

Jiang, F., Liu, Q., Liu, X., Wang, X. H. & Kang, L. 2019. Genomic data reveal high conservation but divergent evolutionary pattern of Polycomb/Trithorax group genes in arthropods. *Insect Sci*, 26, 20-34.

Jin, Y., Peng, Q., Li, S., Su, H., Luo, P., Yang, M., Zhang, X., Li, K., Zang, S. Q., Tang, B. Z. 2022. Aggregation-induced barrier to oxygen—a new AIE mechanism for metal clusters with phosphorescence. *National Science Review*, 9, nwab216.

Juncker, R. B., Lazazzera, B. A. & Billi, F. 2021. The use of functionalized nanoparticles to treat *Staphylococcus aureus*-based surgical-site infections: a systematic review. *J Appl Microbiol*, 131, 2659-2668.

Juncker, R. B., Lazazzera, B. A. & Billi, F. 2021. The use of functionalized nanoparticles to treat *Staphylococcus aureus*-based surgical-site infections: a systematic review. *J Appl Microbiol*, 131, 2659-2668.

Kang, M., Zhang, Z., Xu, W., Wen, H., Zhu, W., Wu, Q., Wu, H., Gong, J., Wang, Z., Wang, D. & Tang, B. Z. 2021. Good Steel Used in the Blade: Well-Tailored Type-I Photosensitizers with Aggregation-Induced Emission Characteristics for Precise Nuclear Targeting Photodynamic Therapy. *Adv Sci (Weinh)*, 8, e2100524.

Kasithevar, M., Periakaruppan, P., Muthupandian, S. & Mohan, M. 2017. Antibacterial efficacy of silver nanoparticles against multi-drug resistant clinical isolates from post-surgical wound infections. *Microb Pathog*, 107, 327-334.

Kumar, K.S.S., Girish, Y.R., Ashrafizadeh, M., Mirzaei, S., Rakesh, K.P., Gholami, M.H., Zabolian, A., Hushmandi, K., Orive, G., Kadumudi, F.B. and Dolatshahi-Pirouz, A., 2021. AIE-featured tetraphenylethylene nanoarchitectures in biomedical application: Bioimaging, drug delivery and disease treatment. *Coordination Chemistry Reviews*, 447, p.214135.

Lakoh, S., Yi, L., Sevalie, S., Guo, X., Adekanmbi, O., Smalle, I. O., Williams, N., Barrie, U., Koroma, C., Zhao, Y., Kamara, M. N., Cummings-John, C., Jiba, D. F., Namanaga, E. S., Deen, B., Zhang, J., Maruta, A., Kallon, C., Liu, P., Wurie, H. R., Kanu, J. S., Deen, G. F., Samai, M., Sahr, F. & Firima, E. 2022. Incidence and risk factors of surgical site infections and related antibiotic resistance in Freetown, Sierra Leone: a prospective cohort study. *Antimicrob Resist Infect Control*, 11, 39.

Lebel, C. P., Ischiropoulos, H. & Bondy, S. C. 1992. Evaluation of the probe 2',7'-dichlorofluorescein as an indicator of reactive oxygen species formation and oxidative stress. *Chem Res Toxicol*, 5, 227-31.

Lee, N.-Y., Ko, W.-C. & Hsueh, P.-R. 2019. Nanoparticles in the treatment of infections caused by multidrug-resistant organisms. *Frontiers in pharmacology*, 10, 1153.

Levy, S.B., 2002. Factors impacting on the problem of antibiotic resistance. *Journal of Antimicrobial Chemotherapy*, 49(1), pp.25-30.

Li, B., Wang, D., Lee, M.M., Wang, W., Tan, Q., Zhao, Z., Tang, B.Z. and Huang, X., 2021. Fabrics attached with highly efficient aggregation-induced emission photosensitizer: toward self-antiviral personal protective equipment. *ACS nano*, 15(8), pp.13857-13870.

Li, M., Jiang, X., Wang, D., Xu, Z. and Yang, M., 2019. In situ reduction of silver nanoparticles in the lignin based hydrogel for enhanced antibacterial application. *Colloids and Surfaces B: Biointerfaces*, 177, pp.370-376.

Li, X., Li, J., Shan, G. and Wang, X., 2023. Identification of long non-coding RNA and circular RNA associated networks in cellular stress responses. *Frontiers in Genetics*, 14, p.1097571.

Liu, M., Chen, Y., Guo, Y., Yuan, H., Cui, T., Yao, S., Jin, S., Fan, H., Wang, C., Xie, R. and He, W., 2022. Golgi apparatus-targeted aggregation-induced emission luminogens for effective cancer photodynamic therapy. *Nature Communications*, 13(1), p.2179.

Liu, P., Li, D., Kang, M., Pan, Y., Wen, Z., Zhang, Z., Wang, D. and Tang, B.Z., 2023. Emerging Applications of Aggregation-Induced Emission Luminogens in Bacterial Biofilm Imaging and Antibiofilm Theranostics. *Small Structures*, 4(5), p.2200329.

Liu, Y., Li, F., Guo, Z., Xiao, Y., Zhang, Y., Sun, X., Zhe, T., Cao, Y., Wang, L., Lu, Q. and Wang, J., 2020. Silver nanoparticle-embedded hydrogel as a photothermal platform for combating bacterial infections. *Chemical Engineering Journal*, 382, p.122990.

Ma, K., Zhe, T., Li, F., Zhang, Y., Yu, M., Li, R. and Wang, L., 2022. Sustainable films containing AIE-active berberine-based nanoparticles: A promising antibacterial food packaging. *Food Hydrocolloids*, 123, p.107147.

Macgregor, M. and Vasilev, K., 2019. Perspective on plasma polymers for applied biomaterials nanoengineering and the recent rise of oxazolines. *Materials*, 12(1), p.191.

Macgregor, M.N., Michelmore, A., Safizadeh Shirazi, H., Whittle, J. and Vasilev, K., 2017. Secrets of plasma-deposited polyoxazoline functionality lie in the plasma phase. *Chemistry of Materials*, 29(19), pp.8047-8051.

Macgregor-Ramiasa, M.N., Cavallaro, A.A. and Vasilev, K., 2015. Properties and reactivity of polyoxazoline plasma polymer films. *Journal of Materials Chemistry B*, 3(30), pp.6327-6337.

Mammari, N., Lamouroux, E., Boudier, A. and Duval, R.E., 2022. Current knowledge on the oxidative-stress-mediated antimicrobial properties of metal-based nanoparticles. *Microorganisms*, 10(2), p.437.

Martin-Sanchez, F., Iakovidis, I., Nørager, S., Maojo, V., de Groen, P., Van der Lei, J., Jones, T., Abraham-Fuchs, K., Apweiler, R., Babic, A. and Baud, R., 2004. Synergy between medical informatics and bioinformatics: facilitating genomic medicine for future health care. *Journal of biomedical informatics*, 37(1), pp.30-42.

MENACHEM FROMER, C. Y., MICHAL LINIAL 2009. Design of multispecific protein sequences using probabilistic graphical modeling. *Proteins: Structure, Function, and Bioinformatics*, 78(3).

Michl, T.D., Tran, D.T.T., Kuckling, H.F., Zhalgasbaikyzy, A., Ivanovská, B., García, L.E.G., Visalakshan, R.M. and Vasilev, K., 2020. It takes two for chronic wounds to heal: Dispersing bacterial biofilm and modulating inflammation with dual action plasma coatings. *RSC advances*, 10(13), pp.7368-7376.

Ming-Hsuang Cho, A. N., Ruili Huang, James Inglese, Christopher P. Austin, Terry Riss, Menghang Xia 2008. A bioluminescent cytotoxicity assay for assessment of membrane integrity using a proteolytic biomarker. *Toxicology in Vitro*, 22(4).

Mittal, L., Camarillo, I.G., Varadarajan, G.S., Srinivasan, H., Aryal, U.K. and Sundararajan, R., 2020. High-throughput, label-free quantitative proteomic studies of the anticancer effects of electrical pulses with turmeric silver nanoparticles: an in vitro model study. *Scientific Reports*, 10(1), p.7258.

Mohamed, M.A., Jaafar, J., Ismail, A.F., Othman, M.H.D. and Rahman, M.A., 2017. Fourier transform infrared (FTIR) spectroscopy. In *Membrane characterization* (pp. 3-29). elsevier.

Mohammadi, G., Nokhodchi, A., Barzegar-Jalali, M., Lotfipour, F., Adibkia, K., Ehyaei, N. and Valizadeh, H., 2011. Physicochemical and anti-bacterial performance characterization of clarithromycin nanoparticles as colloidal drug delivery system. *Colloids and Surfaces B: Biointerfaces*, 88(1), pp.39-44.

Ninan, N., Joseph, B., Visalakshan, R.M., Bright, R., Denoual, C., Zilm, P., Dalvi, Y.B., Priya, P.V., Mathew, A., Grohens, Y. and Kalarikkal, N., 2021. Plasma assisted design of biocompatible 3D printed PCL/silver nanoparticle scaffolds: in vitro and in vivo analyses. *Materials Advances*, 2(20), pp.6620-6630.

NingáLi, N., ZhiáLi, J., CunáChen, J., FengáHu, X., MingáLi, C. and QunáXu, L., 2017. An antimicrobial peptide with an aggregation-induced emission (AIE) luminogen for studying bacterial membrane interactions and antibacterial actions. *Chemical Communications*, 53(23), pp.3315-3318.

Okubo, T., Suzuki, T., Yokoyama, Y., Kano, K. and Kano, I., 2003. Estimation of estrogenic and anti-estrogenic activities of some phthalate diesters and monoesters by MCF-7 cell proliferation assay in vitro. *Biological and Pharmaceutical Bulletin*, 26(8), pp.1219-1224.

Owens, C.D. and Stoessel, K., 2008. Surgical site infections: epidemiology, microbiology and prevention. *Journal of hospital infection*, 70, pp.3-10.

Paladini, F. and Pollini, M., 2019. Antimicrobial silver nanoparticles for wound healing application: progress and future trends. *Materials*, 12(16), p.2540.

Panthihage Ruvini, L. D., Akash, B., Emma, P.-L. & Krasimir, V. 2021. Surface nanotopography mediated albumin adsorption, unfolding and modulation of early innate immune responses. *Materials Today Advances*, 12, 100187.

Putman, M., Burton, R. & Nahm, M. H. 2005. Simplified method to automatically count bacterial colony forming unit. *J Immunol Methods*, 302, 99-102.

Rai, M., Yadav, A. and Gade, A., 2009. Silver nanoparticles as a new generation of antimicrobials. *Biotechnology advances*, 27(1), pp.76-83.

Reithofer, M.R., Lakshmanan, A., Ping, A.T., Chin, J.M. and Hauser, C.A., 2014. In situ synthesis of size-controlled, stable silver nanoparticles within ultrashort peptide hydrogels and their anti-bacterial properties. *Biomaterials*, 35(26), pp.7535-7542.

Rodríguez-Ezpeleta, N., Hackenberg, M. and Aransay, A.M. eds., 2011. *Bioinformatics for high throughput sequencing*. Springer Science & Business Media.

Rupp, F., Scheideler, L. and Geis-Gerstorfer, J., 2002. Effect of heterogenic surfaces on contact angle hysteresis: dynamic contact angle analysis in material sciences. *Chemical Engineering & Technology: Industrial Chemistry–Plant Equipment–Process Engineering–Biotechnology*, 25(9), pp.877-882.

Russo, P.L., Stewardson, A.J., Cheng, A.C., Bucknall, T. and Mitchell, B.G., 2019. The prevalence of healthcare associated infections among adult inpatients at nineteen large Australian acute-care public hospitals: a point prevalence survey. *Antimicrobial Resistance & Infection Control*, 8, pp.1-8.

Sael, L., Chitale, M. and Kihara, D., 2012. Structure-and sequence-based function prediction for non-homologous proteins. *Journal of structural and functional genomics*, 13, pp.111-123.

Sekar, G., Mukherjee, A. and Chandrasekaran, N., 2014. Synthesis, Characterization and Application of Silver Nanoparticles as Chemical and Biological Sensors Towards Metal Ion Sensing. *Sensor Letters*, 12(12), pp.1694-1702.

Senem Kamiloglu, G. S., Tugba Ozdal, Esra Capanoglu 2020. Guidelines for cell viability assays. *Food Frontiers*, 1(3).

Serial Dilution Problem help (no date). <https://www.uvm.edu/~btessman/calc/serhelp.html>.

Severi, L., Losi, L., Fonda, S., Taddia, L., Gozzi, G., Marverti, G., Magni, F., Chinello, C., Stella, M., Sheouli, J. and Braicu, E.I., 2018. Proteomic and bioinformatic studies for the characterization of response to pemetrexed in platinum drug resistant ovarian cancer. *Frontiers in Pharmacology*, 9, p.454.

Silhavy, T.J., Kahne, D. and Walker, S., 2010. The bacterial cell envelope. *Cold Spring Harbor perspectives in biology*, 2(5), p.a000414.

Smith, K.C.A. and Oatley, C.W., 1955. The scanning electron microscope and its fields of application. *British Journal of Applied Physics*, 6(11), p.391.

SSI (no date). <https://www.gnsh.org/30-minute-weekly-initiative/weekly-challenge/healthcare-associated-infections/ssi/#:~:text=In%20Australia%2C%20infection%20of%20the,approximately%203%25%20of%20surgical%20procedures&text=over%2021%2C000%20cases%20of%20SSI%20occur%20annually.>

Surgical wound dehiscence (no date). <https://www.woundsource.com/patientcondition/surgical-wounds.>

Swanton, C., Larkin, J.M., Gerlinger, M., Eklund, A.C., Howell, M., Stamp, G., Downward, J., Gore, M., Futreal, P.A., Escudier, B. and Andre, F., 2010. Predictive biomarker discovery through the parallel integration of clinical trial and functional genomics datasets. *Genome medicine*, 2, pp.1-10.

Taheri, S., Cavallaro, A., Christo, S.N., Majewski, P., Barton, M., Hayball, J.D. and Vasilev, K., 2015. Antibacterial plasma polymer films conjugated with phospholipid encapsulated silver nanoparticles. *ACS Biomaterials Science & Engineering*, 1(12), pp.1278-1286.

Taheri, S., Cavallaro, A., Christo, S.N., Smith, L.E., Majewski, P., Barton, M., Hayball, J.D. and Vasilev, K., 2014. Substrate independent silver nanoparticle based antibacterial coatings. *Biomaterials*, 35(16), pp.4601-4609.

Tang, Y., Sun, H., Shang, Y., Zeng, S., Qin, Z., Yin, S., Li, J., Liang, S., Lu, G. and Liu, Z., 2019. Spiky nanohybrids of titanium dioxide/gold nanoparticles for enhanced photocatalytic

degradation and anti-bacterial property. *Journal of colloid and interface science*, 535, pp.516-523.

Tian, J., Wong, K.K., Ho, C.M., Lok, C.N., Yu, W.Y., Che, C.M., Chiu, J.F. and Tam, P.K., 2007. Topical delivery of silver nanoparticles promotes wound healing. *ChemMedChem: Chemistry Enabling Drug Discovery*, 2(1), pp.129-136.

Tilli, M., Paulasto-Kröckel, M., Petzold, M., Theuss, H., Motooka, T. and Lindroos, V. eds., 2020. *Handbook of silicon based MEMS materials and technologies*. Elsevier.

Vasilev, K., 2014. Nanoengineered plasma polymer films for biomaterial applications. *Plasma Chemistry and Plasma Processing*, 34, pp.545-558.

Vasilev, K., 2019. Nanoengineered antibacterial coatings and materials: A perspective. *Coatings*, 9(10), p.654.

Vasilev, K., Michelmore, A., Griesser, H.J. and Short, R.D., 2009. Substrate influence on the initial growth phase of plasma-deposited polymer films. *Chemical communications*, (24), pp.3600-3602.

VERA, R. M. 2016. *Management of Surgical Site Infections. Common Problems in Acute Care Surgery*

Verma, J., Kanoujia, J., Parashar, P., Tripathi, C.B. and Saraf, S.A., 2017. Wound healing applications of sericin/chitosan-capped silver nanoparticles incorporated hydrogel. *Drug delivery and translational research*, 7, pp.77-88.

Vizcarra, I. A., Emge, P., Miermeister, P., Chabria, M., Konradi, R., Vogel, V., Moller, J. 2013. Fluorescence-based in situ assay to probe the viability and growth kinetics of surface-adhering and suspended recombinant bacteria. *Biointerphases* 8(1), 22.

Wang, B., Liu, S., Liu, X., Hu, R., Qin, A. and Tang, B.Z., 2021. Aggregation-Induced Emission Materials that Aid in Pharmaceutical Research. *Advanced Healthcare Materials*, 10(24), p.2101067.

Wang, D., Lee, M.M., Shan, G., Kwok, R.T., Lam, J.W., Su, H., Cai, Y. and Tang, B.Z., 2018. Highly efficient photosensitizers with far-red/near-infrared aggregation-induced emission for in vitro and in vivo cancer theranostics. *Advanced Materials*, 30(39), p.1802105.

Wang, D., Su, H., Kwok, R.T., Hu, X., Zou, H., Luo, Q., Lee, M.M., Xu, W., Lam, J.W. and Tang, B.Z., 2018. Rational design of a water-soluble NIR AIEgen, and its application in ultrafast wash-free cellular imaging and photodynamic cancer cell ablation. *Chemical science*, 9(15), pp.3685-3693.

Wang, D., Su, H., Kwok, R.T., Shan, G., Leung, A.C., Lee, M.M., Sung, H.H., Williams, I.D., Lam, J.W. and Tang, B.Z., 2017. Facile synthesis of red/NIR AIE luminogens with simple structures, bright emissions, and high photostabilities, and their applications for specific imaging of lipid droplets and image-guided photodynamic therapy. *Advanced Functional Materials*, 27(46), p.1704039.

Wang, W., Wu, F., Zhang, Q., Zhou, N., Zhang, M., Zheng, T., Li, Y. and Tang, B.Z., 2022. Aggregation-induced emission nanoparticles for single near-infrared light-triggered photodynamic and photothermal antibacterial therapy. *ACS nano*, 16(5), pp.7961-7970.

Wang, W., Wu, F., Zhang, Q., Zhou, N., Zhang, M., Zheng, T., Li, Y., Tang, B. Z. 2022. Aggregation-induced emission nanoparticles for single near-infrared light-triggered photodynamic and photothermal antibacterial therapy. *ACS Nano*, 16, 7961.

Wong, K.K., Tian, J., Ho, C.M., Lok, C.N., Che, C.M., Chiu, J.F. and Tam, P.K., 2006. Topical delivery of silver nanoparticles reduces systemic inflammation of burn and promotes wound healing. *Nanomedicine: Nanotechnology, Biology and Medicine*.

World Health Organization, 2016. Global guidelines for the prevention of surgical site infection. World Health Organization.

Worth, L.J., Bull, A.L., Spelman, T., Brett, J. and Richards, M.J., 2015. Diminishing surgical site infections in Australia: time trends in infection rates, pathogens and antimicrobial resistance using a comprehensive Victorian surveillance program, 2002–2013. *infection control & hospital epidemiology*, 36(4), pp.409-416.

Wu, W. and Liu, B., 2021. Aggregation-induced emission: challenges and opportunities. *National Science Review*, 8(6), p.nwaa222.

Wu, X., Zhu, Z., Liu, Z., Li, X., Zhou, T., Zhao, X., Wang, Y., Shi, Y., Yu, Q., Zhu, W.H. and Wang, Q., 2022. Tricyano-Methylene-Pyridine Based High-Performance Aggregation-Induced Emission Photosensitizer for Imaging and Photodynamic Therapy. *Molecules*, 27(22), p.7981.

Würthner, F., 2020. Aggregation-induced emission (AIE): a historical perspective. *Angewandte Chemie International Edition*, 59(34), pp.14192-14196.

Yang, G., Yao, Y. and Wang, C., 2017. Green synthesis of silver nanoparticles impregnated bacterial cellulose-alginate composite film with improved properties. *Materials Letters*, 209, pp.11-14.

Yang, X.R., Sherman, M.E., Rimm, D.L., Lissowska, J., Brinton, L.A., Peplonska, B., Hewitt, S.M., Anderson, W.F., Szeszenia-Dabrowska, N., Bardin-Mikolajczak, A. and Zatonski, W., 2007. Differences in risk factors for breast cancer molecular subtypes in a population-based study. *Cancer Epidemiology Biomarkers & Prevention*, 16(3), pp.439-443.

Yang, Z., Yin, W., Zhang, S., Shah, I., Zhang, B., Zhang, S., Li, Z., Lei, Z. and Ma, H., 2020. Synthesis of AIE-active materials with their applications for antibacterial activity, specific imaging of mitochondrion and image-guided photodynamic therapy. *ACS Applied Bio Materials*, 3(2), pp.1187-1196.

Yasuda, H. and Gazicki, M., 1982. Biomedical applications of plasma polymerization and plasma treatment of polymer surfaces. *Biomaterials*, 3(2), pp.68-77.

Yasuda, H.K., 2012. Plasma polymerization. Academic press.

Ye, J., Calvo, I.A., Cenzano, I., Vilas-Zornoza, A., Martinez-de-Morentin, X., Lasaga, M., Alignani, D., Paiva, B., Viñado, A.C., Martin-Uriz, S. and Romero, J.P., 2021. Deep deconvolution of the hematopoietic stem cell regulatory microenvironment reveals a high degree of specialization and conservation between mouse and human. *Blood*, 138(Supplement 1), pp.2168-2168.

Yu, Y., Liu, Y., Chen, Y., Chen, J., Feng, G. and Tang, B.Z., 2023. Cationic AIE-active photosensitizers for highly efficient photodynamic eradication of drug-resistant bacteria. *Materials Chemistry Frontiers*, 7(1), pp.96-105.

Zhang, J., Liang, W., Wen, L., Lu, Z., Xiao, Y. and Lang, M., 2021. Antibacterial AIE polycarbonates endowed with selective imaging capabilities by adjusting the electrostaticity of the mixed-charge backbone. *Biomaterials Science*, 9(15), pp.5293-5301.

Zhang, Y., Wang, Y., Wang, J. and Liang, X.J., 2018. Improved pharmaceutical research and development with AIE-based nanostructures. *Materials Horizons*, 5(5), pp.799-812.

Zhao, Q. and Sun, J.Z., 2016. Red and near infrared emission materials with AIE characteristics. *Journal of Materials Chemistry C*, 4(45), pp.10588-10609.

Zhou, T., Hu, R., Wang, L., Qiu, Y., Zhang, G., Deng, Q., Zhang, H., Yin, P., Situ, B., Zhan, C. and Qin, A., 2020. An AIE-active conjugated polymer with high ROS-generation ability and biocompatibility for efficient photodynamic therapy of bacterial infections. *Angewandte Chemie International Edition*, 59(25), pp.9952-9956.

Zuo, Y., Kwok, R.T., Sun, J., Lam, J.W. and Tang, B.Z., 2023. AIE Macromolecular Materials for Antibacterial Applications. *Macromolecular Rapid Communications*, p.2300104.